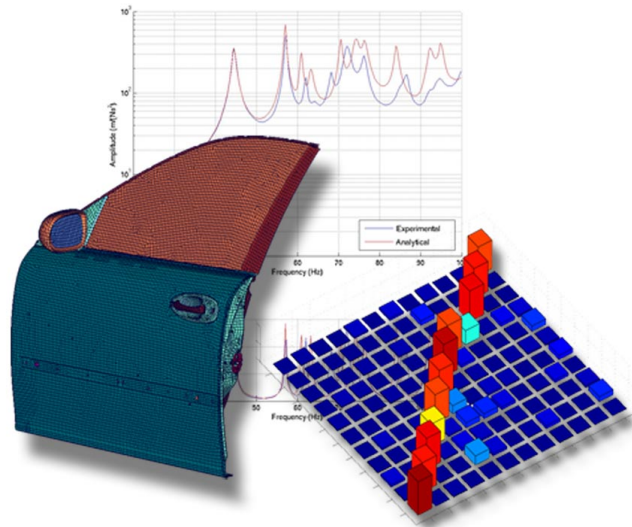




LUND
UNIVERSITY



ANALYSIS AND MEASUREMENTS OF VEHICLE DOOR STRUCTURAL DYNAMIC RESPONSE

MATS HÖRNLUND and
ALEXANDER PAPAZOGLU

Structural
Mechanics

Master's Dissertation

Structural Mechanics

ISRN LUTVDG/TVSM--05/5131--SE (1-167)

ISSN 0281-6679

ANALYSIS AND MEASUREMENTS OF VEHICLE DOOR STRUCTURAL DYNAMIC RESPONSE

Master's Dissertation by
MATS HÖRNLUND and
ALEXANDER PAPAZOGLU

Supervisors:

Göran Sandberg and Per-Erik Austrell,
Div. of Structural Mechanics

Lars Börjesson and Ulrika Johansson,
Saab Automobile AB

Copyright © 2005 by Structural Mechanics, LTH, Sweden.
Printed by KFS I Lund AB, Lund, Sweden, June, 2005.

For information, address:
Division of Structural Mechanics, LTH, Lund University, Box 118, SE-221 00 Lund, Sweden.
Homepage: <http://www.byggmek.lth.se>

Abstract

In order to reduce lead time and cost in the product development of vehicles more development will be made virtually. However, the predictability capability of simulation models is questioned and the simulation models need to be correlated versus hardware measurements and modeling techniques improved.

As part of the process of vehicle system model capability improvements the main objective of this project is to improve the structural dynamic response prediction capability of a vehicle door simulation model in a free-free configuration under steady-state conditions. The actions performed can then be rolled down to: simulate eigenmodes and frequency response, perform hardware measurements, make correlations of simulations versus measurements, using modal assurance criterion, frequency response assurance criterion and sum-blocks, and update simulation model. These actions are performed for four successively more complex door structures starting from a door in white and ending at a trimmed door.

The correlation status of the original model was only reasonably good for the door in white configuration. All other configurations displayed serious correlation mismatch.

By replacing the existing antifrutter models (connecting the side impact rail to outer panel) in the door in white configuration with simple spring elements the correlation for the door in white configuration was improved. With the window and seals attached the correlation problems was solved by introducing stiffness in the plane of the window of the springs acting as seals. The idea was to take friction into account. Also, by adjusting the spring stiffness of the seals, fair correlation could be achieved. The most important issue is to relate these results to component properties known before building simulation models. The following two configurations need more attention for better correlation. By using more detailed models the correlation could be improved, which shows the obvious trade-off between accuracy and computational effort. However, improving the model detail level fall outside the limitations of this project.

Preface

This project constitutes the final degree project within the Master of Science Programme in Mechanical Engineering at Lund Institute of Technology, Lund University, Sweden. The project was performed within the Division of Structural Mechanics under the supervision of Professor Göran Sandberg in collaboration with and on site at Noise and Vibration Center, Saab Automobile, Trollhättan, Sweden under the supervision of simulation engineers Ulrika Johansson and Lars Börjesson.

The authors would like to acknowledge Per-Olof Sturesson for giving us the opportunity to get an inside view of vehicle development in general and simulation engineering in particular as well as for seeing us through the whole of the project, Ulrika Johansson for kick starting the project and Lars Börjesson for picking up the ball after Ulrika. Thanks also to Per Bryntheson for taking us through the door model and for helpful guidance in modeling techniques, Bart Schellens for performing the actual measurements and for much valued input concerning the realm of measurements, Eva-Lotta Saloniemäki for many valuable discussions not only concerning this project, Mats Larsson for helpful insights concerning sheet metal stamping and last but not least all mechanics for helping us with a number of practical issues.

Lund, May 26, 2005

Mats Hörnlund and Alexander Papazoglu

I would also like to thank my fiancée Pernilla for moving to Trollhättan with me and for standing by me throughout this project. I love you Nilla.

Alexander

Notation

Symbols

a	Analytical
\mathbf{A}	General matrix
\mathbf{A}_i	Residues
\mathbf{b}	Body force vector
\mathbf{B}	Differentiated global shape function matrix
\mathbf{B}_i	Upper triangular Lanczos block
c_i	Modal damping
\mathbf{c}	Arbitrary vector
\mathbf{C}	Viscous damping matrix
$CT, CTMIN$	Constraint classification parameters
\mathbf{d}, \mathbf{d}^i	Search direction vector
\mathbf{D}	Constitutive matrix
$\mathbf{D}(\omega)$	Dynamic stiffness matrix in frequency domain
\mathbf{e}_j	Unit vector with non-zero component j
E	Young's modulus of elasticity
f	Frequency
\hat{f}_i	Modal force
$f(\mathbf{x})$	Objective function
\mathbf{f}	Force vector
$\hat{\mathbf{f}}(\omega)$	Complex force vector in frequency domain
\mathbf{f}_b	Boundary traction vector
\mathbf{f}_i	Body force vector
$g_j(\mathbf{x})$	Inequality constraints
G	Shear modulus of elasticity
G_{xx}	Power spectral density
G_{xy}	Cross power spectral density
$h_k(\mathbf{x})$	Equality constraints
$h_{ij}(\omega)$	Elements of $\mathbf{H}(\omega)$

H_1	Scalar function, H_1 estimate
$H_{sum}(\omega)$	Sum-blocks
$\mathbf{H}(\omega)$	Frequency response function matrix
\mathbf{A}^H	Hermitian transpose
i, j, k	Indices
i	imaginary number, $i = \sqrt{-1}$
\mathbf{I}	Identity matrix
J	Set of critical, i.e. active or violated, constraint indices
k_i	Modal stiffness
k_j	Scale factors
\mathbf{K}	Stiffness matrix
\mathbf{l}_i	Modal participation factor
m, n, p	Defines sizes of sets
m	Mass
m_i	Modal mass
\mathbf{M}	Mass matrix
\mathbf{M}_i	Upper triangular Lanczos block
n_x, n_y, n_z	Surface normals
\mathbf{N}	Global shape function matrix
P	Penalty variable
\mathbf{r}_j	Residual vector
\mathbf{R}_j	Residual matrix
\mathbf{R}_L	Lower residual matrix
\mathbf{R}_U	Upper residual matrix
\mathbf{R}	Upper triangular matrix
\mathbf{q}	Inertia force vector
\mathbf{q}_j	Columns of \mathbf{Q}
Q_i	Modal scaling factors
\mathbf{Q}	Orthonormal matrix
S	Surface
\mathbf{s}_i	Columns of \mathbf{S}_j , i.e. eigenvectors to \mathbf{T}_j
$\tilde{\mathbf{s}}_j$	Last p elements of the last column in \mathbf{S}_j
\mathbf{S}_j	Eigenvector matrix to \mathbf{T}_j
t	Time
\mathbf{t}	Surface traction vector
\mathbf{T}_j	Tri-diagonal (block) matrix
\mathbf{A}^T	Transpose
\mathbf{u}	Displacement vector
\mathbf{v}	Arbitrary weight vector
V	Volume

\mathbf{V}	Eigenvector matrix
w_j	Weight factors
x, y, z	Coordinates
x	Experimental
x_i^L, x_i^U	Lower and upper side constraints respectively
\mathbf{x}, \mathbf{x}^i	Vector of design variables
\mathbf{x}	Displacement vector for every degree of freedom
$\hat{\mathbf{x}}(\omega)$	Complex displacement vector in frequency domain
$\dot{\mathbf{x}}, \ddot{\mathbf{x}}$	First and second time derivative of \mathbf{x} , i.e. velocity and acceleration vectors respectively
\mathbf{X}_i	Lanczos block
\mathbf{y}_i	Columns of \mathbf{Y}_j , i.e. eigenvector estimates
\mathbf{Y}_j	Eigenvector matrix estimates
z	Scalar function
\mathbf{z}_k	Iteration vector
\mathbf{Z}_k	Iteration subspace
α_i	Lanczos coefficient
α^*	Optimal step length
$\boldsymbol{\alpha}_r$	Matrix estimated in <i>PolyMAX</i>
β_i	Lanczos coefficient
β^i	Biasing factor
β	β -method objective function
$\boldsymbol{\beta}_r$	Matrix estimated in <i>PolyMAX</i>
$\boldsymbol{\epsilon}$	Strain vector
ζ_i	Modal damping
θ_i	Eigenvalue of \mathbf{T}_j
θ	Direction
$\boldsymbol{\theta}_j$	Diagonal matrix containing the eigenvalues of \mathbf{T}_j
λ_i	Eigenvalue
λ, μ	Lame's constants
$\boldsymbol{\Lambda}$	A diagonal matrix containing the eigenvalues
μ	Eigenvalue
ν	Poisson's ratio
ξ_i	Modal response
$\boldsymbol{\xi}$	Modal response vector
ρ	Material density
σ	Shift constant
$\boldsymbol{\sigma}$	Stress vector
$\boldsymbol{\varphi}, \varphi_i$	Mode shape vector
$\boldsymbol{\Phi}$	Matrix with the mode shapes as columns

ω	Angular frequency
ω_i	Eigenfrequency
*	Complex conjugate
Δt	Sampling time
$\tilde{\nabla}$	Matrix differential operator

Abbreviations

CAD	Computer aided design
DOT	Design optimization tool
<i>DPR</i>	Driving point residue
FE	Finite element
FFT	Fast Fourier transform
<i>FRAC</i>	Frequency response assurance criterion
frf	Frequency response function
<i>MAC</i>	Modal assurance criterion
<i>WADPR</i>	Weighted average driving point residue

Contents

1	Introduction	1
1.1	Background	1
1.2	Objective	3
1.3	Disposition	3
2	Methodology	5
2.1	Door Configurations	5
2.2	Measurement and Analysis Reconciliation	7
2.3	Discussion	8
3	Finite Element Model	9
3.1	Finite Element Formulation	9
3.2	The Door Model	13
3.2.1	Bulk Data Entries	13
3.2.2	Door Components	15
4	Structural Dynamics	21
4.1	Modal Analysis	22
4.1.1	Formulation of the Eigenvalue Problem	22
4.1.2	Normalization of Modes	23
4.1.3	Solution Method of the Eigenvalue Problem	24
4.2	Frequency Response Analysis	33
4.2.1	Formulation of the Frequency Response Function	34
4.2.2	Solution Method for the Frequency Response Analysis	35
5	Pre-Test Analysis	39
5.1	Finding the Optimal Test Set-Up	40
5.1.1	Frequency Range Selection	40
5.1.2	Excitation Point Selection	40
5.1.3	Response Point Selection	42
5.2	Pre-Test Analysis of Door	44

5.2.1	Frequency Range	44
5.2.2	Response Point Selection	45
5.2.3	Excitation Point Selection	48
5.3	Discussion	49
6	Experimental Modal Analysis	51
6.1	Boundary Conditions	51
6.2	Structure Excitation	52
6.3	Measuring the Response Motion	52
6.4	Post Processing the Data	53
6.4.1	Estimation of the Modal Parameters	54
6.5	Modal Model Validation	56
6.5.1	Frequency Response Function Synthesis	56
6.5.2	Modal Assurance Criterion	57
6.6	Test Set-Up	57
6.6.1	Response Location Positioning	57
6.6.2	Boundary Conditions	58
6.6.3	Structure Excitation	58
6.6.4	Measuring the Response	60
6.6.5	Post Processing the Data	60
6.7	Measurement Results	62
6.8	Discussion	63
7	Measurement and Analysis Reconciliation	65
7.1	Correlation Methods	66
7.1.1	Direct Comparison	67
7.1.2	Comparison of Mode Shapes	67
7.1.3	Comparison of Frequency Response Functions	68
7.2	Correlation of Original Model	69
7.2.1	Door in White	69
7.2.2	Door in White, Window	70
7.2.3	Door in white, Window, Misc	70
7.2.4	Trimmed Door	70
8	Model Updating	73
8.1	Model Updating Process	74
8.2	Iterative Parameter Updating Procedure	75
8.2.1	Constraint Classification	77
8.2.2	Finding a Usable-Feasible Search Direction	78
8.2.3	The One-Dimensional Search	81
8.2.4	Convergence Check	82

Contents

8.2.5	The β -method	82
8.2.6	Comments on Optimization	83
8.3	Updating the Door Model	84
8.3.1	Updating Inertia Properties	84
8.3.2	Door in White	85
8.3.3	Door in White, Window	96
8.3.4	Door in White, Window, Misc	102
8.3.5	Trimmed Door	107
9	Conclusions	111
9.1	The Modeling of Doors	111
9.2	Model Updating Methodology	113
10	Future Work	115
A	Normal Modes Analysis in MSC.Nastran	117
A.1	MSC.Nastran SOL 103 Input File	118
B	Modal Frequency Response Analysis in MSC.Nastran	119
B.1	MSC.Nastran SOL 111 Input File	121
C	Pre-Test Results	123
C.1	Excitation Point Selection	123
C.2	Response Point Selection	124
C.2.1	Door in White	124
C.2.2	Door in White, Guide Rails	125
C.2.3	Door in White, Window	126
C.2.4	Door in White, Window, Misc	127
C.2.5	Trimmed Door	128
D	Measurement Results	129
D.1	Mode Maps	129
D.2	Model Validation	132
D.3	Sum-Blocks with Separated Excitations	138
E	Correlation Results	143
E.1	Door in White	143
E.2	Door in White, Window	146
E.3	Door in White, Window, Misc	149
E.4	Trimmed Door	152

F Optimization in MSC.Nastran	155
F.1 MSC.Nastran SOL 200 Input File	157

Chapter 1

Introduction

1.1 Background

The development of new automotive vehicles is a resource consuming and costly process. In order to reduce lead time and cost in the product development of vehicles more development will be made virtually. In an increasing pace of development and constant demands of cost reduction the building of prototypes is considered too expensive. Fewer and fewer prototypes are build in every prototype cycle of new automotive model development but the vehicle performance still need to be evaluated before the vehicles reach the market. In this light, with increasing computational power, simulation models seem a natural successor to conventional prototypes.

Within the engineering community hardware measurements always surpass simulations when it comes to reliability. The predictability capability of simulation models is questioned. Therefore the simulation models need to be correlated versus hardware measurements and modeling techniques improved.

In the field of noise and vibrations simulations are used to evaluate the structural dynamical and acoustic properties of components, sub-systems and vehicle systems during the whole of the development process. Since structure borne noise and vibrations are properties of the vehicle system the overall performance is highly dependent on the basic structure and is set at an early stage in the development process, often at a stage when it is not possible to evaluate hardware. This means that virtual prototyping is an important part of defining the overall noise and vibration performance of a new vehicle.

When performing structure borne road and engine noise simulations on vehicle system models the doors play an important part. In the simulations the vehicle structure interacts with the compartment cavity and the air pres-

sure response at the occupants' ears is the interesting output. The doors are fixed to the vehicle structure through hinges, a lock mechanism and door seals. This gives the door some freedom of motion and since the doors comprise large surfaces this motion have great impact on the air pressure in the compartment. This accentuates the necessity of good predictive performance of door models, including attachment points, when performing vehicle system simulations.

An effective and comfortable approach to analyze structural dynamics is to work under steady-state conditions in the frequency domain. The models considered here are used in eigenmodes and frequency response simulations.

To validate the simulation capability of the models measurements on hardware are used as reference. This implies that the frequency response of hardware must be measured and an experimental modal analysis performed.

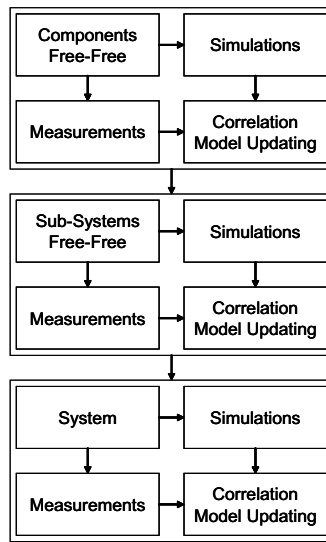


Figure 1.1 *Process employed when developing simulation models and techniques.*

The ideal simulation model development process addresses model improvements in several steps, see figure 1.1. Beginning at component level the simulation models are updated using hardware measurements as reference. Then, the components are assembled into sub-systems and finally the assembled system can be analyzed. When working on component and sub-system level attachments to the system are left out and the models are analyzed in a free-free configuration.

1.2. Objective

1.2 Objective

As part of the process of vehicle system model capability improvement the main objective of this project is to:

Improve the structural dynamic response prediction capability of vehicle door simulation model in a free-free configuration under steady-state conditions.

The actions of this project can then be rolled down to:

- Simulate eigenmodes and frequency response of door structure.
- Perform measurements on hardware.
- Make correlations of simulations and measurements.
- Update door simulation model.

1.3 Disposition

The report begins with a description of the methodology employed throughout the work in chapter 2. Then, the finite element formulation of the equation of motion and the finite element model is presented in chapter 3. In chapter 4 the subject of structural dynamics is covered including formulation of the eigenvalue problem, solution method used to solve the same problem and modal frequency response analysis. Then, the project enters into the realm of hardware measurements. First, a pre-test analysis procedure is explained in chapter 5 and then the actual hardware measurements are presented in chapter 6. The following chapter concerns the measurement and analysis reconciliation and presents the status of the door model. In chapter 8 the process of updating a simulation model is described, including the iterative parameter updating procedure used, the modification of the model and the correlation results of the improved model. Finally, the conclusions are presented in chapter 9 and suggested future work in chapter 10.

Chapter 2

Methodology

In this chapter the methodology employed throughout the work is explained. Since the main objective is to improve a simulation model a certain task that lies ahead is to change or update some model properties. To be able to relate what can be considered flaws in the model to the correct properties and/or components of the model it is preferable that the measurement and analysis reconciliation is performed for several different hardware and model configurations. Different aspects of the model properties can then be addressed in each configuration. In this project the reconciliation is performed for four door configurations explained below.

Since this project comprises only one step in the overall model development process in figure 1.1 only free-free configurations will be addressed.

For every door configuration a number of simulations and analyzes are performed. What they are, why they are used here, their individual order and what conclusions can be expected are then outlined in the following section.

2.1 Door Configurations

The actual door consists of a number of different components and materials. Basically the main structure is build up by spotwelded panels. The trim and accessories are attached in different ways.

How to choose or divide the door in different configurations is mainly a question of resource capacity, the more configurations the better.

In this project five configurations was chosen initially, see figure 2.1. The first being the basic door structure of spotwelded panels hereafter called *door in white*. To take the door apart even more the spotwelds needed to be broken up, which is not desirable. Performing measurements and simulations on this

configuration would give a sound understanding of the basic dynamics of the door.

Then, the window guide rails with attached electrical motor and gear box was added. This configuration was named *door in white, guide rails*. The idea with this setup was to separate the dynamics of the window and window seals from all other parts.

The third configuration, named *door in white, window*, then includes the window and window seals. This way the dynamics of the window and seals could be explored.

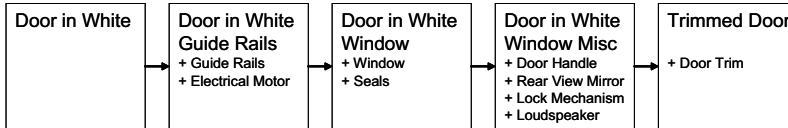


Figure 2.1 *Door configurations*

In the next configuration the door handle, lock mechanism, loudspeaker and rear view mirror are attached. These are all parts that cannot be expected to contribute significantly to the stiffness of the structure but will contribute with mass. This configuration was named *door in white, window, misc*.

Finally the door trim is attached. This plastic trim covers most of the inside of the door structure and causes difficulties when performing measurements of the structure in such way that it is not possible to attach instruments behind. Also, the stiffness impact of the trim is uncertain and the model is extensively simplified. The final configuration was named *trimmed door*.

This said, there still exists door parts not included in the analyzes. All electrical wiring was removed from the actual door and never included in the models. Also, three plastic trims, one on the outside of the outer panel, one on the lower door edge and the door arch trim, was excluded since they cannot be expected to have any major impact on the dynamics due to weak couplings and light, soft material. Further on, crash blocks or styrofoam blocks placed between the inner and outer panel was excluded due to low mass and questionable connections. These are mainly squeezed between the panels.

As is explained here the process starts from the door in white configuration and then components are added through the following configurations. This is the preferred strategy when considering simulation and analyzes. However, when working on the actual door it seems intuitive to start from

2.2. Measurement and Analysis Reconciliation

a complete door and the remove parts. This is also how the work was performed.

2.2 Measurement and Analysis Reconciliation

The different tasks performed for every door configuration in the measurement and analysis reconciliation is shown schematically in figure 2.2.

The main task, also depicted in the objective of the project, is the *model updating*. This is where the simulation model is improved. Based on how well the model predicts the actual dynamic response of the door, the model parameters can be updated. Here, the engineering judgement plays a vital role and the model is thoroughly studied to decide how to change and what parameters to change. Also, an iterative updating procedure can be employed.

To be able to tell anything about how well the model performs the simulation predictions are *correlated* versus hardware measurements. This is done through a series of correlation methods explained later. The simulations correlated are *eigenmodes simulations* and *frequency response simulations*.

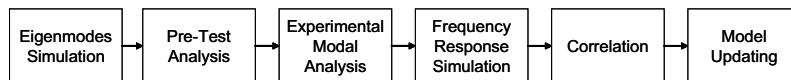


Figure 2.2 Analysis steps

The hardware measurements consists of an *experimental modal analysis* based on a huge number of spatially distributed frequency response measurements. In the experimental modal analysis the vibration mode shapes, resonance frequencies, modal participation factors and modal damping is estimated.

The estimated modal damping is used as input in the modal frequency response analysis which explains the individual ordering of the frequency response simulations.

To ensure good measurements a *pre-test analysis* is performed based on *eigenmodes simulation* of the original model. With an initial idea of the vibration mode shapes it is possible to select response locations that captures the interesting dynamical behavior of the structure. Also, excitation locations are determined.

This way the measurement and analysis reconciliation can be outlined as in figure 2.2.

It should be noted here that in this project all but the model updating step was performed for all door configurations at once, i.e. first the eigenmodes simulations for all configurations was performed then the pre-test analysis and so on. The model updating step was then performed for each configuration successively so that all updates made previously was inherited throughout the process.

2.3 Discussion

At first glance the methodology seems intuitive. However, some questions are raised. One concerns the frequency response simulations.

Is it not possible to perform frequency response simulations without first performing hardware measurements? Yes, of course, but then assumptions must be made concerning the damping. In this project modal frequency response analysis is used in the simulations which implies that the vibration modes have individual damping. Another way to reason is to apply a uniform structural damping using some rule of thumb value of damping. When adding trim to the structure it is reasonable that the damping is also increased and when considering the door structure only the first few modes can be categorized as global modes why also local damping properties are important.

The second major concern is if the original model performs well enough to be used in the pre-test analysis. If the model updating of the different configurations alters the dynamic response considerably it might be preferable to apply the whole of the measurement and analysis reconciliation shown in figure 2.2 to every configuration and in that way use updated models in the pre-test analysis.

Chapter 3

Finite Element Model

The dynamic motion of a system is described by the system force equilibrium equation called the equation of motion. This differential equation for a continuous system is complicated to solve by classical analytical methods. However, it can be solved in an approximate manner using the finite element method. This numerical method solves differential equations by making a discrete system of a continuum body using finite elements.

The finite element method can be studied further in a wide range of literature. An introduction to the method is given in Ottosen and Pettersson (1992).

In this chapter the finite element formulation of the equation of motion is derived with damping neglected. Damping is introduced in section 4.2.2. Finally, a description of the door and how it is modeled using finite elements is given.

3.1 Finite Element Formulation

The forces acting on an undamped three dimensional continuum body is described by the differential equations of equilibrium given by;

$$\tilde{\nabla}^T \boldsymbol{\sigma} + \mathbf{b} = \mathbf{q} \quad (3.1)$$

where $\boldsymbol{\sigma}$ is the stress vector, \mathbf{b} the body force vector and \mathbf{q} the inertia force vector. The inertia force vector can be written as;

$$\mathbf{q} = \rho \frac{\partial^2 \mathbf{u}}{\partial t^2} \quad (3.2)$$

3. Finite Element Model

where ρ is the density of the material, t the time and \mathbf{u} the displacement vector. $\tilde{\nabla}^T$ is a matrix differential operator defined as:

$$\tilde{\nabla}^T = \begin{bmatrix} \frac{\partial}{\partial x} & 0 & 0 & \frac{\partial}{\partial y} & \frac{\partial}{\partial z} & 0 \\ 0 & \frac{\partial}{\partial y} & 0 & \frac{\partial}{\partial x} & 0 & \frac{\partial}{\partial z} \\ 0 & 0 & \frac{\partial}{\partial z} & 0 & \frac{\partial}{\partial x} & \frac{\partial}{\partial y} \end{bmatrix} \quad (3.3)$$

In order to derive the finite element formulation of the differential equations of equilibrium the objective is to first determine the weak form (Davidsson, 2004). Multiplying equation (3.1) with an arbitrary weight function $\mathbf{v} = [v_x v_y v_z]^T$ and integrating over the volume V results in:

$$\int_V \mathbf{v}^T \left(\tilde{\nabla}^T \boldsymbol{\sigma} + \mathbf{b} - \rho \frac{\partial^2 \mathbf{u}}{\partial t^2} \right) dV = 0 \quad (3.4)$$

An integration by parts using Green-Gauss theorem on the first term of equation (3.4) yields:

$$\int_V \mathbf{v}^T \tilde{\nabla}^T \boldsymbol{\sigma} dV = \int_S \mathbf{v}^T \mathbf{t} dS - \int_V (\tilde{\nabla} \mathbf{v})^T \boldsymbol{\sigma} dV \quad (3.5)$$

The vector $\mathbf{t} = [t_x t_y t_z]$ is a surface traction vector which acts on the boundary S of the body. Its components are given by;

$$\begin{aligned} t_x &= \sigma_{xx}n_x + \sigma_{xy}n_y + \sigma_{xz}n_z \\ t_y &= \sigma_{yx}n_x + \sigma_{yy}n_y + \sigma_{yz}n_z \\ t_z &= \sigma_{zx}n_x + \sigma_{zy}n_y + \sigma_{zz}n_z \end{aligned} \quad (3.6)$$

where n_x , n_y and n_z are normals pointing out from the surface of the structure. Insertion of equation (3.5) in equation (3.4) yields:

$$\int_V \mathbf{v}^T \rho \frac{\partial^2 \mathbf{u}}{\partial t^2} dV + \int_V (\tilde{\nabla} \mathbf{v})^T \boldsymbol{\sigma} dV = \int_S \mathbf{v}^T \mathbf{t} dS + \int_V \mathbf{v}^T \mathbf{b} dV \quad (3.7)$$

This is the weak form of the differential equations of equilibrium (3.1) subjected to the boundary conditions stated in equation (3.6). This weak form holds for any constitutive relation as no assumptions are made yet. Introducing the finite element approximations, the displacement vector \mathbf{u} will be approximated by;

$$\mathbf{u} = \mathbf{N} \mathbf{x} \quad (3.8)$$

where \mathbf{x} is a vector of dimension $n_{dof} \times 1$ containing the displacement for every degree of freedom of the body. \mathbf{N} is the global shape function matrix

3.1. Finite Element Formulation

for the system. Next, the weight vector is chosen in accordance with the *Galerkin method* (Ottosen and Petterson, 1992) as:

$$\mathbf{v} = \mathbf{N}\mathbf{c} \quad (3.9)$$

The fact that \mathbf{v} is arbitrary, makes the matrix \mathbf{c} arbitrary. From equation (3.9) it follows that:

$$\begin{aligned} \tilde{\mathbf{V}}\mathbf{v} &= \mathbf{B}\mathbf{c} \\ \mathbf{B} &= \tilde{\mathbf{V}}\mathbf{N} \end{aligned} \quad (3.10)$$

Inserting equations (3.9) and (3.10) into equation (3.7), taking into account that \mathbf{c} is independent of the coordinates, yields:

$$\mathbf{c}^T \left(\int_V \mathbf{N}^T \rho \mathbf{N} dV \ddot{\mathbf{x}} + \int_V \mathbf{B}^T \boldsymbol{\sigma} dV - \int_S \mathbf{N}^T \mathbf{t} dS - \int_V \mathbf{N}^T \mathbf{b} dV \right) = 0 \quad (3.11)$$

As \mathbf{c} is an arbitrary matrix the following expression is true:

$$\int_V \mathbf{N}^T \rho \mathbf{N} dV \ddot{\mathbf{x}} + \int_V \mathbf{B}^T \boldsymbol{\sigma} dV = \int_S \mathbf{N}^T \mathbf{t} dS + \int_V \mathbf{N}^T \mathbf{b} dV \quad (3.12)$$

At this point the elasticity is introduced assuming small displacements and that the material is isotropic. Consequently, the stresses and strains are related by the following constitutive model;

$$\boldsymbol{\sigma} = \mathbf{D}\boldsymbol{\epsilon} \quad (3.13)$$

assuming the initial strains to be zero. \mathbf{D} is the constitutive matrix given by;

$$\mathbf{D} = \begin{bmatrix} \lambda + 2\mu & \lambda & \lambda & 0 & 0 & 0 \\ \lambda & \lambda + 2\mu & \lambda & 0 & 0 & 0 \\ \lambda & \lambda & \lambda + 2\mu & 0 & 0 & 0 \\ 0 & 0 & 0 & \mu & 0 & 0 \\ 0 & 0 & 0 & 0 & \mu & 0 \\ 0 & 0 & 0 & 0 & 0 & \mu \end{bmatrix} \quad (3.14)$$

and $\boldsymbol{\epsilon}$ is the strain vector. The coefficients λ and μ in the constitutive matrix are called *Lame's constants*. They can be expressed in the modulus of elasticity E , the shear modulus G and Poisson's ratio ν as:

$$\lambda = \frac{\nu E}{(1 + \nu)(1 - 2\nu)} \quad (3.15)$$

$$\mu = G = \frac{E}{2(1 + \nu)} \quad (3.16)$$

3. Finite Element Model

Using the kinematic expression for the strains they can be written as:

$$\boldsymbol{\epsilon} = \tilde{\mathbf{N}}\mathbf{u} \quad (3.17)$$

Equations (3.8) and (3.9) then result in:

$$\boldsymbol{\epsilon} = \mathbf{B}\mathbf{x} \quad (3.18)$$

Inserting equation (3.18) into equation (3.13) the constitutive model becomes:

$$\boldsymbol{\sigma} = \mathbf{D}\mathbf{B}\mathbf{x} \quad (3.19)$$

Inserting this expression into equation (3.12) we arrive at the finite element formulation:

$$\int_V \mathbf{N}^T \rho \mathbf{N} dV \ddot{\mathbf{x}} + \int_V \mathbf{B}^T \mathbf{D} \mathbf{B} dV \mathbf{x} = \int_S \mathbf{N}^T \mathbf{t} dS + \int_V \mathbf{N}^T \mathbf{b} dV \quad (3.20)$$

In order to write this in a compact form, the following matrices are defined;

$$\begin{aligned} \mathbf{M} &= \int_V \mathbf{N}^T \rho \mathbf{N} dV \\ \mathbf{K} &= \int_V \mathbf{B}^T \mathbf{D} \mathbf{B} dV \\ \mathbf{f}_b &= \int_S \mathbf{N}^T \mathbf{t} dS \\ \mathbf{f}_l &= \int_V \mathbf{N}^T \mathbf{b} dV \end{aligned} \quad (3.21)$$

where \mathbf{M} is the mass matrix, \mathbf{K} the stiffness matrix, \mathbf{f}_b the boundary traction vector and \mathbf{f}_l the body force vector. Defining the force vector \mathbf{f} as;

$$\mathbf{f} = \mathbf{f}_b + \mathbf{f}_l \quad (3.22)$$

the standard finite element formulation for a system without damping is obtained as:

$$\mathbf{M}\ddot{\mathbf{x}} + \mathbf{K}\mathbf{x} = \mathbf{f} \quad (3.23)$$

Both \mathbf{x} and \mathbf{f} are time dependent vectors. Different methods to solve this equation using the finite element method by transforming the problem into the frequency domain is presented in chapter 4. Also, one way to apply damping by assigning each mode an individual damping value, so called modal damping, is described in section 4.2.2.

3.2. *The Door Model*

3.2 The Door Model

The door is modeled in MSC.Nastran with different entries in the bulk data section of the MSC.Nastran input file.

The first section describes the bulk data entries, i.e. entries of grid data, finite elements, element and material properties. The next section describes how these entries define the door model.

3.2.1 Bulk Data Entries

The bulk data section contains entries that specify model geometry, element connectivity, element and material properties, boundary conditions and loads. The entries described below are all used in the door model. Only entry fields that are used in the FE model of this project are described. More detailed information about the bulk data entries can be found in MSC.Software Corporation (2003b).

The descriptions below has the same structure as the bulk data file of the model, i.e. the entries are described in the same order as they are entered in the input file.

GRID

The **GRID** entry defines the location of a geometric grid point, also called node. Each node has six degrees of freedom, three translational and three rotational. The location of the node in a rectangular coordinate system is given by its x , y and z coordinates. Each node has a unique grid point identification number which is referenced by element definitions.

CONM2

The **CONM2** entry defines a finite element of concentrated mass at a grid point. Each mass element refers to a grid point identification number defining the location of the mass. The mass value is entered as a real number. Also general mass inertia properties can be entered in the element definition.

RBE2

The **RBE2** entry defines a multipoint constraint element with independent degrees of freedom specified at single grid point and dependent degrees of freedom specified at an arbitrary number of grid points.

RBE3

The **RBE3** entry defines an interpolation constraint finite element which defines the motion at a reference grid point as the weighted average of the motion at a set of other grid points. The identification number of the reference grid point is given together with its components. In the following fields the weighting factor for components of motion, the component numbers and the grid point identification number are specified for each of the other grid points.

CBUSH

The **CBUSH** entry defines a spring element. Each element refers to a **PBUSH** entry in which the properties of the spring is entered. The spring connection points are given as two grid point identification numbers. These are allowed to be coincident meaning that the element has zero length. This avoids coupling between translational and rotational degrees of freedom at the grids even when no rotational spring are specified on the **PBUSH** entry. If stiffness is to be given in other directions than the direction of the element axis an orientation vector must be specified on the **CBUSH** entry. This can be done by entering the components of the orientation vector in the x , y and z directions of the global coordinate system.

CTRIA3

The **CTRIA3** entry defines an iso-parametric membrane-bending or plane strain triangular plate element. Each element refers to a **PSHELL** entry where the element properties are entered. The connection points are entered as three unique grid point identification numbers.

CQUAD4

The **CQUAD4** entry defines an iso-parametric membrane-bending or plane strain quadrilateral plate element. Each element reference a **PSHELL** entry where the element properties are entered. The connection points are entered as four unique grid point identification numbers.

CTETRA

The **CTETRA** entry defines a four sided solid element with four to ten grid points. Each element refers to a **PSOLID** entry where the element properties

3.2. *The Door Model*

are specified. The connection points are entered as a minimum of four unique grid point identification numbers. The mid edge points are optional.

CHEXA

The CHEXA entry defines a six sided solid element with eight to twenty grid points. The element properties are specified in a PSOLID entry and referred to by the property identification number. The connection points are entered as a minimum of eight grid point identification numbers. The edge points are optional.

PSHELL

The PSHELL entry defines the element properties for shell elements. Here the membrane thickness, bending moment of inertia ratio, transverse shear thickness ratio and nonstructural mass per unit area are specified. Each property card refers to a MAT1 entry by its material identification number, where the material properties are given. Each property entry is given an unique property identification number.

PSOLID

The PSOLID entry defines the properties of solid elements. If the material is isotropic each property card reference a MAT1 entry by its material identification number, where the material properties are specified. Each PSOLID entry is given an unique property identification number.

PBUSH

Defines the properties of a spring element where the spring stiffness values for each degree of freedom are specified. Each PBUSH entry is given an unique property identification number.

MAT1

The MAT1 entry defines the material properties, such as Young's modulus, Poission's ratio and mass density, for isotropic materials.

3.2.2 Door Components

The components of the door are modeled by the bulk data entries described above and then assembled to a door complete using different connections.

3. Finite Element Model

Only isotropic materials are used and all elements have linear properties, i.e no frequency or load dependency.

The coordinate system used in this project is defined with the origin at the front end of the vehicle, the x -axis in the front to rear direction and the z -axis pointing upward.

Panels, Trim and Window

Each panel of the door are modeled with **CTRIA3** and **CQUAD4** elements defining the panel midsurface, meaning that the panel is approximated by two dimensional plates. The plate elements belonging to a specific panel all reference the same **PSHELL** entry which in turn reference only one **MAT1** entry resulting in uniform element and material properties throughout the panel. The panels are given the properties of steel or aluminum and the nominal thickness of the sheet metal, according to CAD data, before stamping. Figure 3.1 shows the finite element model of the door in white configuration where some of the panels can be seen.



Figure 3.1 *Finite element model of the door in white configuration.*

The trim is modeled in the same manner as the panels using plate elements that represents the midsurface of the trim. The finite element model of the trim can be seen in figure 3.2. The whole trim has uniform element and material properties. Because the actual trim consists of several different materials with different thicknesses that are replaced with one uniform midsurface the element and material properties of the trim FE model has no physical counterpart. The trim is fixed to the door with plastic clip tower to clip connections. The clip towers are modeled using plate elements and each

3.2. The Door Model

clip is represented by a CBUSH spring element, with stiffness in the direction of the element axis. One end of the spring element is then connected to the tower and the other to the door by one RBE3 element in each end. This gives an assembly with some flexibility.



Figure 3.2 *Finite element model of the trim.*

The window is also represented by its midsurface, modeled with plate elements given the properties of glass. The window can be seen in figure 3.3. The figure also represents the guide rails, electrical motor and gear box.

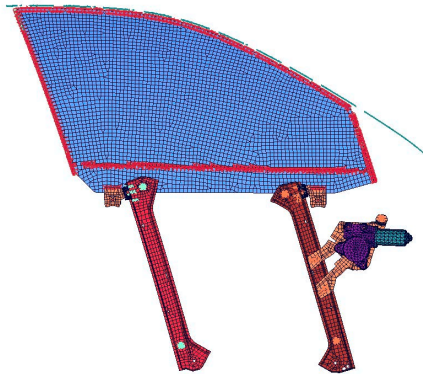


Figure 3.3 *Finite element model of the window, guide rails, electrical motor and gear box.*

Spotwelds, Hemflange and Adhesives

Spotwelds are modeled using CHEXA elements with eight grid points. The solids are connected to the surrounding grid points of the panels that are welded together with a number of RBE3 elements. The welds has the material properties of steel.

Hemflange is the connection of two panels by folding. In this connection a hemflange adhesive is used.

The antiflutter adhesive is a sticky rubber material that among other things joins together the outer panel and the side impact rail. The hemflange and antiflutter adhesive are modeled in the same manner as spotwelds with CHEXA and RBE3 elements but are given rubber like properties.

Seals and Friction Connections

Rubber seals are modeled using one CBUSH element per seal unit length. The springs are only given stiffness in the direction of the element axis.

Friction connections are modeled in the same way but the springs are given stiffness in all three translational directions. The two stiffnesses perpendicular to the element axis are given the same value and as a fraction of the element axis stiffness.

Bolt Connections

Each bolt is modeled with a so called star of RBE2 elements that connects the nodes at the periphery of the holes through which the bolt runs on the physical door.

Rear View Mirror, Lock, Handle and Loudspeaker

The rear view mirror, consisting of several different details, is exclusively modeled with plate elements of different properties and connected to the door by rigid elements representing three bolts. The finite element model of the rear view mirror is presented in figure 3.4.

The lock, see figure 3.5, is modeled with solid elements giving the lock its correct outer geometry but the mass distribution is homogeneous. Over the solid elements a shell of plate elements is placed to avoid numerical problems for some solutions sequences in MSC.Nastran.

The handle, shown in figure 3.6, is modeled with both plate elements and solid elements. For instance the counterweight is represented with solid elements giving the weight its right mass and mass distribution and on top of that a layer of plate elements with almost zero mass to solve numerical

3.2. The Door Model

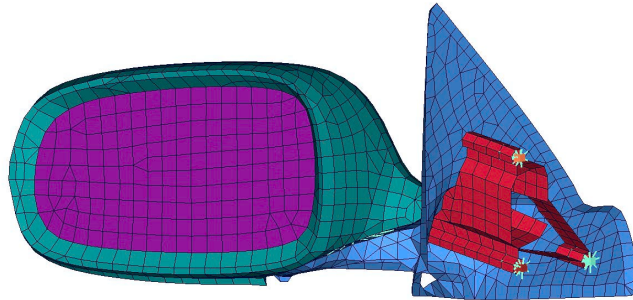


Figure 3.4 *Finite element model of the rear view mirror.*

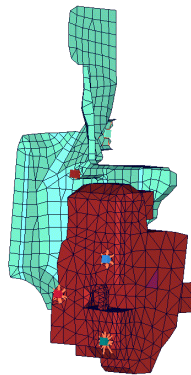


Figure 3.5 *Finite element model of the lock.*

3. Finite Element Model

problems in MSC.Nastran. The physical handle consists of moving parts joined together by hinges. These parts are locked in the FE model by rigid RBE2 elements. The handle is connected to the door by spring elements representing a rubber seal and rigid elements modeling a bolt.

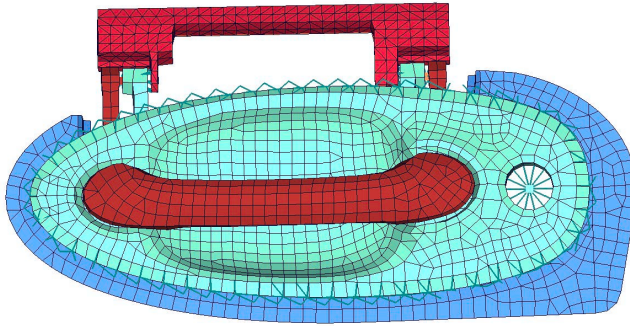


Figure 3.6 *Finite element model of the handle.*

The loudspeaker is modeled with several layers of plate elements of different properties over each other. The layers are connected using coincident nodes. The magnet is modeled with solid elements. The loudspeaker is connected to the door by RBE2 elements representing bolts. The finite element model of the loudspeaker can be seen in figure 3.7.

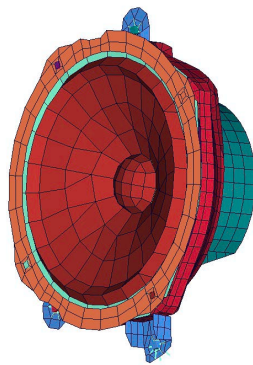


Figure 3.7 *Finite element model of the loudspeaker.*

Chapter 4

Structural Dynamics

Structural dynamics describes the behavior of a structure due to dynamic loading. Dynamic loads are applied as a function of time resulting in time varying responses. Due to computational cost and convenience these time varying loads are often transformed into the frequency domain before computing the responses of the structure. As a result the responses, i.e. the displacements, velocities, accelerations, forces and stresses are obtained as functions of frequency. To obtain the responses analytically a dynamic analysis is performed with the objective to solve the equation of motion;

$$\mathbf{M}\ddot{\mathbf{x}}(t) + \mathbf{C}\dot{\mathbf{x}}(t) + \mathbf{K}\mathbf{x}(t) = \mathbf{f}(t) \quad (4.1)$$

where $\mathbf{M}\ddot{\mathbf{x}}(t)$ are the inertia forces, which are functions of the mass matrix \mathbf{M} and the nodal acceleration vector $\ddot{\mathbf{x}}(t)$, $\mathbf{C}\dot{\mathbf{x}}(t)$ the viscous damping forces, which are functions of the damping matrix \mathbf{C} and the nodal velocities $\dot{\mathbf{x}}(t)$, $\mathbf{K}\mathbf{x}(t)$ are the elastic forces, which are functions of the stiffness matrix \mathbf{K} and the nodal displacement vector $\mathbf{x}(t)$, and $\mathbf{f}(t)$ are the applied loads. The equation of motion accounts for the forces acting on the structure at each instant in time. To find a solution there are several dynamic analysis methods available. The necessary solution approach is dependent of the extent of information required from the dynamic analysis. Two different solution approaches are described in the following sections. Modal analysis is used to determine the basic dynamic characteristics of a structure. Frequency response analysis is an efficient method for finding the steady-state response to harmonic excitation. Both methods are performed in the frequency domain.

In the following sections the (t) indicating a time dependent variable is omitted from the equations. If a variable is defined in the frequency domain this is indicated with (ω) after the variable.

4.1 Modal Analysis

The objective with modal analysis is to determine the natural frequencies and vibration mode shapes of a structure. This is usually the first and in many cases the only dynamic analysis performed. Most often damping is neglected. The results from this analysis characterize the basic dynamic behavior and are an indication of how the structure will respond to dynamic loading. The natural frequencies of a structure are the frequencies at which the structure naturally tends to vibrate if it is subjected to a disturbance. The deformed shape of the structure at a specific frequency is called its mode shape or normal mode. When damping is neglected the eigenvalues are real numbers (The MacNeal-Schwendler Corporation, 1996). The solution for the undamped natural frequencies and mode shapes is called real eigenvalue analysis or normal modes analysis. The structures' natural frequencies and mode shapes are functions of the structural properties and boundary conditions and are computed by solving an eigenvalue problem.

In this section the formulation of the eigenvalue problem is derived, followed by a section covering the normalization of modes. Then, a solution method for solving the eigenvalue problem is covered.

Normal modes analysis is implemented in MSC.Nastran by the executive control command `SOL 103`. A description of the entries and an input file used to perform modal analysis on the door in MSC.Nastran are presented in appendix A.

4.1.1 Formulation of the Eigenvalue Problem

Equation (4.1) is called the equation of motion. In this case, when performing modal analysis, the free vibrations of the structure are of interest. This means that there are no external forces applied. Also, damping is neglected. This reduces the equation of motion to:

$$\mathbf{M}\ddot{\mathbf{x}} + \mathbf{K}\mathbf{x} = \mathbf{0} \quad (4.2)$$

To solve equation (4.2) assume a harmonic solution of the form;

$$\mathbf{x} = \boldsymbol{\varphi} \sin \omega t \quad (4.3)$$

where $\boldsymbol{\varphi}$ is the mode shape vector and ω the corresponding angular frequency. Differentiating equation (4.3) and substituting it into the equation of motion (4.2) results in:

$$-\omega^2 \mathbf{M}\boldsymbol{\varphi} \sin \omega t + \mathbf{K}\boldsymbol{\varphi} \sin \omega t = \mathbf{0} \quad (4.4)$$

4.1. Modal Analysis

Simplifying this equation and dividing by the time dependent term $\sin \omega t$ yields the equation of motion in the frequency domain:

$$(\mathbf{K} - \omega^2 \mathbf{M}) \boldsymbol{\varphi} = \mathbf{0} \quad (4.5)$$

This equation is called the eigenequation and has a non-trivial solution when:

$$\det(\mathbf{K} - \omega^2 \mathbf{M}) = 0 \quad (4.6)$$

Equation (4.6) is called the system characteristic equation. The roots of this equation are the eigenvalues of the system. They are as many as the degrees of freedom, n_{dof} . The n_{dof} roots determine the n_{dof} natural frequencies ω_i ($i = 1, 2, \dots, n_{dof}$) of vibration. Each eigenvalue $\lambda_i = \omega_i^2$ has a corresponding eigenvector or mode shape $\boldsymbol{\varphi}_i$, which fulfills equation (4.6). Therefore the system can be written as;

$$(\mathbf{K} - \lambda_i \mathbf{M}) \boldsymbol{\varphi}_i = \mathbf{0} \quad (4.7)$$

or expressed for all eigenvalues and eigenmodes:

$$\mathbf{K}\boldsymbol{\Phi} = \boldsymbol{\Lambda}\mathbf{M}\boldsymbol{\Phi} \quad (4.8)$$

This is the generalized eigenvalue problem to be solved in free vibration modal analysis. There are several numerical approaches available for extracting the natural frequencies and mode shapes. A selection of these are described in section 4.1.3.

4.1.2 Normalization of Modes

An important characteristic of mode shapes is that the scaling or magnitude of the eigenvectors is arbitrary. This means that the eigenvalue problem, stated in equation (4.7), determines the natural modes only as relative quantities (Chopra, 2001). If two or more mode shapes are proportional to each other they are essentially the same natural mode because they all satisfy equation (4.7). Scale factors are sometimes applied to natural modes to standardize their elements associated with various degrees of freedom. In computer programs it is common to use a normalization method called *mass normalization*. This method scales each eigenvector to result in a unit value of generalized mass:

$$\boldsymbol{\varphi}_i^T \mathbf{M} \boldsymbol{\varphi}_i = 1 \quad (4.9)$$

This method results in a modal mass matrix that is the identity matrix and simplifies both computational and data storage requirements (The MacNeal-Schwendler Corporation, 1996). In another method called *max normalization*

each mode is normalized so that the largest modal displacement is unity. This method can be useful in the determination of the relative participation of an individual mode. If each mode is normalized so that the element corresponding to a particular degree of freedom at which the modal displacement is set to 1 or -1 the method is called point normalization. This method can cause numerical round off problems if the chosen degree of freedom in the non-normalized mode shape have a very small value of displacement. This will result in very large numbers in the mode shapes when larger numbers are normalized by this small value.

4.1.3 Solution Method of the Eigenvalue Problem

The problem of determining the natural vibration frequencies and the associated mode shapes of a mechanical system always leads to solving the generalized eigenvalue problem;

$$\mathbf{K}\Phi = \Lambda\mathbf{M}\Phi \quad (4.10)$$

where \mathbf{K} denotes the stiffness matrix, \mathbf{M} the mass matrix, Λ is a diagonal matrix of eigenvalues λ_i and Φ is a matrix with columns of eigenvectors. With mass normalized eigenvectors the orthogonality relations;

$$\Phi^T\mathbf{M}\Phi = \mathbf{I} \quad \Phi^T\mathbf{K}\Phi = \Lambda \quad (4.11)$$

hold. \mathbf{I} denotes the identity matrix.

The matrices \mathbf{K} and \mathbf{M} are nearly always symmetric and positive definite. However, numerical problems arise when this is not true, which is the case in many structural dynamic applications. The mass matrix becomes semi-positive definite when some degrees of freedom are not mass supplied. Also, if the system contains rigid body modes additional problems are introduced. These situations must be dealt with in numerical implementations. Problems with the mass matrix are avoided by only using the matrix in multiplications and rigid body modes are dealt with by introducing artificial constraints during factorization procedures. These problems will not be addressed further in this project.

There are several ways to go about solving the eigenvalue problem. The choice of method depends on the number of degrees of freedom of the system, the number of required eigenvalues or the required frequency range, ability to separate close eigenvalues, rate of convergence, computational cost and automatic extraction of rigid body modes.

When working with the finite element method the problem at hand usually consists of several thousand degrees of freedom and only a few of the

4.1. Modal Analysis

lowest eigenfrequencies or mode shapes are needed. When dealing with unsupported structures, rigid body modes are present. Symmetries or repetition of the same component in the structure leads to solutions with very close eigenvalues and puts restrictions on the solution method. The method chosen must comply with these problems and be computationally efficient.

To cope with these problems iterative solution methods are employed and where one of the most powerful is the *Lanczos method*.

Since this method is the main tool used to determine the natural vibration frequencies and associated mode shapes in this project the method is outlined below. This will only be a brief introduction and will only describe the general idea of the method. All mathematical intricacies and convergence properties of the method and how it is implemented in MSC.Nastran will not be addressed here. For a more thorough deduction the reader is referred to Golub and Van Loan (1983), Spanne (1994) and Komzisk (2001).

Many iterative solution methods employed to solve the eigenvalue problem can be categorized as *eigenvector iteration methods*, so also the Lanczos method. The origin of all eigenvector iteration methods is the *power algorithm*. To get a general idea of how these methods work this algorithm will be the starting point in the solution method description.

The Power Algorithm

With the power algorithm, in its raw form, it is possible to extract only the required eigenvalues and eigenvectors. Its convergence rate is independent of the size of the system to be solved, which makes it very useful when dealing with large systems. However, it is also flawed with some drawbacks, which will be explained below.

Consider the eigenvalue problem on standard form:

$$\mathbf{Ax} = \lambda \mathbf{x} \quad (4.12)$$

Assuming that the matrix \mathbf{A} is diagonalizable the solution to the problem is obtained by iteration, starting from an arbitrary vector \mathbf{z}_0 , of the relation:

$$\mathbf{z}_{k+1} = \mathbf{Az}_k \quad (4.13)$$

The starting vector can be written as a linear combination of the eigenvectors of \mathbf{A} as;

$$\mathbf{z}_0 = \sum_{i=1}^n \alpha_i \mathbf{x}_i \quad (4.14)$$

where the n eigenvectors \mathbf{x}_i and the corresponding eigenvalues λ_i are ordered in decreasing modular order as:

$$\lambda_1 \geq \lambda_2 \geq \dots \geq \lambda_n \quad (4.15)$$

Then k successive iterations yield:

$$\begin{aligned}\mathbf{z}_k &= \mathbf{A}^k \mathbf{z}_0 = \sum_{i=1}^n \alpha_i \mathbf{A}^k \mathbf{x}_i = \sum_{i=1}^n \alpha_i \lambda_i^k \mathbf{x}_i = \\ &= \lambda_1^k \left(\alpha_1 \mathbf{x}_1 + \sum_{i=2}^n \alpha_i \left(\frac{\lambda_i}{\lambda_1} \right)^k \mathbf{x}_i \right)\end{aligned}\quad (4.16)$$

As a consequence of decreasing modular order and disregarding from the case of multiple eigenvalues for now, the quotients (λ_i/λ_1) are less than 1 and their powers $(\lambda_i/\lambda_1)^k$ tend to zero when k is sufficiently large. Thus for $k \rightarrow \infty$;

$$\mathbf{z}_k \rightarrow \lambda_1^k \alpha_1 \mathbf{x}_1 \quad (4.17)$$

and:

$$\mathbf{z}_{k+1} \rightarrow \lambda_1^{k+1} \alpha_1 \mathbf{x}_1 \quad (4.18)$$

If $\alpha_1 \neq 0$ the quotient between two corresponding non-zero components of two successive iteration vectors tend toward the largest eigenvalue λ_1 according to;

$$\lambda_1 = \frac{\mathbf{z}_{k+1}^T \mathbf{e}_j}{\mathbf{z}_k^T \mathbf{e}_j} \quad (4.19)$$

and \mathbf{z}_{k+1} tends toward the corresponding eigenvector. \mathbf{e}_j denotes a unit vector with non-zero component j . The operation in equation (4.19) will only be computed for the largest corresponding components of the iteration vectors \mathbf{z}_k .

In order to avoid unnecessary large or small numbers during the iteration procedure the iteration vectors are normalized in such way that the procedure takes the following form:

$$\begin{aligned}\mathbf{z}_{k+1}^* &= \mathbf{A} \mathbf{z}_k \\ \mathbf{z}_{k+1} &= \frac{\mathbf{z}_{k+1}^*}{\|\mathbf{z}_{k+1}^*\|}\end{aligned}\quad (4.20)$$

The requirement of $\alpha_1 \neq 0$ is not critical since the progressive buildup of round off errors will introduce a small component parallel to \mathbf{x}_1 in the iteration vectors, but it will slow down convergence. In the case where the largest eigenvalues are equal, the algorithm will converge toward their common value and the associated eigenvector is any linear combination of the vectors \mathbf{x}_i .

The iteration procedure is stopped with a suitable convergence criterion.

The power algorithm has a number of serious drawbacks that keeps it from being useful in practical applications. If the largest eigenvalue is complex or multiple the iteration process will not converge. Also, the convergence of the algorithm is highly dependent on the distance between the two largest

4.1. Modal Analysis

eigenvalues. Since the approximation error is of size $O\left(\frac{\lambda_2}{\lambda_1}\right)$ the convergence will be extremely slow for close eigenvalues. And last, only the largest eigenpair will be solved. To solve for another eigenpair the algorithm has to be restarted after a projection and re-orthogonalized in every iteration. Despite this, the general idea of eigenvector iteration methods are proven and to cope with the problem mentioned some modification are introduced.

The Inverse Iteration Concept

Instead of using the matrix \mathbf{A} as iteration matrix, its inverse can be employed. The deduction is much like in equations (4.16), (4.17) and (4.18) and the iteration relation now takes the form:

$$\begin{aligned} \mathbf{z}_{k+1}^* &= \mathbf{A}^{-1} \mathbf{z}_k \\ \mathbf{z}_{k+1} &= \frac{\mathbf{z}_{k+1}^*}{\|\mathbf{z}_{k+1}^*\|} \end{aligned} \quad (4.21)$$

Instead of multiplying a matrix with a vector a linear system must be solved. At first glance this looks cumbersome but since it is the same matrix \mathbf{A} used in every iteration, some clever matrix decomposition is introduced and the effort becomes compatible with the power algorithm. In this way the iteration procedure solves for the smallest eigenvalue.

Introducing Shifts

If σ is a scalar the matrix $\mathbf{A} - \sigma \mathbf{I}$ has the same eigenvector as \mathbf{A} and eigenvalues $\lambda_1 - \sigma \geq \lambda_2 - \sigma \geq \dots \geq \lambda_n - \sigma$. Consequently, the smallest eigenvalue of $\mathbf{A} - \sigma \mathbf{I}$ corresponds to the eigenvalue of \mathbf{A} that is closest to σ . An inverse iteration of $\mathbf{A} - \sigma \mathbf{I}$ will converge to the eigenvalue $\mu = 1/(\lambda_i - \sigma)$ and the eigenvector \mathbf{x}_i . In this way it is possible to choose what eigenvalue λ_i to solve for.

Introducing shifts also leads to an efficient way of determining how many eigenvalues there is in a certain interval. This is implemented in MSC.Nastran to decide if all eigenvalues have been solved for.

If a matrix \mathbf{A} is symmetric of size $n \times n$, then suppose that during Gaussian elimination (usually performed initially when working with shifted and inverted algorithms) of the matrix $\mathbf{A} - \sigma \mathbf{I}$ the number of positive pivot elements is p and the number of negative pivot elements are $m = n - p$. Then p is the number of eigenvalues larger than σ and m is the number of eigenvalues smaller than σ .

This is used when some eigenvalues in an interval have been solved. Then, the last Gaussian elimination reveals if all eigenvalues have been solved. Implementation needs to be more elaborated but will not be addressed here.

The main advantage with the shifted and inverted iteration procedure is however a complete separate matter. By choosing σ as a fairly good approximation to λ_i one iteration step will result in a good approximation of the eigenvector \mathbf{x}_i . However, to be able to get acceptable results the iteration matrix must be transformed to a more suitable form (tri-diagonal or *Hessenberg*) (Spanne, 1994). This transformation is necessary for other reasons explained later and the inverse iteration with shifts can be an efficient way of extracting eigenvectors from already computed eigenvalues.

Subspace Iteration

Up to this point the iteration procedures have only been able to solve for single eigenpairs. By the introduction of *subspace iteration methods* (Spanne, 1994) this will change. The concept is simple. Instead of just using a vector, \mathbf{z} in the iterations a whole subspace is used. When working with subspaces it is preferable to work with orthonormal bases. This is implemented by using the well-known *QR factorization* (Spanne, 1994). There are several variations of methods performing QR factorizations. The choice depends on the problem at hand. The QR factorization transforms a non-singular $n \times m$ matrix to the product between a unitary $n \times n$ matrix \mathbf{Q} containing orthonormal column vectors and an upper-triangular $n \times m$ matrix \mathbf{R} . Starting from an arbitrary matrix \mathbf{Q}_0 the subspace iteration routine can be expressed as;

$$\begin{aligned} \mathbf{Z}_k &= \mathbf{A}\mathbf{Q}_{k-1} \\ \mathbf{Q}_k\mathbf{R}_k &= \mathbf{Z}_k \end{aligned} \quad (4.22)$$

where the last equation represents the QR factorization of the $n \times m$ iteration subspace \mathbf{Z}_k . In this case a multiplication with the matrix \mathbf{A} is necessary in every iteration and in this form the QR factorization is costly. However, it can be shown that when k tends to infinity the matrices \mathbf{R}_k tend to \mathbf{R} such that;

$$\mathbf{Q}^H\mathbf{A}\mathbf{Q} = \mathbf{R}, \quad \mathbf{A} = \mathbf{Q}\mathbf{R}\mathbf{Q}^H \quad (4.23)$$

where H denotes *Hermitian transpose*. This is just a *Shur factorization* of \mathbf{A} and the eigenvalues can be found on the diagonal of \mathbf{R} (Spanne, 1994).

Denote the matrix $\mathbf{Q}_k^H\mathbf{A}\mathbf{Q}_k$ with \mathbf{T}_k . Then this matrix \mathbf{T}_k , and thus the eigenvalues, can be recursively determined without involving the matrix \mathbf{A} again since;

$$\mathbf{T}_{k-1} = \mathbf{Q}_{k-1}^H\mathbf{A}\mathbf{Q}_{k-1} = \mathbf{Q}_{k-1}^H\mathbf{Z}_k = (\mathbf{Q}_{k-1}^H\mathbf{Q}_k)\mathbf{R}_k \quad (4.24)$$

and:

$$\begin{aligned} \mathbf{T}_k &= \mathbf{Q}_k^H\mathbf{A}\mathbf{Q}_k = \mathbf{Q}_k^H\mathbf{A}\mathbf{Q}_{k-1}^H\mathbf{Q}_{k-1}\mathbf{Q}_k \\ &= \mathbf{Q}_k^H\mathbf{Z}_k\mathbf{Q}_{k-1}^H\mathbf{Q}_k = \mathbf{R}_k(\mathbf{Q}_{k-1}^H\mathbf{Q}_k) \end{aligned} \quad (4.25)$$

4.1. Modal Analysis

Thus, \mathbf{T}_k is determined by computing the QR factorization of \mathbf{T}_{k-1} ;

$$\mathbf{T}_{k-1} = (\mathbf{Q}_{k-1}^H \mathbf{Q}_k) \mathbf{R}_k \quad (4.26)$$

and then multiplying the factors together in reversed order. The subspace iteration procedure, now called the *QR method* then becomes;

$$\begin{aligned} \mathbf{Q}_k \mathbf{R}_k &= \mathbf{T}_{k-1} \\ \mathbf{T}_k &= \mathbf{R}_k \mathbf{Q}_k \end{aligned} \quad (4.27)$$

with the initialization of $\mathbf{T}_0 = \mathbf{A}$.

The QR method in the form described here still contain some serious drawbacks. Every iteration step is too costly, the convergence is slow (at best linear) and complex eigenvalues to real matrices breaks down the algorithm. The first problem is solved by transforming the matrix \mathbf{A} to tri-diagonal form using the Lanczos method outlined below. The second problem is taken care of by introducing shifts and the last can be solved by some modifications but will not be addressed here due to the fact that in the undamped vibration problems discussed here, complex eigenvalues do not occur.

Lanczos Method

The Lanczos method or algorithm was derived for the purpose of solving the eigenvalue problem for large, sparse and symmetric matrices. As can be expected at this point it is a derivative of the previous methods and takes the subspace iteration techniques one step further.

The Lanczos iterations sole purpose is to generate a sequence of tri-diagonal matrices \mathbf{T}_j with eigenvalues that are progressively better estimates of eigenvalues of the original matrix \mathbf{A} . Then, the QR method can be used to extract the eigenvalues of \mathbf{T}_j . With the tri-diagonal structure the QR method becomes computationally efficient.

The tri-diagonalization of $\mathbf{A} \in \mathbf{R}^{n \times n}$ can be expressed as $\mathbf{T} = \mathbf{Q}^T \mathbf{A} \mathbf{Q}$ where \mathbf{Q} contains the orthonormal columns \mathbf{q}_j and:

$$\mathbf{T} = \begin{bmatrix} \alpha_1 & \beta_1 & 0 & \cdots & 0 \\ \beta_1 & \alpha_2 & \beta_2 & & \\ 0 & \beta_2 & \alpha_3 & \ddots & \\ \vdots & & \ddots & \ddots & \beta_{n-1} \\ 0 & & & \beta_{n-1} & \alpha_n \end{bmatrix} \quad (4.28)$$

Using the orthogonality of \mathbf{Q} , that is $\mathbf{Q}^T \mathbf{Q} = \mathbf{I}$, the columns in $\mathbf{A} \mathbf{Q} = \mathbf{Q} \mathbf{T}$ can be equated:

$$\mathbf{A} \mathbf{q}_j = \beta_{j-1} \mathbf{q}_{j-1} + \alpha_j \mathbf{q}_j + \beta_j \mathbf{q}_{j+1} \quad (4.29)$$

Since the \mathbf{q}_j 's are orthonormal the relation;

$$\alpha_j = \mathbf{q}_j^T \mathbf{A} \mathbf{q}_j \quad (4.30)$$

holds. And if;

$$\mathbf{r}_j = (\mathbf{A} - \alpha_j \mathbf{I}) \mathbf{q}_j - \beta_{j-1} \mathbf{q}_{j-1} \quad (4.31)$$

is nonzero, then;

$$\mathbf{q}_{j+1} = \mathbf{r}_j / \beta_j \quad (4.32)$$

where:

$$\beta_j = \|\mathbf{r}_j\|_2 \quad (4.33)$$

By sequencing these equations properly the Lanczos iterations can be written;

$$\begin{aligned} \alpha_j &= \mathbf{q}_j^T \mathbf{A} \mathbf{q}_j \\ \mathbf{r}_j &= (\mathbf{A} - \alpha_j \mathbf{I}) \mathbf{q}_j - \beta_{j-1} \mathbf{q}_{j-1} \\ \beta_j &= \|\mathbf{r}_j\|_2 \\ \mathbf{q}_{j+1} &= \mathbf{r}_j / \beta_j \end{aligned} \quad (4.34)$$

with the initialization $\beta_1 = 0$, $\mathbf{q}_0 = \mathbf{0}$ and \mathbf{q}_1 as an arbitrary vector with $\|\mathbf{q}_1\|_2 = 1$.

The iterations are stopped when the eigenpairs are determined satisfactory accurate in a 2-norm sense. This can be determined without the complete computation of an eigenpair as will be explained later. The Lanczos method described so far is still not ready for implementation. As was the case with the power algorithm, the Lanczos method has a block analog.

Block Lanczos Method

The block Lanczos method works in the same manner as the one deduced above only now on a block of vectors.

Suppose $n = rp$ and consider the tri-diagonalization;

$$\mathbf{Q}^T \mathbf{A} \mathbf{Q} = \mathbf{T} = \begin{bmatrix} \mathbf{M}_1 & \mathbf{B}_1^T & \mathbf{0} & \cdots & \mathbf{0} \\ \mathbf{B}_1 & \mathbf{M}_2 & \mathbf{B}_2^T & & \\ \mathbf{0} & \mathbf{B}_2 & \mathbf{M}_3 & \ddots & \\ \vdots & & \ddots & \ddots & \mathbf{B}_{r-1}^T \\ \mathbf{0} & & & \mathbf{B}_{r-1} & \mathbf{M}_r \end{bmatrix} \quad (4.35)$$

where $\mathbf{Q} = [\mathbf{X}_1, \dots, \mathbf{X}_r]$, $\mathbf{X}_i \in \mathbf{R}^{n \times p}$ is orthogonal, and every $\mathbf{M}_i \in \mathbf{R}^{p \times p}$, $\mathbf{B}_i \in \mathbf{R}^{p \times p}$ is upper triangular. p determines the size of the blocks.

Comparing blocks in $\mathbf{A} \mathbf{Q} = \mathbf{Q} \mathbf{T}$ gives:

$$\mathbf{A} \mathbf{X}_j = \mathbf{X}_{j-1} \mathbf{B}_{j-1}^T + \mathbf{X}_j \mathbf{M}_j + \mathbf{X}_{j+1} \mathbf{B}_j \quad (4.36)$$

4.1. Modal Analysis

Again, the orthogonality of \mathbf{Q} leads to;

$$\mathbf{M}_j = \mathbf{X}_j^T \mathbf{A} \mathbf{X}_j \quad (4.37)$$

further on;

$$\mathbf{X}_{j+1} \mathbf{B}_j = \mathbf{R}_j \quad (4.38)$$

represents the QR factorization of:

$$\mathbf{R}_j = \mathbf{A} \mathbf{X}_j - \mathbf{X}_j \mathbf{M}_j - \mathbf{X}_{j-1} \mathbf{B}_{j-1}, \quad \mathbf{R}_j \in R^{n \times p} \quad (4.39)$$

Thus, starting from \mathbf{X}_1 such that $\mathbf{X}_1^T \mathbf{X}_1 = \mathbf{I}^{p \times p}$, $\mathbf{X}_0 \mathbf{B}_0^T = \mathbf{0}$ and computing $\mathbf{M}_1 = \mathbf{X}_1^T \mathbf{A} \mathbf{X}_1$ the block Lanczos method can be written:

$$\begin{aligned} \mathbf{R}_j &= \mathbf{A} \mathbf{X}_j - \mathbf{X}_j \mathbf{M}_j - \mathbf{X}_{j-1} \mathbf{B}_{j-1} \\ \mathbf{X}_{j+1} \mathbf{B}_j &= \mathbf{R}_j \\ \mathbf{M}_{j+1} &= \mathbf{X}_{j+1}^T \mathbf{A} \mathbf{X}_{j+1} \end{aligned} \quad (4.40)$$

With proper storage of the blocks \mathbf{M}_j and \mathbf{B}_j the now block tri-diagonal matrix \mathbf{T}_j can be produced. This matrix contain estimates of a block of eigenpairs of the original matrix \mathbf{A} .

The Lanczos method implemented in MSC.Nastran uses a generalized *modified Gram-Schmidt orthogonalization* procedure in the QR factorization of \mathbf{R}_j , where only two multiplications of the mass matrix are needed (Komzsik, 2001). These multiplications are needed due to that the blocks \mathbf{X}_j are kept mass orthogonal meaning $\mathbf{X}_j^T \mathbf{M} \mathbf{X}_j = \mathbf{I}$ (\mathbf{M} now denotes the mass matrix).

The block-tri-diagonal matrix \mathbf{T}_j is essentially a banded matrix. Before extracting the eigenvalues this matrix has to be tri-diagonalized. This is done efficiently using *Givens rotations*. The eigenvalues of the now tri-diagonal matrix can be solved with the QR method outlined in equation (4.27). The computational effort is now drastically lower when the iteration matrix is tri-diagonal. Again the Givens rotations are used to zero off the off-diagonal elements in the QR factorizations of \mathbf{T}_j (Komzsik, 2001).

To terminate the iterations a convergence criterion must be established. After j iterations;

$$\mathbf{S}_j^T \mathbf{T}_j \mathbf{S}_j = \boldsymbol{\theta}_j, \quad \boldsymbol{\theta}_j = \text{diag}(\theta_1, \dots, \theta_{jp}) \quad (4.41)$$

is the Shur decomposition of \mathbf{T}_j obtained during the solution of the eigenvalues of \mathbf{T}_j . The eigenvectors of \mathbf{T}_j can be found as the columns, \mathbf{s}_i of the matrix \mathbf{S}_j with corresponding eigenvalues θ_i . Further on, define the matrix \mathbf{Y}_j as;

$$\mathbf{Y}_j = \mathbf{Q}_j \mathbf{S}_j \quad (4.42)$$

\mathbf{Y}_j now contains estimates of \mathbf{A} 's eigenvectors and the corresponding eigenvalues are contained in $\boldsymbol{\theta}$ and a suitable convergence criterion for eigenpair i can be expressed as;

$$\|\mathbf{A}\mathbf{y}_i - \theta_i\mathbf{y}_i\|_2 < \epsilon \quad (4.43)$$

where \mathbf{y}_i is the i^{th} column of \mathbf{Y}_j and ϵ is a small scalar set to certain a tolerance. Put this way it seems that a complete eigenpair must be computed in every iteration, which is a costly operation. As it turns out this is not necessary due to structure of the matrix \mathbf{T}_j and the operation can be reduced to;

$$\|\mathbf{B}_j\tilde{\mathbf{s}}_j\| < \epsilon \quad (4.44)$$

where $\tilde{\mathbf{s}}_j$ is the last p elements of the last column in \mathbf{S}_j . In this way the convergence check is made for the whole block of size p .

Orthogonality

The Lanczos algorithm is extensively dependent on the orthogonality of the Lanczos blocks, \mathbf{X}_i , and in turn the Lanczos vectors (columns of \mathbf{X}_i). In exact arithmetics the algorithm produces an orthonormal set of Lanczos vectors but this is not the case when implemented in a numerical environment. Round off errors causes the Lanczos vectors to loose their orthogonality and brakes down the convergence properties of the algorithm. This problem is, however, well understood and can be handled in different ways (Komzsisik, 2001).

Without getting too detailed it should be said that when the algorithm was first introduced a complete re-orthogonalization was used where each new Lanczos block was orthogonalized against all previous blocks. This procedure was computationally cumbersome and required unnecessary storage. But as the problem was investigated further new solutions became available.

Loss of orthogonality can occur in four different areas:

- Internally Within a given block of Lanczos vectors.
- Locally With respect to the previous two Lanczos blocks.
- Globally With respect to the whole set of previously computed
Lanczos vectors.
- Externally With respect to eigenvectors from different shifts.

All areas are treated differently. The first two are solved by introducing some orthogonalization routine such as the modified Gram-Schmidt orthogonalization, which includes updating the iteration variables. The third can be efficiently handled due to the fact that estimates of the orthogonality and convergence can be cheaply monitored during the iterations and that it is sufficient to have an orthogonality at the level of the square root of the

4.2. Frequency Response Analysis

machine's precision to get reasonable results. Also, the beauty of the algorithm allows for orthogonalization against only a few of the newly converged eigenvectors and still maintain global orthogonality. This method is then called *selective orthogonalization*. Finally, the fourth, is not due to the algorithm itself and the problem is solved by keeping track of the eigenvalues and eigenvectors extracted from previous Lanczos runs and then applying selective orthogonalization.

Transforming the Generalized Eigenvalue Problem

The solution method for solving the eigenvalue problem for vibration problems implemented in MSC.Nastran is a block Lanczos algorithm with a shifted and inverted iteration matrix. Considering the generalized eigenvalue problem in equation (4.10) again, now expressed for a single eigenpair:

$$\mathbf{K}\boldsymbol{\varphi} = \lambda\mathbf{M}\boldsymbol{\varphi} \quad (4.45)$$

Introducing the shift;

$$\lambda = \mu + \sigma \quad (4.46)$$

and moving the σ to the left hand side yields:

$$(\mathbf{K} - \sigma\mathbf{M})\boldsymbol{\varphi} = \mu\mathbf{M}\boldsymbol{\varphi} \quad (4.47)$$

Assuming $\mathbf{K} - \sigma\mathbf{M}$ is invertible, pre-multiply both sides by $\mathbf{M}(\mathbf{K} - \sigma\mathbf{M})^{-1}$ and use equation (4.46). Then, the problem can be expressed as a standard eigenvalue problem;

$$\mathbf{M}(\mathbf{K} - \sigma\mathbf{M})^{-1}\mathbf{M}\boldsymbol{\varphi} = \frac{1}{\lambda - \sigma}\mathbf{M}\boldsymbol{\varphi} \quad (4.48)$$

and it is this problem that is solved with the Lanczos method in MSC.Nastran. It is important to notice that the mass matrix is only used in multiplications. In this way problems with semi-positive definite mass matrices are avoided.

4.2 Frequency Response Analysis

The objective of frequency response analysis is to determine the frequency response function matrix of a structure. The frequency response function is defined as the response in one degree of freedom due to an input in the same or another degree of freedom. It is used to compute structural response

to steady-state oscillatory excitation, where the excitation is defined in the frequency domain.

In this section the expression for the frequency response function matrix is derived. Then a numerical method, the modal frequency response analysis, for solving the frequency response is described.

Frequency response function analysis is implemented in MSC.Nastran by the executive control command `SOL 111`. A description of the entries and an input file used to perform frequency response analysis on the door in MSC.Nastran are presented in appendix B.

4.2.1 Formulation of the Frequency Response Function

Starting from the equation of motion for the system;

$$\mathbf{M}\ddot{\mathbf{x}} + \mathbf{C}\dot{\mathbf{x}} + \mathbf{K}\mathbf{x} = \mathbf{f} \quad (4.49)$$

where \mathbf{M} is the mass matrix, \mathbf{C} the viscous damping matrix, \mathbf{K} the complex stiffness matrix, \mathbf{f} the force vector and \mathbf{x} the displacement vector. In the case of harmonic excitation a steady-state solution is sought and the force and the corresponding response can be expressed as harmonic functions (Davidsson, 2004) as;

$$\mathbf{f} = \hat{\mathbf{f}}(\omega) e^{i\omega t} \quad (4.50a)$$

$$\mathbf{x} = \hat{\mathbf{x}}(\omega) e^{i\omega t} \quad (4.50b)$$

where $\hat{\mathbf{f}}(\omega)$ is the complex force vector and $\hat{\mathbf{x}}(\omega)$ the complex displacement vector. Taking the first and second derivatives of equation (4.50b) and inserting the results together with equation (4.50) into equation (4.49) gives;

$$-\omega^2 \mathbf{M} \hat{\mathbf{x}}(\omega) e^{i\omega t} + i\omega \mathbf{C} \hat{\mathbf{x}}(\omega) e^{i\omega t} + \mathbf{K} \hat{\mathbf{x}}(\omega) e^{i\omega t} = \hat{\mathbf{f}}(\omega) e^{i\omega t} \quad (4.51)$$

where t is the time and $i = \sqrt{-1}$. Dividing by the time dependence $e^{i\omega t}$, results in the equation of motion in the frequency domain:

$$(-\omega^2 \mathbf{M} + i\omega \mathbf{C} + \mathbf{K}) \hat{\mathbf{x}}(\omega) = \hat{\mathbf{f}}(\omega) \quad (4.52)$$

Expressing this equation with the dynamic stiffness matrix $\mathbf{D}(\omega)$ defined in the frequency domain as;

$$\mathbf{D}(\omega) = (-\omega^2 \mathbf{M} + i\omega \mathbf{C} + \mathbf{K}) \quad (4.53)$$

results in:

$$\mathbf{D}(\omega) \hat{\mathbf{x}}(\omega) = \hat{\mathbf{f}}(\omega) \quad (4.54)$$

4.2. Frequency Response Analysis

Solving this equation for the vector $\hat{\mathbf{x}}(\omega)$ leads to the definition of the frequency response function matrix $\mathbf{H}(\omega)$:

$$\begin{aligned}\hat{\mathbf{x}}(\omega) &= \mathbf{H}(\omega) \hat{\mathbf{f}}(\omega) \\ \mathbf{H}(\omega) &= \mathbf{D}(\omega)^{-1}\end{aligned}\tag{4.55}$$

This equation can be solved by the numerical method described below.

4.2.2 Solution Method for the Frequency Response Analysis

This section is entirely based on The MacNeal-Schwendler Corporation (1996).

The structural response could be computed at discrete excitation frequencies by inserting the forcing frequency ω into;

$$(-\omega^2\mathbf{M} + i\omega\mathbf{C} + \mathbf{K}) \hat{\mathbf{x}}(\omega) = \hat{\mathbf{f}}(\omega)\tag{4.56}$$

and then solving these equations at each input frequency using complex arithmetic. This is called direct frequency response analysis. However, when dealing with large models, there is a much more efficient solution method available called modal frequency response analysis used to solve for a frequency range.

Modal Frequency Response Analysis

Modal frequency response analysis is an alternate approach for solving the frequency response of a structure. This method uses the mode shapes of the structure to reduce the size, uncouple the equations of motion and makes the numerical solution more efficient than in direct frequency response analysis. Note that it is only in the case of no damping or modal damping that the mode shapes can be used to uncouple the equations. The case of modal damping is covered below.

First, the variables are transformed to modal coordinates by assuming the following;

$$\hat{\mathbf{x}}(\omega) = \mathbf{\Phi}\boldsymbol{\xi}(\omega)\tag{4.57}$$

where $\mathbf{\Phi}$ is the mode shape matrix and $\boldsymbol{\xi}(\omega)$ is a vector containing the modal responses. This operation transforms the problem in terms of the behavior of the modes as opposed to the behavior of the grid points. At this point damping is temporarily neglected, resulting in the undamped equation for harmonic motion;

$$-\omega^2\mathbf{M}\hat{\mathbf{x}}(\omega) + \mathbf{K}\hat{\mathbf{x}}(\omega) = \hat{\mathbf{f}}(\omega)\tag{4.58}$$

4. Structural Dynamics

at forcing frequency ω . Inserting equation (4.57) into equation (4.58) yields:

$$-\omega^2 \mathbf{M} \Phi \boldsymbol{\xi}(\omega) + \mathbf{K} \Phi \boldsymbol{\xi}(\omega) = \hat{\mathbf{f}}(\omega) \quad (4.59)$$

This is the equation of motion in terms of the modal coordinates. To uncouple the equations equation (4.59) is pre-multiplied by Φ^T to obtain;

$$-\omega^2 \Phi^T \mathbf{M} \Phi \boldsymbol{\xi}(\omega) + \Phi^T \mathbf{K} \Phi \boldsymbol{\xi}(\omega) = \Phi^T \hat{\mathbf{f}}(\omega) \quad (4.60)$$

where $\Phi^T \mathbf{M} \Phi$ is the modal generalized mass matrix, $\Phi^T \mathbf{K} \Phi$ the modal generalized stiffness matrix and $\Phi^T \hat{\mathbf{f}}(\omega)$ the modal force vector. The generalized mass and stiffness matrices do not have the off-diagonal terms that couple the equation of motion and the equations are uncoupled. Therefore, the equations of motion can be expressed as a set of uncoupled single degree freedom systems;

$$-\omega^2 m_i \xi_i(\omega) + k_i \xi_i(\omega) = \hat{f}_i(\omega) \quad (4.61)$$

where m_i , k_i the and $\hat{f}_i(\omega)$ are the i^{th} modal mass, modal stiffness and modal force respectively. In the case of modal damping each mode is assigned the damping c_i where:

$$c_i = 2m_i \omega_i \zeta_i \quad (4.62)$$

Here ζ_i specifies fraction of critical damping. The equations of motion remain uncoupled and have the form;

$$-\omega^2 m_i \xi_i(\omega) + i\omega c_i \xi_i(\omega) + k_i \xi_i(\omega) = \hat{f}_i(\omega) \quad (4.63)$$

for each mode. The modal responses are then computed as:

$$\xi_i(\omega) = \frac{\hat{f}_i(\omega)}{-m_i \omega^2 + i\omega c_i + k_i} \quad (4.64)$$

Once the individual modal responses are computed the physical responses are recovered as the summation of the modal responses using equation (4.57). Note that this equation represents an equality only if all modes are used, which is rarely the case. To get a fair approximation all the modes whose resonance frequencies lie within the range of forcing frequencies need to be retained. This is the absolute minimum and for better accuracy at least all the modes up to two or three times the highest forcing frequency should be retained. Another way is to model the influence of the out-of-band modes by the use of so called residual vectors, which is described below.

With the displacements computed as above it is easy to recover the velocities and accelerations by pre-multiplying the displacements with $i\omega$ and $(i\omega)^2$ respectively.

4.2. Frequency Response Analysis

Residual Vectors

This section is entirely based on reference MSC.Software Corporation (2003a) where a more detailed description of residual vectors is given.

Modal solutions such as the one described in section 4.2.2 involves reduction of the model size. This modal reduction may capture most of the structures dynamic response. However, the static response may be incomplete due to modal truncation of higher frequency modes that may contribute statically to the total response. Residual vectors are used in an attempt to account for the response of these modes.

To calculate the residual vectors a set of base vectors is used. Although any vector can be used as a residual vector, as long as it is partially independent of the modal vectors, it is desirable to use a vector that does not destroy the diagonal properties of the reduced mass and stiffness matrices when added to the modes for matrix reduction. To ensure this the following steps are preformed:

1. Ensure that loads are linearly independent with the modal inertial forces.
2. Determine base vectors from static response due to loads.
3. Ensure that base vectors are linearly independent.
4. Orthogonalize the base vectors with respect to the modal vectors to produce residual vectors. These vectors will result in diagonal mass and stiffness matrices.

The base vectors can be determined from the structures static response to structural, viscous and inertial forces due to enforced motion. Before calculating the base vectors the inertial forces of the normal mode shapes are removed from these loads. The deformations that serve as base vectors are then determined by applying the modified loads to the structure. Now, the base vectors are made linear independent removing vectors that are linear combinations of other vectors. The remaining base vectors are then made orthogonal with respect to the mass and stiffness matrices. The resulting orthogonal vectors are the residual vectors.

Chapter 5

Pre-Test Analysis

The preparations of an experimental modal analysis consist of two important tasks:

1. The selection of response points.
2. The selection of excitation points.

The experimental modal analysis should be designed based on as much information of the system at hand as possible and to meet certain criteria. The measured modes must correspond to the actual modes of motion and they should be easily distinguishable. The excitation locations should be chosen such that all modes of interest are sufficiently excited. The measured data should contain all the information needed for the analyst depending on the context of the analysis. For practical reasons it is desirable to visualize the measured mode shapes. Since the test design is based on experience from previous tests and on analytical models, which contain inaccuracies, certain robustness in the test design is vital. The test procedure should not be too sensitive to these inaccuracies. Finally, all measurement locations must be accessible.

Since the objective of the test, in this case, is to examine the prediction performance of an analytical model, it is reasonable to use this model as starting point in the response and excitation location selection process.

Discretizing a continuous system introduces errors and to achieve a reasonable accuracy in the analytical model often several thousands degrees of freedom are necessary. However, when performing modal analysis tests the number of response locations are reduced to, at most, a couple of hundred. First, it is not necessary to have a fine mesh of measurement points for an experimental modal analysis. Accurate results can be achieved with a reasonable coarse mesh. Second, many of the degrees of freedom in the analytical

model are located internally in the structure and cannot be accessed with measurement instruments. Third, motion in rotational degrees of freedom is difficult to capture using traditional measurement hardware.

Most correlation and model updating methods require a one-to-one correspondence of analytical and testing degrees of freedom. The location and number of degrees of freedom must be identical for both data sets. The problem at hand is to reduce the number of degrees of freedom in the analytical model to a manageable amount without losing too much information about the dynamics of the system and still meet practical test requirements.

5.1 Finding the Optimal Test Set-Up

The following sections describes methods for finding optimal shaker and response locations. First, the frequency range is considered.

5.1.1 Frequency Range Selection

An important part of test preparations is the decision of a relevant frequency range or which modes are to be considered interesting. This decision is mainly based on the purpose of the analysis as a whole, i.e. in what context the analysis should be used. This decision turns out to have great impact later on in the pre-test analysis and in the measurements. The wider the frequency range, the larger number of modes to be analyzed and the more measurement locations needed to distinguish between the different modes. It turns out to be a trade-off between good accuracy for a small number of modes and bad for a large, given the number of measurement locations. Also, a frequency range too wide may have the effect that not enough energy will be put into the structure. This can cause poor excitation of the relevant modes.

5.1.2 Excitation Point Selection

The selection of excitation points is often less restrictive than the selection of response points. Still, there are methods to help the analyst in order to minimize the risk of missing modes due to poorly chosen excitation locations. The task is to choose the point most likely to excite all the modes of interest. One technique is based upon the study of driving point residues. A complete derivation of driving point residues can be found in Heylen et al. (1997). To introduce the concept of residues, consider the frequency response function

5.1. Finding the Optimal Test Set-Up

in equation (4.55), i.e.:

$$\begin{aligned}\hat{\mathbf{x}}(\omega) &= \mathbf{H}(\omega) \hat{\mathbf{f}}(\omega) \\ \mathbf{H}(\omega) &= \mathbf{D}(\omega)^{-1} = \frac{\text{adj}(\mathbf{D}(\omega))}{\det(\mathbf{D}(\omega))}\end{aligned}\quad (5.1)$$

As mentioned in section 4.1 the determinant of $\mathbf{D}(\omega)$ set to zero is called the system characteristic equation. Since the eigenvalues are the roots of the characteristic equation, the equation for the frequency response function matrix can be rewritten as;

$$\mathbf{H}(\omega) = \frac{\text{adj}(\mathbf{D}(\omega))}{\prod_{i=1}^m E (i\omega - \lambda_i) (i\omega - \lambda_i^*)} \quad (5.2)$$

where E is a constant, λ_i the eigenvalue of modal vector $\boldsymbol{\varphi}_i$, λ_i^* the complex conjugate to the eigenvalue λ_i and m is the number of modes. If the theory of partial fraction is applied, this expression can be rewritten to:

$$\mathbf{H}(\omega) = \sum_{i=1}^m \left(\frac{\mathbf{A}_i}{(i\omega - \lambda_i)} + \frac{\mathbf{A}_i^*}{(i\omega - \lambda_i^*)} \right) \quad (5.3)$$

In this analysis the frequency response function matrix is defined between all possible response degrees of freedom n , hence $\mathbf{H}(\omega) \in \mathbf{C}^{n \times n} \forall \omega$. The terms \mathbf{A}_i and \mathbf{A}_i^* are called the residues. These residues are related to the mode shapes;

$$\mathbf{A}_i = Q_i \boldsymbol{\varphi}_i \boldsymbol{\varphi}_i^T \quad (5.4)$$

where Q_i are modal scaling factors. For a system with no damping, scaled for unity modal mass, the modal scaling factors can be written as:

$$Q_i = \frac{1}{i2\omega_i} \quad (5.5)$$

Note that there are two different i's, one denoting the mode number and one $\sqrt{-1}$. Inserting equation (5.5) into equation (5.4) yields:

$$\mathbf{A}_i = \frac{\boldsymbol{\varphi}_i \boldsymbol{\varphi}_i^T}{i2\omega_i} \quad (5.6)$$

A driving point is defined as any point in the structure where the excitation degree of freedom is the same as the response degree of freedom. Therefore, the residue at the driving point, i.e. the driving point residue (*DPR*) for mode i and degree of freedom j , can be found as the i^{th} a_{jj} , where a_{pq} are elements in \mathbf{A}_i .

Driving point residues are proportional to the magnitudes of the resonance peaks when measuring the frequency response in the driving point and are a measure of how much each mode is excited, or has participated in the overall response, at the driving point (von Langenhove and Brughmans, 1999). A close study of the driving point residues for all candidate excitation points and for all modes of interest gives information concerning the selection of the excitation degree of freedom. Generally, degrees of freedom with large *DPR* values for as many modes as possible will be good excitation points (Heylen et al., 1997). These points can be found by looking at the *weighted average driving point residues* for the modes of interest (Bedrossian et al., 2000). The weighted average driving point residue over the m considered modes for degree of freedom j is defined as:

$$WADPR(j) = \min_{i=1}^m DPR(i, j) \sum_{i=1}^m \frac{DPR(i, j)}{m} \quad (5.7)$$

The degree of freedom with the largest weighted average driving point residue is the optimum location for excitation, i.e. shaker placement.

The use of driving point residues in the selection of excitation points only give suggestions of excitations in one direction. Care must be taken to make sure that the structure is excited in all directions.

5.1.3 Response Point Selection

The selection of response locations when performing experimental modal analysis on a structure is a critical step in the correlation work. If the response points are chosen bad the analyst will not be able get as much information from the test results as needed and the future correlation work will suffer.

The modal vectors for the full system are linear independent. When omitting degrees of freedom from the full system this is no longer completely true for some of the modal vectors. If the eliminated degrees of freedom are poorly chosen the analyst will have difficulties separating them both visually and analytically. They will become linear dependent to some degree. To avoid this the choice of degrees of freedom to keep in the reduced model must be made with great caution so that the modal vectors stay independent after the reduction. The *modal assurance criterion (MAC)* can help the analyst to make this choice. The *MAC* value, in the form shown here, is a measure of independence for each pair of the reduced analytical modal vectors extracted in modal analysis of the finite element model. The *MAC* value between

5.1. Finding the Optimal Test Set-Up

mode i and j is given by;

$$MAC_{ij} = \frac{(\boldsymbol{\varphi}_i^T \boldsymbol{\varphi}_j)^2}{(\boldsymbol{\varphi}_i^T \boldsymbol{\varphi}_i)(\boldsymbol{\varphi}_j^T \boldsymbol{\varphi}_j)} \quad (5.8)$$

where $\boldsymbol{\varphi}_i$ are $\boldsymbol{\varphi}_j$ are the i^{th} and j^{th} modal vectors reduced to the retained degrees of freedom. When comparing the reduced modal vectors to each other and sorting all MAC_{ij} values in a matrix the diagonal will always be equal to unity. If the selected degrees of freedom enable all the modes to be easily distinguished from each other then the dependency between the modes should be small and the off-diagonal values in the matrix should be low. If the selected response locations show high off-diagonal values, this indicates that they are insufficient to adequately describe the different mode shapes. Such a group of locations does not contain enough measurement points to separate modes that differ in reality. In this case the analyst must add additional degrees of freedom to the initial group of response locations in order to lower the off-diagonal MAC values. This can be done in an iterative procedure to determine which degrees of freedom will have the greatest impact in lowering the high off-diagonal MAC values. By adding degree of freedom k to the reduced modal vectors $\boldsymbol{\varphi}_i$ and $\boldsymbol{\varphi}_j$ the analyst easily can evaluate the effect of an additional response degree of freedom according to

$$MAC_{ij} = \frac{(\boldsymbol{\varphi}_i^T \boldsymbol{\varphi}_j + \boldsymbol{\varphi}_i(k) \boldsymbol{\varphi}_j(k))(\boldsymbol{\varphi}_i^T \boldsymbol{\varphi}_j + \boldsymbol{\varphi}_i(k) \boldsymbol{\varphi}_j(k))}{(\boldsymbol{\varphi}_i^T \boldsymbol{\varphi}_i + \boldsymbol{\varphi}_i(k) \boldsymbol{\varphi}_i(k))(\boldsymbol{\varphi}_j^T \boldsymbol{\varphi}_j + \boldsymbol{\varphi}_j(k) \boldsymbol{\varphi}_j(k))} \quad (5.9)$$

One alternative is to track all off-diagonal MAC values during each iteration, and another one is to track the largest off-diagonal MAC values only. The latter is used in this project and described below.

Iterative Procedure

The addition of new locations follows a procedure in three steps starting from the initial MAC matrix already calculated.

Step 1 New MAC matrices are calculated for every candidate location. Each matrix extends the initial matrix with the degrees of freedom corresponding to each candidate location. The position of the maximum off-diagonal MAC value in the initial matrix is determined. The same positions in the new matrices are compared. The candidate matrix that has the lowest value in this position is examined further. The maximum off-diagonal MAC value in that candidate matrix is compared to the maximum value in the initial matrix. If it is lower the procedure continues to step 3 otherwise to step 2.

Step 2 Two positions in every candidate matrix are compared; The position of the maximum off-diagonal value in the initial matrix and the position of the maximum off-diagonal value in the candidate matrix that had the lowest value in the position corresponding to the maximum in the initial, both determined in step 1. The two positions are compared individually for every candidate matrix and the highest of the two is determined for every candidate. The candidate that has the lowest maximum off-diagonal *MAC* value is retained.

Step 3 Extending the retained candidate matrix by the corresponding degrees of freedom forms new *MAC* matrices, one for every candidate location left. The same matrix positions as in step 2 are compared and the candidate that minimizes both values is determined. The maximum off-diagonal *MAC* value of this matrix is compared to the maximum of the initial. If it is lower, the candidate and the corresponding location is selected and the procedure starts over using this candidate's *MAC* matrix as initial. Otherwise step 2 is repeated now examining three positions in the new candidate matrices. The procedure continues until a stopping criteria is met.

When using the methods described here the analyst starts out with an initial set of degrees of freedom. It is wise to closely study the dynamics of the structure and to use this initial set of response points to help visualize the structure and the first global modes.

5.2 Pre-Test Analysis of Door

The main tool used to prepare the measurements is the pre-test software LMS Gateway Pretest. It features the necessary tools for a complete pre-test analysis.

Since rotational degrees of freedom cannot be measured with conventional accelerometers they are omitted in the pre-test analysis.

5.2.1 Frequency Range

When considering the frequency range of interest a problem arises. In this project the frequency range was initially set between 0 and 400 Hz and the door structure is fairly complex. This means that within the frequency range a huge number of modes will be present. When performing the correlation of simulation and test data it is desirable that at least the global modes correlate well. So, in the pre-test analysis the frequency range and the number of modes must be reduced further. In this case the range is reduced to 0

5.2. Pre-Test Analysis of Door

to 100 Hz. This range was determined by performing the response location selection process a number of times on an ad hoc basis to see, given a reasonable amount of measurement locations, how many modes could be captured and result in fair off-diagonal *MAC* values. This procedure seems questionable but it is important to keep in mind the purpose of the modal analysis and correlation process as a whole. Even at this stage it is not expected that the measurements and the correlation will be perfect in the entire frequency range of interest. Since the modal analysis and correlation will be performed for a number of different structural set-ups it seems desirable to have a common basis of evaluation parameters for all set-ups during the pre-test analysis. This is due to the practicality of using as many measurement locations common to the different set-ups.

5.2.2 Response Point Selection

The pre-test module in LMS Gateway uses the iterative procedure described in section 5.1.3 to find the optimal response points.

Since the correlation and model correction process will go through a number of different stages, beginning from a door in white and ending up with a complete door, as detailed as possible, the measurements and thus the pre-test analysis must follow the same stages.

Since it is still the same door structure going through all stages it is practical and reasonable to have as many common measurement locations through all stages as possible. When new components are added, new measurement locations can be expected. When parts that cover previous accessible locations are added, measurement locations have to be removed or replaced. The result of the response location selection process for door in white was used as input into the next stage. Then, new locations were added which in turn were used as input into the following stage, and so on until the complete door was assembled. This iteration procedure results in as many common locations as possible between the different stages.

Due to the mathematical definition of the *MAC* value and the nature of mode shapes, a greater number of response points does not always lead to lower off-diagonal *MAC* values and vice versa. This means that in some cases adding additional response locations on the door will actually make the modes more dependent of each other according to the *MAC* value. This is specially evident in the last pre-test step where adding 14 response nodes increase the maximum off-diagonal *MAC* value from 0.43 to 0.46, see table 5.1. This does not necessarily mean that the mode shapes will actually be harder to separate visually when animating the reduced mode shapes. However, it points out an important fact, the final response locations can not

5. Pre-Test Analysis

be chosen exclusively based on the points given by the iterative procedure, section 5.1.3. It is therefore of great importance to study the dynamics, i.e. animate the mode shapes, to get a fair understanding of the structure at hand before performing a pre-test analysis. The final decision of response locations should be based not only on the *MAC* values but also on that understanding. Some of the final response locations were suggested by the software, others were chosen based on the study of the mode shapes.

Also, the iterative procedure, described in section 5.1.3, has a tendency to choose response locations in clusters. Obviously this area is interesting to lower the off-diagonal *MAC* value but placing accelerometers in clusters is not desirable from a testing point of view. One accelerometer is sufficient to capture the motion of that area. Therefore, only one of the cluster points was kept in the pre-test.

In the pre-test procedure the aim was to reach off-diagonal values below 0.05 to make sure the mode shapes could be separated later on in the correlation work. Due to limitations in the number of accelerometers that could be used in the test this aim was not always possible to reach.

After the response locations selection was complete one of the response points was chosen as an excitation point why it was omitted, see section 5.2.3.

A summary of the results of the response point selection procedure is seen in table 5.1.

Door in White

The response location selection results for this configuration are presented in appendix C.2.1.

Starting out with an initial set consisting of 27 nodes was chosen to help visualize the door in a wire frame, see figure C.2, and to make sure to capture the first global modes, an initial *MAC* matrix was calculated for this set, see figure C.2. As can be seen in table 5.1 the highest off-diagonal *MAC* value is quite high. Using the iterative procedure described in section 5.1.3 additional response nodes were added to lower the off-diagonal *MAC* values below the threshold value. This was archived for this step but some of the points suggested had to be removed because they were too close to each other. Other response nodes suggested had to be removed or moved because of their physical locations on edges. Then, the point that was used as excitation point was removed. This results in the final set of sensor points consisting of 33 locations for this configuration, see figure C.3.

5.2. Pre-Test Analysis of Door

Door in White, Guide Rails

The response location selection results for this configuration are presented in appendix C.2.2.

In this step the guide rails were added in the pre-test analysis. The final nodes from the previous step were used as initial nodes. Also, three more locations were added on the new parts, one on each guide rail and one on the electrical motor, see figure C.4, before calculating the optimal response locations. Again, some of the suggested points had to be removed or moved and the point used as excitation location was omitted resulting in the final set of 39 response locations, see figure C.5.

Door in White, Window

The response location selection results for this configuration are presented in appendix C.2.3.

The final response locations from the previous step were used as initial in this step. The window were added in the analysis so some extra nodes were added to the initial set, see figure C.6, before performing the calculations. Some points suggested where moved or removed together with the excitation point, resulting in the final set of 48 response locations, see figure C.7.

Door in White, Guide Rails, Window, Misc

The response location selection results for this configuration are presented in appendix C.2.4.

The final response locations from the previous step were used as initial in this step. New locations were added on the new parts, in this case on the rear view mirror, the loudspeaker and the lock, see figure C.8, before calculating the optimal sensor locations. Some of the suggested locations were removed or moved. Then, the excitation locations was omitted. Also, some other points where later on excluded in the test because of the impossibility to place sensors on these locations. This resulted in final set of 56 response locations, see figure C.9.

Trimmed Door

The response location selection results for this configuration are presented in appendix C.2.4.

In this step the trim were present in the analysis, meaning that all response locations not accessible when the trim is assembled on the door had to be removed. The other locations were kept from the previous configuration

5. Pre-Test Analysis

as the initial set of nodes in this set-up, see figure C.10. Optimal response locations were calculated. Again some of the suggested points had to be removed or moved. Then, the excitation point was excluded resulting in the final set of 49 response locations, see figure C.11. The frequency range was changed for this last step because it was impossible to get a fair separation of the modes up to 100 Hz. The pre-test was performed for the ten first modes.

Table 5.1 *Response location selection results. Step 5 denotes diw, step 4 diw, grs, step 3 diw, win, step 2 diw, win, misc and step 1 td. Columns: initial set of response points, temporary set after the iterative procedure, first final set after moving and omitting some points from the temporary set and the final set of response locations after omitting the excitation point and other points for some configurations. The sub-columns show number of locations and maximum off-diagonal MAC values for each set.*

Step	Init		Temp		1 st Final		Final	
	Nodes	MAC	Nodes	MAC	Nodes	MAC	Nodes	MAC
5	27	0.30	39	0.05	34	0.09	33	0.08
4	37	0.09	43	0.05	40	0.08	39	0.08
3	46	0.08	56	0.07	49	0.06	48	0.09
2	54	0.06	64	0.07	59	0.07	56	0.08
1	46	0.43	60	0.46	50	0.43	49	0.38

5.2.3 Excitation Point Selection

In LMS Gateway it is possible to use driving point residues, described in section 5.1.2, to find which degree of freedom is the most efficient in exciting the different modes. In this project degrees of freedom with high *WADPR* values, see equation (5.7), was chosen to make sure that as many modes as possible was excited. The selection base consisted of the already chosen response locations. From these sets five degrees of freedom with the highest *WADRP* for each configuration was chosen. Then, the location common for as many configurations as possible was selected. The reason for this was that it is preferred not to excite the door in different locations in every test set-up. This resulted in one point on the outer panel.

For practical reasons it is not always possible to excite the structure in the points calculated so the final decision has to be made by the test engineer based on engineering judgment and experience.

The door was excited in two points. One of the points was calculated using *WADPR* the other one was chosen by the test engineer. The excitation

5.3. Discussion

point selected using *WADPR* was then excluded from the set of response locations, hence the last column in table 5.1. The two excitation points are shown in figure C.1. For more information about the test set-up see section 6.6.

5.3 Discussion

The goal with the response location selection process is to achieve a fair number of locations to measure and still be able to describe and distinguish between all the modes of interest. A large number of modes and a small number of retained degrees of freedom will cause high off-diagonal *MAC* values. There is a trade-off between reasonable off-diagonal *MAC* values and the number of modes to be considered interesting given a fixed number of retained degrees of freedom. If all modes in the frequency range are to be considered in the pre-test analysis then the off-diagonal *MAC* values will surely be high. Even for the first few modes of motion, which is not desirable since these are the most interesting ones and concerns the global behavior of the structure.

When performing a pre-test analysis in the manner described in this chapter there is a number of flaws that the analyst must take into account. Looking at the selection of response points, the goal for the software is to lower the off-diagonal *MAC* values, i.e. the only objective for the iterative loop. It does not have the ability to decide if a location is actually of use in the measurements later on. If most of the suggested points has to be omitted then the response point selection procedure is a waste. By limiting the selectable points, only using nodes that are of use, this can be avoided. Also, the selectable nodes should have some geometrical spread to avoid clusters. This was not done in this project, which led to that many of the suggested points had to be omitted.

Considering the excitation point selection, one of the points where chosen because of its high *WADPR* value. Looking at the definition of *DPR*, a high value seems to indicate a degree of freedom with large amplitudes of motion. Is this really a good point to excite the structure in? Points that have large amplitudes of motion are often located in weak areas. If the area that are used to excite the structure is to weak the energy will not be distributed to its surroundings and the structure will be poorly excited. Never the less, the study of driving point residues serves only one purpose, to find good excitation points, but use it with care.

Also, the model correlation procedure was planned to go through five different stages but due to the lack of measurement time and the decision

5. Pre-Test Analysis

to skip one stage only four stages were completed. However the decision was taken after the pre-test analysis with the implications that the response locations selection is affected by the omitted stage. Also, the result of the omitted stage location selection process was used as input into the following and thereby affected the result in total.

Chapter 6

Experimental Modal Analysis

This chapter gives a short description to the concept of experimental modal analysis. For a more detailed description the reader is referred to Heylen et al. (1997).

The objective with experimental modal analysis is to estimate the modal parameters of a structure defined by the natural frequency, the modal damping and the mode shape for each mode. This is done by exciting the structure, measuring the response motion in the response points and post processing the vibration data. This chapter gives an overview of these steps and how to validate the test results using frequency response function synthesis. The first section describes the boundary conditions of the structure.

6.1 Boundary Conditions

There will always exist a boundary condition for the test object. This boundary condition can be chosen to some extent and are dependent on the aim of the test. If the aim is to compare the test results with the results computed with a finite element model, the boundary conditions should match each other. Often, preferred boundary conditions are free-free conditions, which means that no connections with the environment should exist. In practice these conditions will be approximated by hanging the test object on very soft springs or bungies. To minimize the influence of the suspension the connections points should be at points that are close to nodal points of as many modes as possible.

6.2 Structure Excitation

In modal testing, measurements are usually made under controlled conditions, where the structure is artificially excited by using either an impact hammer, or one or more shakers driven by broadband signals. Impact hammers have two main advantages, the simple set-up and it does not affect the dynamics of the test object by mass loading. The major disadvantages are the concentration of the energy in a very short time, eventually causing overloading and non-linearity problems, and the number of impacts needed for larger objects. The main advantage of shaker excitation is the wide variety of possible excitation signals. The main disadvantages are the test set-up and the mass loading effect, especially on light weight objects.

It is recommended to apply multiple inputs. Multiple inputs will better distribute the input energy over the entire structure. This minimizes the chance of not exciting modes. In general the exciters will be located spatially separated to generate a good energy distribution. The exciters should be oriented in different direction to make sure that modes in all directions are excited.

A shaker is usually attached to the structure using a stinger so that the shaker will only impart force to the structure along the axis of the stinger. The excitation force is measured by a force transducer, which is attached between the structure and the stinger.

When multiple shakers are used care must be taken to insure that the shaker signals are uncorrelated. A variety of excitation signals exists for making shaker measurements with fast Fourier transform analyzers (FFT). The burst random excitation results in leakage free signals. This means that both the response signals and the excitations signals are periodic within the sampling window. This is done by turning the signal off prior to the end of the sampling window time period. The random signal generator must be turned off early enough to allow the structural response to decay to zero or nearly zero before the end of the sampling window.

6.3 Measuring the Response Motion

Once the structure is vibrating due to an exciter, input and output quantities need to be measured. As mentioned in section 6.2, the force induced by a shaker or impact hammer is measured by a force transducer. The system outputs generally are the accelerations at the response locations on the structure, but can also be the displacements or the velocities. Motion transducers will measure these outputs. The fact that displacement and velocity

6.4. Post Processing the Data

transducers are relatively heavy makes the accelerometer more favorable to use, (Heylen et al., 1997). The lesser influence on the structure results in a more accurate measurement.

An additional factor that underlines the benefit of accelerometers is the fact that an acceleration signal can easily be integrated electronically to obtain velocity and displacement. Electronic differentiation used with velocity and displacement transducers is much more difficult, (Heylen et al., 1997).

The accelerometer is a simple mass-spring-damper system, which produces a signal proportional to the acceleration in a frequency band well below its proper resonance. This yields quite stiff and light weight transducers that are very robust.

When the three dimensional motion of each response point is desired, as in most cases, a tri-axial accelerometer is used.

6.4 Post Processing the Data

Experimental modal parameters are obtained from a set of frequency response function (*frf*) measurements. The frequency response function describes the input-output relationship between two single response degrees of freedom on the structure as a function of frequency. If the response motion is measured as acceleration the frf is a measure of how much acceleration response the structure has at an output degree of freedom per unit of excitation force at an input degree of freedom. In this case the frf is called inertance or receptance. Although the frequency response function is defined as the output in the frequency domain divided by the input in the frequency domain, see equation (4.55), it is computed differently in all modern FFT analyzers. This is done to remove random noise and non-linearities from the frf estimates. All methods for calculating the frf is built around the tri-spectrum averaging loop. In this loop three spectral estimates are performed, a *power spectral density* for each channel and the *cross power spectral density* between the two channels for each input-output signal pair. From these three basic spectral estimates the frf is then calculated. This can be done in several different ways. The most common way is the H_1 estimate, where random noise and distortion are assumed to be summed up into the output. In this case the frf is calculated as;

$$H_1 = \frac{G_{xy}}{G_{xx}} \quad (6.1)$$

where G_{xy} denotes the cross power spectral density estimate between the input and the output signals and the G_{xx} the power spectral density of the

input signal. If the noise and the randomly excited non-linearities are modeled as Gaussian noise added to the output it can be shown that the H_1 estimate is a least square error estimate of the frf (Schwarz and Richardson, 1999).

6.4.1 Estimation of the Modal Parameters

Modal parameters are most commonly identified by curve fitting a set of frfs. In general, curve fitting is a process of matching a mathematical expression to a set of empirical data points. This is usually done in two steps where the system poles, damping and modal participation factors are estimated in the first step and the mode shapes in the second. However, this process involves subjective decisions and thus engineering judgement.

The method used in this project is called the *LMS PolyMAX*, which is implemented in the software LMS Test.Lab and was recently developed by LMS International.

In the first step a set of frfs are used as primary data and assumes the so called *right matrix fraction model*, (LMS International, 2003), to represent the test data as;

$$\mathbf{H}(\omega) = \sum_{r=1}^n z^r \boldsymbol{\beta}_r \left(\sum_{r=1}^n z^r \boldsymbol{\alpha}_r \right)^{-1} \quad (6.2)$$

where $\mathbf{H}(\omega) \in \mathbf{C}^{l \times m}$, $\boldsymbol{\alpha}_r \in \mathbf{R}^{m \times m}$, $\boldsymbol{\beta}_r \in \mathbf{R}^{l \times m}$, l is the number of outputs, m the number of inputs and n the modal order. Also;

$$z = e^{-i\omega\Delta t} \quad (6.3)$$

where Δt is the sampling time. The matrix $\mathbf{H}(\omega)$ can be computed for all frequencies ω within the range of interest. Then the unknown parameters $\boldsymbol{\alpha}_r$ and $\boldsymbol{\beta}_r$ can be estimated in a least squares sense after linearization.

The system poles and modal participation factors can now be found in the solution of the eigenvalue problem:

$$\begin{bmatrix} \mathbf{0} & \mathbf{I} & \mathbf{0} & \cdots & \mathbf{0} \\ \mathbf{0} & \mathbf{0} & \mathbf{I} & \cdots & \mathbf{0} \\ \vdots & \vdots & \ddots & \ddots & \vdots \\ \mathbf{0} & \mathbf{0} & \cdots & \mathbf{0} & \mathbf{I} \\ -\boldsymbol{\alpha}_1^T & -\boldsymbol{\alpha}_2^T & \cdots & -\boldsymbol{\alpha}_{n-1}^T & -\boldsymbol{\alpha}_n^T \end{bmatrix} \mathbf{V} = \mathbf{V}\boldsymbol{\Lambda} \quad (6.4)$$

The modal participation factors are contained in the last m rows of the eigenvector matrix $\mathbf{V} \in \mathbf{C}^{mn \times mn}$ and the system (discrete time) poles $e^{-\lambda_i \Delta t}$ on the diagonal of the eigenvalue matrix $\boldsymbol{\Lambda} \in \mathbf{C}^{mn \times mn}$.

6.4. Post Processing the Data

The system poles, eigenfrequencies and modal damping ratios are now related according to;

$$\lambda_i, \lambda_i^* = -\zeta_i \omega_i \pm i \sqrt{1 - \zeta_i^2} \omega_i \quad (6.5)$$

where * denotes complex conjugate.

Now a stabilization diagram can be constructed with increasing modal order n and with certain stability criteria for eigenfrequencies, modal damping and modal participation factors. For each number of poles it indicates where on the frequency axis the poles are found. Physical poles will not change with increasing number of assumed poles. On the contrary, computational modes that try to model the noise in the data will be different for increasing number of assumed modal order. The order are the decision of the test engineer. A rule of thumb is to use twice as many poles plus two as there are physical modes in the frequency band. This requires a first estimate of the number system poles. One obvious way is to count the peaks in the amplitude of the frequency response functions. The summation of the amplitudes of all measured frequency response functions globalizes this information in one curve. The function, called sum-blocks, is calculated as;

$$H_{sum}(\omega) = \sum_{i=1}^m \sum_{j=1}^l \left| \operatorname{Re}(h_{ij}(\omega)) \right| + i \left| \operatorname{Im}(h_{ij}(\omega)) \right| \quad (6.6)$$

where $h_{ij}(\omega)$ are elements of the frequency response function matrix $\mathbf{H}(\omega)$. This operation moves all the frfs to the first quadrant. The highest peaks in this curve indicate the resonances with the largest total modal displacements. Small peaks indicate modes with small displacements or local modes.

When a pole in the stabilization diagram has stabilized frequency, damping and modal participation factors this pole is marked with a s . Again it is up to the test engineer which s to choose for each pole. This selection is not always a clear cut process. Since it is allowed to select physical poles from different model orders, i.e. from different horizontal lines in the diagram it has become common practice to look at each pole for a s with consistent values. The analyst can get some indication of the quality of the pole selection by looking at the damping estimate. Higher than 8% of critical damping often indicates a non-physical pole. To obtain a better estimation of the modal parameters it is recommended to part the frequency range where every part is analyzed separately. From practical and numerical point of view there should hardly ever be more than 10 physical modes in the selected frequency band.

It is in this first step that the test engineer need to put his/her experience to the test and select the correct parameters for a valid modal model. With

a highly damped structure this can be very difficult without prior knowledge of the dynamics of the structure. When performing correlation work a simulation model exists and can guide the test engineer in the decision.

The next step is to estimate the modal vectors. The least squares frequency domain method is used in this project. The mode shapes are then found by considering the so called *pole-residue model*;

$$\mathbf{H}(\omega) = \sum_{i=1}^n \left(\frac{\boldsymbol{\varphi}_i \mathbf{l}_i^T}{i\omega - \lambda_i} + \frac{\boldsymbol{\varphi}_i^* \mathbf{l}_i^H}{i\omega - \lambda_i^*} \right) - \frac{\mathbf{R}_L}{\omega^2} + \mathbf{R}_U \quad (6.7)$$

where $\boldsymbol{\varphi}_i \in \mathbf{C}^{l \times 1}$ is the mode shape vector for mode i and $\mathbf{l}_i \in \mathbf{C}^{m \times 1}$ is the modal participation factor, now expressed as the columns of the last m rows in \mathbf{V} , \mathbf{R}_L the lower residual term matrix and \mathbf{R}_U the upper residual term matrix, both in $\mathbf{R}^{l \times m}$. They approximate the effect of modes below and above the frequency band of interest. The mode shapes and the residual terms are estimated from this model. The prior knowledge of system poles and participation factors turns this non-linear technique into a linear least squares method where the squared error is minimized.

6.5 Modal Model Validation

Modal model validation verifies the results from the modal parameter estimation. Below two quite simple model validation methods are described, frequency response function synthesis and the study of the *MAC* matrix. More detailed information on the subject of model validation can be found in Heylen et al. (1997).

6.5.1 Frequency Response Function Synthesis

One way to evaluate the quality of the estimated modal model is to compare the synthesized frequency response functions with the already measured ones (Heylen et al., 1997). The knowledge of the modal parameters allows the calculation of any frequency response between any two of the measured degrees of freedom according to:

$$\mathbf{H}(\omega) = \sum_{i=1}^n \left(\frac{\boldsymbol{\varphi}_i \mathbf{l}_i^T}{i\omega - \lambda_i} + \frac{\boldsymbol{\varphi}_i^* \mathbf{l}_i^H}{i\omega - \lambda_i^*} \right) \quad (6.8)$$

A visual inspection of the synthesized frfs give a good hint of the quality of the experimental modal analysis.

6.5.2 Modal Assurance Criterion

The modal assurance criterion (*MAC*) value can be used in the model validation process to make sure that it is in fact different modes that are estimated. The *MAC* value was defined in chapter 5 but needs to be redefined here. Looking at the *MAC* value for two measured modes the new definition becomes;

$$MAC_{ij} = \frac{(\varphi_i^{xT} \varphi_j^x)^2}{(\varphi_i^{xT} \varphi_i^x)(\varphi_j^{xT} \varphi_j^x)} \quad (6.9)$$

where the x indicates experimental modes. If two modes has high *MAC* value and lies close in frequency they may be the same mode and one of them needs to be omitted from the test data or the test needs to be redone.

6.6 Test Set-Up

This section describes how the measurements were set up and how the experimental modal analysis was performed on the door. Before the testing could take place the response locations had to be positioned on the door with millimeter precision to match the coordinates of the response locations found in the pre-test analysis. The first section describes this procedure.

6.6.1 Response Location Positioning

The response location selection process, based on the analytical model, employed here does not take into account the physical geometry of the structure more than the possibility to place accelerometers on the selected locations. An automobile door is a quite complex structure with curved surfaces and enclosed space. When dealing with a virtual model it is easy to access all locations with the click of button. When considering the physical structure this task becomes difficult but all response locations must be positioned on the actual door. The pre-test analysis results in a set of coordinates for response locations. Here, the global coordinate system of the car was used. To position the response location coordinates on the actual door a position measurement system with an accuracy of a thousand of a millimeter was used. The actual door was aligned in the cars global coordinate system using existing geometry data and three known locations. Then, the response location coordinates could be positioned on the actual door. It turned out to be impossible to access some location due to limitations in the position measurement system. These locations had to be excluded or moved. The

6. Experimental Modal Analysis

position measurement system together with the door is shown in figure 6.1 below.



Figure 6.1 *Position measurement system used to determine the response locations.*

6.6.2 Boundary Conditions

The door was suspended using four soft bungies simulating the free-free boundary condition as shown in figure 6.2. This makes sure that the six rigid body modes lie well below the first flexible mode in frequency (below 1 Hz).

6.6.3 Structure Excitation

The door was excited using two shakers of the same sort. One of the shakers together with the force transducer is shown in figure 6.3. The excitation locations are shown in figure 6.4.

The burst random signal described in section 6.2 was used as excitation signal. The signal was active 80% of the sampling window time period.

6.6. Test Set-Up

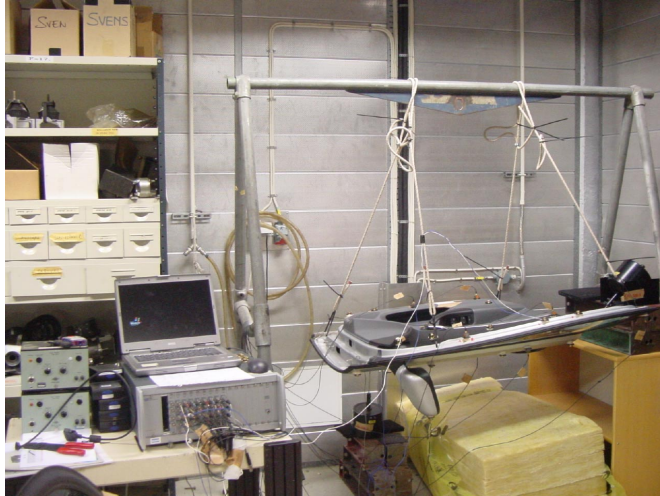


Figure 6.2 *The suspension of the door in four soft bungees simulating the free-free condition.*

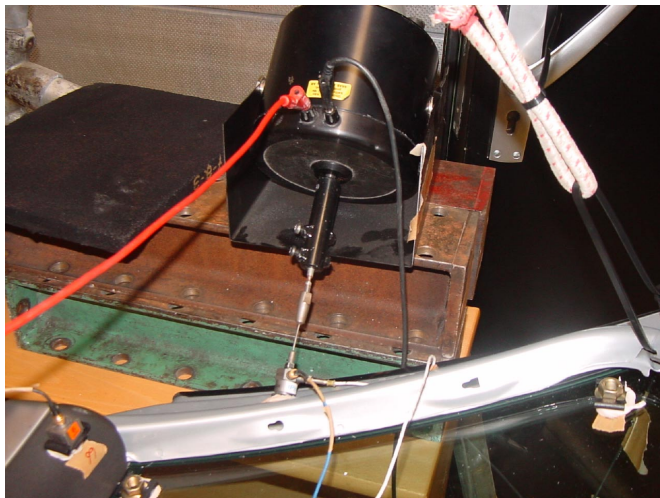


Figure 6.3 *Shaker used to excite the door.*

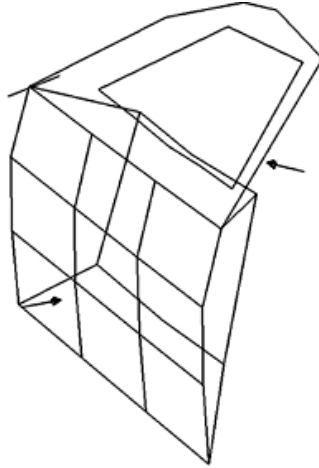


Figure 6.4 *Excitation locations.*

6.6.4 Measuring the Response

The acceleration was measured in the response locations using tri-axial accelerometers shown in figure 6.5. The accelerometers were attached to the door by clips. To avoid measuring Euler angles these were glued on using X-60 which makes it possible to align the three axes of the accelerometer with the global coordinate system. When this was not needed, i.e. on surfaces parallel to the global xy -, xz - or yz -plane, a strong fast drying glue called Loctite was used. Because of the limited number of channels in the frontend only nine tri-axial accelerometers could be used at the same time. This means that for each configuration the measurement was performed in different runs, moving the nine accelerometers around the clips until all response locations were measured. Doing this changes the mass distribution for each measurement run affecting the results in a negative way. To avoid this and to get the same mass loading through each run dummy weights were placed on the unused clips as shown in figure 6.6.

6.6.5 Post Processing the Data

The response data was processed by the FFT analyzer using the H_1 estimate shown in equation 6.1 to calculate the measured frfs.

As mentioned before the LMS Test.Lab software, in which the LMS Poly-Max theory described in section 6.4.1, was used to estimate the modal para-

6.6. Test Set-Up

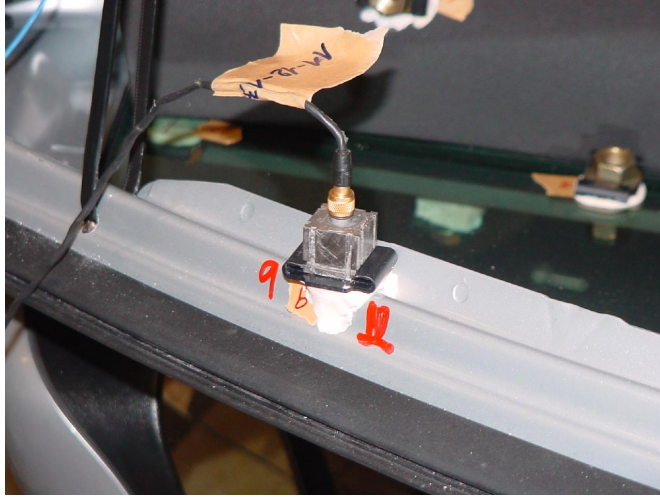


Figure 6.5 *Tri-axial accelerometer used to measure the acceleration of the response locations.*

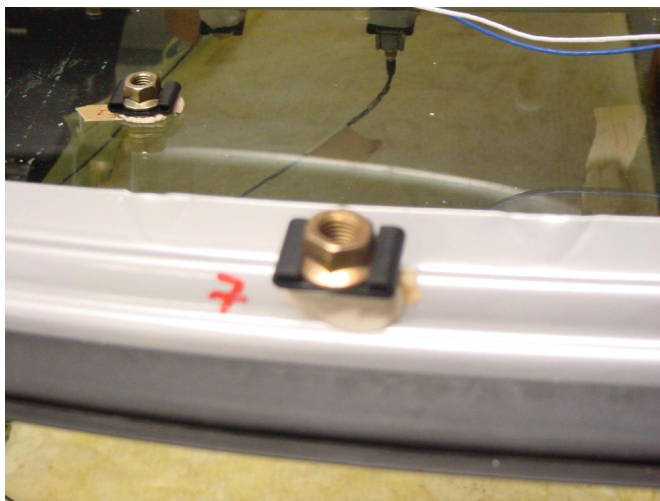


Figure 6.6 *Dummy weight on unused clip. Used to avoid change in mass distribution between different measurement runs.*

meters.

6.7 Measurement Results

The measurement results are all presented in appendix D.

Mode Maps

Tables D.1, D.2, D.3 and D.4 gives a listing of the test results for each configuration. The modal damping mean value increases for each measurement set-up as can be expected. When adding structural parts the system becomes more damped. The largest increase is between the door in white, window, misc configuration and the trimmed door configuration, with an increase from 1.02% to 1.81% of critical damping, see tables D.3 and D.4. Apparently the trim has great impact on the damping properties of the door.

Also, some mode switching occur between different measurement set-ups. The global torsion mode and the global lateral bending mode switch place between the door in white configuration and the door in white, window configuration, see tables D.1 and D.2, and then switches back in the door in white, window, misc configuration, see table D.3.

Looking at table D.4, the first mode is different from the other configurations. A window lateral bending mode appears at 36 Hz. Even if the window is apparent in two other configurations this mode can only be seen in this last measurement set-up. The reason for this is unknown.

Model Validation

A visual comparison of the synthesized frfs and the measured ones, shown in figures D.1, D.2, D.3 and D.4, seem to validate that the estimation of the modal parameters was good. There are no critical differences between the two, although the synthesized frfs shows somewhat more accentuated resonances.

Looking at the *MAC* matrices, presented in figures D.5, D.6, D.7 and D.8, all the estimated modes seem to be unique. Only in the trimmed door configuration, figure D.8, there are high off-diagonal values. They are not that high so none of the modes are omitted as duplicates. However, they will probably be hard to separate later on in the correlation work.

6.8. Discussion

Sum-Blocks with Separated Excitations

Figures D.9, D.10, D.11 and D.12 shows the sum-blocks for all configuration with separated excitations. The location with high $WADPR$ value on the front panel is labeled with *y-direction* and the one on the arch with *xy-plane*. Looking at these figures one important conclusion can be drawn: the excitation on the front panel excited a greater number of modes and gave better response in all measurement set-ups. For instance, for the door in white configuration the excitation on the arch failed to excite the first mode whereas the shaker on the front panel had good response from this mode, see figure D.9.

6.8 Discussion

In section 5.3 it was discussed whether the DPR is a good criteria for finding optimal excitation locations. The question was if the points with high DPR values is to weak to distribute the energy. Looking at the test results presented in 6.7 and appendix D.3, nothing can be said about that with great certainty but it can be seen that the point with high $WADPR$ value was the better excitation location of the two.

The window lateral bending mode which appeared for the last measurement configuration is somewhat of a mystery and the measurements for this set-up has to be questioned. There is always the risk of changing the structural properties of a system when interfering with it between measurements. This is probably what happened when the door was prepared for this set-up. Otherwise this mode would have been present in all the configurations in which the window was assembled. To be sure, the measurements should have been redone. Due to lack of time this was never possible.

Chapter 7

Measurement and Analysis Reconciliation

At this point the dynamic response predictions of the numerical model and the corresponding measured data are available. The question is how well do they correlate? In this chapter the correlation between the analytical and the experimental model is addressed. It is the outcome of the correlation that the model updating is based on.

To be able to evaluate the correlation certain sensible criteria must be established. There exists a number of more or less complicated methods in the literature covering multiple aspects of correlation (Heylen et al., 1997):

1. Direct comparison of resonance frequencies and mass.
2. Mode shape correlation.
3. Frequency response correlation.
4. Mode shape vector orthogonality check.

Also, the problem can be put in a statistical point of view.

When selecting the appropriate methods it is important to keep in mind the amount of data available and how the outcome of the methods are to be presented and analyzed. It is difficult to bring down information of a structures complete behavior into a manageable criterion. When performing modal analysis the data contains information about each degree of freedom and vibration mode and it is easy to see that the amount of data is vast.

On the other hand it is important to use as many methods as possible and not simply rely on one or two. The different methods highlights different aspects of correlation.

7.1 Correlation Methods

The correlation methods employed in this project are divided in three categories: direct comparison, comparison of mode shapes and comparison of frequency response. All outlined in this section.

When using mode shape vector orthogonality in correlation the system matrices of the FE model must be reduced to the degrees of freedom measured. This involves some reduction technique that introduces errors in the system matrices. Also, the interpretation of the orthogonality are not always clear (Heylen et al., 1997). These methods are left out here.

An interesting point of view when performing correlation is to introduce some statistical method. Due to statistical variations in measurements and in the production of hardware a perfect deterministic correlation is impossible. The problem with statistical correlation methods is the number of measurement and/or simulation runs needed. With large models and many response locations this becomes too resource intensive.

Still, attempts to develop statistical methods exists. One example is the study performed by Cafeo et al. (2000). Here a number of experimental modal analyzes was performed to build a sufficient data set and estimate both product-to-product and test-to-test variability. No less than 63 different analyzes were made. Based on the data set a model of the mode shape distribution could be developed assuming normal distribution based on both an estimated mean and a subjective measure.

Next, assuming that a simulation model adequately represents the true mode shapes in a mean sense, samples of 2000 virtual test modes could be extracted using the distributional assumption established. Then, each sample was correlated against the originally simulated mode shape using the modal assurance criterion, which gives a distribution of *MAC* values. Finally the *MAC* value for the originally simulated mode shape against an experimental mode shape was calculated. Now, conclusions about correlation in a statistical sense could be drawn. If the experimental/simulated *MAC* value falls within the distribution of virtually computed *MAC* values the conclusion that the correlations is inadequate cannot be drawn. In turn this means that the model need not be changed.

The main drawbacks with this method is, first, the effort needed to establish a sound statistical distribution, second, the subjective measure used in the establishment of the distribution. This measure was based on the test engineers opinion of the quality of the experimental mode shapes extraction. This measure will certainly differ between engineers and is not a reliable measure.

That said, the method still puts correlation work in a new point of view

7.1. Correlation Methods

but these considerations will not be pursued further in this work.

7.1.1 Direct Comparison

The most simple correlation check is the direct comparison of model and hardware mass. The mass of the FE model and its constituents is easily calculated in FE software and by weighing hardware on a simple scale a comparison can be made. Not only the global mass is important but also mass distribution.

Another simple check is the direct comparison of resonance frequencies.

7.1.2 Comparison of Mode Shapes

Next the vibration mode shapes are considered. Although matching resonance frequencies tells a lot about correlation it is not enough. It is important that the mode shapes correlate as well. With high modal density it is possible for mode shapes to be very similar and appear in different order between measurements and simulation. A thorough study of the mode shapes is needed.

A mode shape comparison is easily done visually by animating the measured and simulated mode shapes in some computer software. Again, the engineering judgement becomes important. When performing model updating and the initial correlation is not satisfactory, it is not always easy to pair experimental and analytical mode shapes visually. The analyst must be clear on which modes to pair to be able to identify problems and to relate the mismatch to model parameters. To aid the analyst a quantitative criterion is helpful.

Modal Assurance Criterion

The Modal Assurance Criterion was already introduced in equation (5.8). Then, the MAC matrix of only the analytical mode shape vectors was calculated but the criterion looks the same when used in correlation and is repeated here;

$$MAC_{ij} = \frac{(\varphi_i^{aT} \varphi_j^x)^2}{(\varphi_i^{aT} \varphi_i^a)(\varphi_j^{xT} \varphi_j^x)} \quad (7.1)$$

where φ is the mode shape vectors reduced to the degrees of freedom measured, a denotes analytical and x experimental. Perfect correspondence of two mode shape vectors gives a MAC value of unity, no correspondence zero. The main advantages of using MAC matrices are that the correlation of two vectors are expressed as a single scalar, the ease of calculation and that the

normalization method of mode shape vectors is irrelevant. The main drawbacks are that mode shape variability is not addressed and that one relatively large element of the mode shape vectors can dominate the correlation, i.e. a large local motion dominates the criterion (Cafeo, 1998).

7.1.3 Comparison of Frequency Response Functions

The frequency response function, defined in section 4.2 and 6.4 respectively, describes the input-output relationship between two single response degrees of freedom. When processing data this is expressed as the frequency response function matrix $\mathbf{H}(\omega)$. Correlation of frequency response is important because it, in contrary to the previous methods, addresses the magnitude of the structures dynamic response.

The frequency response is quite intuitive when the response in a single or a few degrees of freedom are considered, as is the case in many applications. Then, the response in the degrees of freedoms considered can be plotted as function of excitation frequency and conclusions made there of. With increasing number of response degrees of freedoms this becomes a problem. The data is simply too vast. Another way to visualize the frequency response is through the sum-blocks plot defined in equation (6.6) and repeated here:

$$H_{sum}(\omega) = \sum_{i=1}^m \sum_{j=1}^l \left| \text{Re}(h_{ij}(\omega)) \right| + i \left| \text{Im}(h_{ij}(\omega)) \right| \quad (7.2)$$

To complement the visualization a quantitative measure much like the *MAC* value can be used.

Frequency Response Assurance Criterion

Frequency response assurance criterion (FRAC) correlates the dynamic response of a structure on the level of frequency response in the same manner as the *MAC* value does on mode shape level and is defined as:

$$FRAC_{ij} = \frac{\left| \langle h_{ij}^a(\omega), h_{ij}^x(\omega) \rangle \right|^2}{\langle h_{ij}^a(\omega), h_{ij}^a(\omega) \rangle \langle h_{ij}^x(\omega), h_{ij}^x(\omega) \rangle} \quad (7.3)$$

Here h_{ij} are elements of the analytical and experimental frequency response function matrices, i and j denote input and output degree of freedom respectively and $\langle \rangle$ is the scalar product over the frequency ω . The analytical and experimental functions are distinguished by a and x respectively. *FRAC* then compares the response in the j^{th} degree of freedom due to excitation in i .

7.2. Correlation of Original Model

Perfect correspondence gives a *FRAC* value of unity and no correspondence zero.

The major drawback with *FRAC* is that a slight difference in resonance frequencies between model predictions and measurements will give poor correlation according to *FRAC*.

7.2 Correlation of Original Model

The correlation of the original model will give an indication of what to expect during the model updating process. The correlation of resonance frequencies and mode shapes is straight forward but when frequency response is considered the question of how to implement damping in the model must be addressed. The damping model used is crucial for frequency response correlation.

The experimental modal analysis provides data on modal damping and it seems reasonable to use this data when performing modal frequency response analysis for the model. Since several local vibration mode shapes exists in the frequency range considered local damping properties can be expected. Therefore modal damping is preferred to applying a uniform structural damping. However, this requires that analysis modes and experimental modes can be paired, which is not always the case. As the second best solution the mean value of measured modal damping is applied as uniform structural damping.

7.2.1 Door in White

The *MAC* matrix for the door in white configuration, see figure E.1, shows fairly good correlation for mode shapes and resonance frequencies, especially for the first three global modes. Some discrepancies in frequencies can be observed with a maximum relative error of 5.13%. The corresponding test mode to the analytical at 92.1 Hz could not be extracted in the experimental modal analysis.

As can be seen in the sum-blocks plot in figure E.2 the modes in the frequency range of 80 to 100 Hz are not that pronounced and presented difficulties in the experimental modal analysis. Since the *MAC* matrix shows good correlation modal damping could be used in modal frequency response analysis according to table D.1. With this damping model the sum-blocks plot shows fairly good correlation of inertance level, which indicates a good correlation in frequency response as a whole. Frequency discrepancies are obviously visible. Above 80 Hz the model seems under-damped.

7. Measurement and Analysis Reconciliation

The *FRAC* values, see figures E.3 and E.4, indicate poor frequency response correlation. This is mainly due to the frequency discrepancies and the definition of *FRAC*.

7.2.2 Door in White, Window

The door in white, window configuration shows poor correlation over all. The vibration mode shapes are difficult to pair and the modal density in the model seems to high, see figure E.5. The only mode that correlates is the first global mode. This indicates a major flaw in the model and that there is an overall stiffness mismatch.

Without being able to pair experimental and analytical modes, a uniform structural damping of 0.95% of critical damping (mean of experimental modal damping in table D.2) is applied in the modal frequency response analysis. Again, the level of inertance correlate well as a whole but above 75 Hz the model seems under-damped, see figure E.6. The sum-blocks plot also shows the frequency discrepancies and modal density mismatch. *FRAC* indicates poor frequency response correlation, see figures E.7 and E.8.

7.2.3 Door in white, Window, Misc

The situation in the door configuration door in white, window, misc is similar to the previous one. It is impossible to pair mode shapes and there is a severe resonance frequency mismatch. In the range between the first and second experimental mode no less than three analytical modes can be found. This mismatch cannot be traced to only the inherited flaws from the previous configuration. The parts added worsens the case, see figure E.9.

These problems are also clearly visible in the sum-blocks plot, see figure E.10. Here a uniform structural damping of 1.02% of critical damping was applied to the model. The plot also reveals the same damping problems with the model as previously mentioned. *FRAC* strengthens the observation of poor frequency response correlation, see figures E.11 and E.12.

7.2.4 Trimmed Door

The last configuration, trimmed door, shows poor correlation for resonance frequencies, mode shapes and frequency response, see figures E.13 and E.14. All problems with previous configurations are inherited. In this configuration the response locations has been moved considerably due to accessibility of hidden locations by the door trim. The pre-test analysis also showed diffi-

7.2. Correlation of Original Model

culties for modes higher than the tenth mode, which means good correlation at higher frequencies cannot be expected.

An interesting observation in this configuration is the experimental mode at 35.9 Hz, which has not occurred previously. It can be categorized as a rigid body mode of the door trim, but also the window shows motion not seen before.

In the modal frequency response analysis a uniform structural damping of 1.81% of critical damping was used.

Chapter 8

Model Updating

The main objective of this project is to, through a model updating process, achieve the best possible correlation between FE model prediction and hardware measurements. The FE model can be altered in numerous ways. The mesh can be made denser or more detailed, the model parameters, such as Young's modulus or shell element thickness, can be altered.

It should be noted here that the updated model and parameters must still have a physical interpretation and be reasonable. When hardware measurements exist it is possible to achieve good correlation with non-reasonable model parameters. The model can be fitted to the measured data without bearing any physical relevance. Often, when performing correlation or model updating the results are used to establish guidelines for future modeling. Then, the physical interpretation of model parameters becomes more important since models are essentially only geometry and material data.

When dealing with model updating of complex structures the engineering judgement becomes very important. It is impossible to formulate an all-purpose algorithm that solves the updating problem. The engineer must rely on his/her knowledge of the dynamics of the structure and what changes must be done for better correlation.

That said, different tools can be effectively employed and guide the engineer. The criteria mentioned in chapter 7 can act as a quality measure of changes in model parameters and guide the engineer. Also, it is possible to employ iterative procedures in the model updating process. But as will be explained later, these are limited and should only be used to fine-tune the model.

8.1 Model Updating Process

The model updating process employed in this project goes through the steps outlined in figure 8.1.

A general overview to check that the model parameters are up to date with the current specification of the measured hardware. This seems trivial, but cannot be stressed enough. When developing complex structures with thousands of components it is not always easy to keep track of recent developments and changes.

The mass of each component is then considered. The mass of a component often differ due to simplifications done when meshing a structure. Not only the total mass is considered but also the distribution, since this affects the components mass moment of inertia. It is difficult to get a complete correspondence but it is important to be as thorough as possible. The inertia properties can be updated through material density, shell element thickness and by individual point inertia. Also, new components may be added.

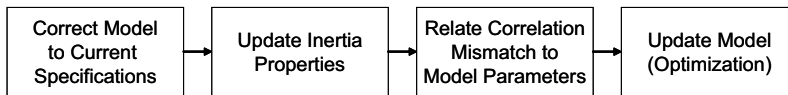


Figure 8.1 *Model updating process.*

With updated inertia properties the task is then to identify correlation problems and relate these to governing model parameters. This is where the engineering judgement comes in handy. Also, some trial and error can lead the way. In this step the major concern is coarse mismatches and changes. Often small changes can imply major increase in correlation. By using the correlation criteria and by visualizing the measured and analytical mode shapes the correlation mismatch can be identified and related to model parameters.

When relating correlation problems to the FE model one must also consider certain physical phenomenon that are hard to model using a linear modal analysis. For instance contact, friction and non-linear material properties. Effects of these phenomenon cannot be fully captured with a linear model but the correlation can improve by introducing linear elements as counterparts. As an example, linear springs can be introduced to simulate some flexibility in a contact point. The difficulties are what properties to assign to the springs.

When the coarse model updating is complete the fine tuning of parameters can be performed with an iterative procedure. The one employed in this

8.2. Iterative Parameter Updating Procedure

work is outlined in section 8.2. These procedures are effective when several parameters must be updated simultaneously. The procedures generally tries to vary all parameters to achieve the best possible solution, which is very cumbersome for the engineer to do one by one.

8.2 Iterative Parameter Updating Procedure

The iterative parameter updating procedure used here is a numerical constrained optimization routine applied to what is called the β -method. The routine is put to practice through the *design optimization tool*, DOT, developed by Vanderplaats Research & Development Inc. implemented in MSC.Nastran. Without getting too detailed the routine will be presented here.

The general optimization problem is stated as;

$$\min_{\mathbf{x}} f(\mathbf{x}) \quad \text{Objective Function} \quad (8.1a)$$

subject to;

$$g_j(\mathbf{x}) \leq 0 \quad j = 1, \dots, n_{IC} \quad \text{Inequality Constraints} \quad (8.1b)$$

$$h_k(\mathbf{x}) = 0 \quad k = 1, \dots, n_{EC} \quad \text{Equality Constraints} \quad (8.1c)$$

$$x_i^L \leq x_i \leq x_i^U \quad i = 1, \dots, n_{SC} \quad \text{Side Constraints} \quad (8.1d)$$

where \mathbf{x} contains the design variables, n_{IC} are number of inequality constraints, n_{EC} are number of equality constraints, n_{SC} are number of side constraints (L and U denotes lower and upper respectively). It is within the space defined by the constraints that the optimizer searches for an optimal solution. The problem is stated as a minimization but the maximization is just the negative of the same.

Due to the use of numerics when running the optimization and the inability to establish when a number is exactly zero, each of the equality constraints in equation (8.1c) are transformed to two inequality constraints in equation (8.1b) and assigned a tolerance.

The optimization method that is used in DOT is called *modified method of feasible directions*. The method works iteratively, starting from an initial vector \mathbf{x}^0 , and alters the design variables in a certain direction to minimize the objective function. The step taken during an iteration is expressed as;

$$\mathbf{x}^{i+1} = \mathbf{x}^i + \alpha^* \mathbf{d}^{i+1} \quad (8.2)$$

where α^* is a scalar factor determining the optimal step length and \mathbf{d} is the search direction.

Box 8.1 *Overall optimization procedure*

Initialization

- Initialize iteration variable, $i = 0$
- Initialize design variables, $\mathbf{x} = \mathbf{x}^0$

Until convergence do

- Evaluate objective function, $f(\mathbf{x}^i)$
 - Evaluate constraints, $g_j(\mathbf{x}^i)$, $j = 1, \dots, N_g$
 - Classify constraints and identify the set of critical constraints (active and violated), J
 - Approximate objective function and critical constraint gradients, $\nabla f(\mathbf{x}^i)$, $\nabla g_j(\mathbf{x}^i)$, $j \in J$
 - Determine a feasible-usable search direction, \mathbf{d}^i
 - Perform one-dimensional search for optimal step length, α^*
 - Update design variables, $\mathbf{x}^{i+1} = \mathbf{x}^i + \alpha^* \mathbf{d}^i$
 - Convergence check
 - Update iteration variable, $i = i + 1$
-

8.2. Iterative Parameter Updating Procedure

The overall optimization procedure follows the steps outlined in box 8.1. Starting from an initial vector of design variables the objective function and the constraint values are evaluated. Then, the constraints are classified to the categories inactive, active or violated. The gradients of the objective function and all active and violated constraints are approximated and a usable-feasible search direction is determined. Usable meaning the objective function decreases in the direction and feasible meaning the direction does not violate any constraints, at least not for a small step. Now, the optimal step length can be found by a one-dimensional search and the design variables updated according to equation (8.2). Finally a convergence check is made and the procedure either ends or starts over with updated variables.

The function evaluations of the objective and constraints are, of course, case specific and are often cumbersome. When applying the procedure to a finite element model the evaluations include the complete solution of the FE problem.

The DOT routine supports user supplied objective function and constraint gradients or it can perform the approximation using finite differences. If the objective function or constraints are considered to be black boxes the finite difference approximation requires two function evaluations, which in FE problems are very cumbersome. In MSC.Nastran the gradients are calculated outside the DOT routine and supplied to it. With the use of the chain rule of differentiation the gradients are broken down into more manageable format and can be determined without the second function evaluation. This is due to the knowledge of which structural responses are involved in the objective function and constraints and how design variables are related to model parameters. Still, finite difference techniques are used, but on simpler functions. The computation of gradients are fully explained in Moore (1994).

The important issues of constraint classification, finding a usable-feasible search direction, the one-dimensional search, and the convergence test will be outlined below.

8.2.1 Constraint Classification

The constraint values are classified into the categories inactive, active and violated. To distinguish them the parameters CT and $CTMIN$ are introduced. CT is a small negative number and $CTMIN$ is a small positive number and the two defines a region around zero that determines how the constraints are to be considered when the search direction is established. The

classification is done according to the following:

$$g_j(\mathbf{x}) \leq CT \quad \text{Inactive} \quad (8.3)$$

$$CT \leq g_j(\mathbf{x}) \leq CTMIN \quad \text{Active} \quad (8.4)$$

$$g_j(\mathbf{x}) \geq CTMIN \quad \text{Violated} \quad (8.5)$$

8.2.2 Finding a Usable-Feasible Search Direction

The problem of finding a usable-feasible search direction is now divided in three cases: no active or violated constraints, one or more active but not violated constraints and one or more violated constraints. The cases are outlined below.

Case 1: No Active or Violated Constraints

In this case the problem can be considered unconstrained and all directions are feasible. In many applications this is the case at the initial iteration step.

If it is the initial iteration step or if in the last step constraints were active or violated, the direction chosen is the negative of the gradient of the objective function, also called the *steepest descent direction*.

$$\mathbf{d}^i = -\nabla f(\mathbf{x}^i) \quad (8.6)$$

If during the last iteration step the steepest descent direction was chosen, the direction in the next iteration is chosen as a *conjugate direction*. Two directions \mathbf{d} being conjugate, or more precise *H-conjugate*, if they are linearly independent and $\mathbf{d}_i^T \mathbf{H} \mathbf{d}_j = 0$ when $i \neq j$. The matrix \mathbf{H} is the *hessian* or second partial derivatives of the objective function (Böiers, 2001; Vanderplaats Research & Development Inc., 1995).

In general, conjugate direction methods solves optimization problems of quadratic functions exact in no more than n iterations, where n is the number of design variables. The methods, however, requires knowledge of second order derivatives and are limited to optimization of quadratic functions. With a Taylor expansion any twice differentiable function can be approximated with a quadratic function in the vicinity of local minimum point and the conjugate direction methods can be expected to perform well for such functions close to the stationary point.

The second derivatives are used to determine the optimal step length which can be replaced by an approximate one-dimensional search. Then, the feasible search direction is:

$$\mathbf{d}^i = -\nabla f(\mathbf{x}^i) + \beta^i \mathbf{d}^{i-1} \quad (8.7)$$

8.2. Iterative Parameter Updating Procedure

This direction is just the steepest descent direction with the addition of some factor of the previous direction. This notion is quite intuitive. Two steepest descent directions following each other are perpendicular (Vanderplaats Research & Development Inc., 1995). This leads to a zig-zag pattern of the path to the minimum point. By biasing the direction with the previous, one can cut corners to the optimum. The biasing factor β^i is determined by;

$$\beta^i = \frac{\|\nabla f(\mathbf{x}^i)\|_2^2}{\|\nabla f(\mathbf{x}^{i-1})\|_2^2} \quad (8.8)$$

and the method is known as the *Fletcher-Reeves method*, Böiers (2001).

Case 2: Active but No Violated Constraints

At this point the optimization procedure has encountered a constraint. The next search direction must lead away from or be parallel to the constraint boundary still minimizing the objective function. The direction must be feasible-usable. The usability requirement is stated as:

$$\nabla f(\mathbf{x}^i)\mathbf{d}^i \leq 0 \quad (8.9)$$

This is just the scalar product of the gradient of the objective function and the search direction and can be reformulated as:

$$|\nabla f(\mathbf{x}^i)||\mathbf{d}^i| \cos \theta \leq 0 \quad (8.10)$$

The preferred direction is the steepest descent direction, $\mathbf{d}^i = -\nabla f(\mathbf{x}^i)$, which decreases the objective function the most. This direction implies $\theta = \pi$ and certainly produces a negative scalar product since the magnitudes are positive. A usable direction is then enclosed by $\pi/2 \leq \theta \leq 3\pi/2$. The equalities meaning the direction is parallel to the constraint boundary and does not reduce the objective function.

The feasibility requirement is stated likewise as;

$$\nabla g_j(\mathbf{x}^i)\mathbf{d}^i \leq 0 \quad j \in J \quad (8.11)$$

where J is the set of violated and active constraints indices. Now, the problem of finding a feasible-usable direction can be formulated as the optimization problem:

$$\min_{\mathbf{d}^i} \quad \nabla f(\mathbf{x}^i)\mathbf{d}^i \quad (8.12a)$$

subject to;

$$\nabla g_j(\mathbf{x}^i)\mathbf{d}^i \leq 0 \quad j \in J \quad (8.12b)$$

$$\mathbf{d}^{iT} \mathbf{d}^i \leq 1 \quad (8.12c)$$

The constraint in equation (8.12c) is used to bound the solution of \mathbf{d}^i . Any direction satisfying the usability and feasibility requirements will decrease $\nabla f(\mathbf{x}^i)\mathbf{d}^i$ by an increase in magnitude of \mathbf{d}^i .

The sub-optimization problem is linear in \mathbf{d}^i except for the bounding constraints (8.12c) and is solved with a method much like a *linear programming* algorithm. The details are left out here but can be found in Vanderplaats (1984).

Case 3: One or More Violated Constraints

In this case the last iteration brought the design variables outside the feasible region and the task is now to find a direction back. This is done by introducing a penalty variable, P , in the sub-optimization problem 8.12 as:

$$\min_{\mathbf{d}^i} \quad \nabla f(\mathbf{x}^i)\mathbf{d}^i - w_0P \quad (8.13a)$$

subject to;

$$\nabla g_j(\mathbf{x}^i)\mathbf{d}^i + w_jP \leq 0 \quad j \in J \quad (8.13b)$$

$$\mathbf{d}^{iT}\mathbf{d}^i + P^2 \leq 1 \quad (8.13c)$$

An increase in P will decrease the objective function in equation (8.13a). At the same time, since \mathbf{d}^i is bounded by equation (8.13c), an increase in P will push \mathbf{d}^i closer to $-\nabla g_j(\mathbf{x}^i)$ which is the direction with the shortest distance to the feasible region.

The choice of weights, w_j , is set to:

$$w_j = k \left(1 - \frac{g_j(\mathbf{x}^i)}{CT} \right)^2 \quad j \in J \quad (8.14)$$

This is a quadratic function of the constraint value $g_j(\mathbf{x}^i)$ that increases the more critical a constraint gets. Remember that the constraints are on the form (8.1b), CT is a small negative number and non-critical constraints are left out from the set J . To overcome an ill-conditioned optimization problem the weights are limited to $w_j \leq 50.0$.

The weight w_0 is initially set to 5.0. In DOT the gradient vectors $\nabla f(\mathbf{x}^i)$ and $\nabla g_j(\mathbf{x}^i)$ is normalized so that the scalar product in equation (8.13a) is close to unity and the penalty and weight dominates the optimization. If the step taken in this iteration does not reach back into the feasible region the weight, w_0 is increased with a factor of 10, although limited to 1000 to avoid ill-conditioning.

This concludes the procedure employed to find a usable-feasible search direction.

8.2. Iterative Parameter Updating Procedure

8.2.3 The One-Dimensional Search

With the usable-feasible search direction established the problem left is to find out how far along this direction to go. The original optimization problem is now broken down into a one-dimensional *line search*. A number of line search methods are available to solve the problem, for instance the *golden section method* or the *Armijo rule* (Böiers, 2001). The problem with these methods are the number of costly function evaluations needed to get a reasonable result. Also, the constraints in the original problem must be considered as well. The method implemented in DOT and MSC.Nastran uses approximations of the objective function and constraints to minimize an interpolated polynomial.

The updated objective function can be written;

$$f(\mathbf{x}^{i+1}) = f(\mathbf{x}^i + \alpha \mathbf{d}^i) \quad (8.15)$$

and a first order approximation with respect to α is;

$$f(\mathbf{x}^{i+1}) \approx f(\mathbf{x}^i) + \sum_{k=1}^n \frac{\partial f(\mathbf{x}^i)}{\partial x_k} \frac{dx_k}{d\alpha} \alpha \quad (8.16)$$

where n is the length of vector \mathbf{x}^i . The first factor in the summation is just the k^{th} entry in $\nabla f(\mathbf{x}^i)$ and by differentiation with respect of α of equation (8.2) the second is the k^{th} element in \mathbf{d}^i . The approximation of the objective is then:

$$f(\mathbf{x}^{i+1}) \approx f(\mathbf{x}^i) + \nabla f(\mathbf{x}^i)^T \mathbf{d}^i \alpha \quad (8.17)$$

The approximations of the constraints follows the same derivation.

Depending on how the constraints are classified during each iteration the determination of the optimal value of α must be made case wise and follows an intricate decision process. The details are left out here but can be found in Moore (1994) and Vanderplaats Research & Development Inc. (1995). With the approximations of the objective and constraints a number of candidate values of α can be calculated. Depending on if constraints are inactive, active or violated the calculated values can act as bounds on and as estimates of the optimal solution α^* . Each α -value corresponds to an approximation of the objective and constraints. These are interpolated using linear, quadratic or cubic polynomials depending on the situation. Now, the optimal solution of α can be obtained by minimizing a simple function or, when it comes to constraints, solve for the optimal root.

8.2.4 Convergence Check

After each iteration a convergence check is made and DOT uses a number of stopping criteria.

1. Maximum number of iterations.
2. No feasible solution can be found.
3. Diminishing objective gradient.
4. Diminishing change in design variables.

The iterative process is stopped when a maximum number of iterations is reached. If no feasible solution is found within 20 iterations the process is terminated. In this case the process can end earlier due to the parameter CT is decreased when a feasible solution cannot be found in the previous iteration. The most important stopping criteria considers diminishing objective gradient. The optimization procedure is expected to reach the optimum asymptotically. Therefore the relative change in objective is checked after each iteration and the process stopped if this is less than a predefined tolerance. Also, the absolute change is considered. Finally, the process can be terminated if the maximum of the relative change of individual design variables is less than a tolerance.

8.2.5 The β -method

The problem is to minimize a scalar function subjected to certain constraints. In doing this the correlation of the FE model prediction to the test data should increase. Therefore the objective function must break down all necessary information of the correlation to just a single scalar. There are a number of ways this can be done. Neither will be able to perform perfectly. They all have their advantages and disadvantages. Here, the β -method is employed. Another possible example is the least squared difference between elements of corresponding experimental and analytical mode shape vectors.

8.2. Iterative Parameter Updating Procedure

The optimization problem for the β -method is stated as

$$\begin{aligned}
 & \min_{\beta} \quad \beta \\
 & \text{subject to;} \\
 & k_m \beta - \left| \frac{m^x - m^a}{m^x} \right| \leq 0 \\
 & k_f \beta - \left| \frac{f_i^x - f_i^a}{f_i^x} \right| \leq 0 \\
 & k_{MAC} \beta - (1 - MAC_{ii}(\mathbf{x})) \leq 0
 \end{aligned} \tag{8.18}$$

where k_j is a scale factor, m is mass, f is modal frequency, a denotes analytical, x denotes experimental, MAC is the modal assurance criterion, defined in section 7.1.2, \mathbf{x} contain the design variables and i is the mode number.

As can be seen the β -method works solely with constraints. The objective function is independent of the design variables. Formulated like this the procedure maximizes the diagonal elements of the MAC matrix, working only on the lowest one while minimizing the relative error of mass and modal frequencies. The scale factors are used to scale the problem appropriately.

8.2.6 Comments on Optimization

The implementation of an all-purpose optimization algorithm is difficult since every problem has its own case specific details. Therefore, several parameters to fine tune the procedure have been established in this case. How to set these parameters depends highly on experience of related problems and trial and error runs.

Also, the optimization procedures will only find local minima. Nothing can be stated concerning the global minimum point.

When used in the context of this project the optimization procedures must be simplified. The mathematical treatment of optimization problems found in the literature differs from the applications here. When developed the procedures usually involves far more function evaluation. This is not possible when working with finite element models due to computational effort needed. The approximation implemented will affect the convergence properties and the accuracy of the results. Still, if used correctly, optimization procedures can be effective.

The β -method used here is only one possible way to roll down the dynamics of a structure to a single scalar. Other attempts is of course possible. The choice here is mainly based on intuition and trial and error. Other methods were tried without success.

8.3 Updating the Door Model

Based on the correlation results the updating of the door model follows the four different door configurations beginning from the door in white. In this way only parameters added in every configuration need to be updated and it is possible to distinguish what parameters are important for the different parts of the structure. As mentioned above the first action performed is the updating of inertia properties.

Table 8.1 *Physical door and model mass comparison.*

Part	Mass (g)			
	Physical	Model	Diff	Diff (%)
DiW	18500	18650	-150	-0.8%
Window	3249	2868	381	11.7%
Guide Rails	2113	1940	173	8.2%
Inner Window Waist Seal	87	100	-13	-14.9%
Outer Window Waist Seal	195	219	-24	-12.3%
Window Arch Seal	635	439	196	30.9%
Total DiW, Win	24779	24216	563	3.3%
Rear View Mirror	1611	1390	221	13.7%
Lock	758	803	-45	-5.9%
Handle	1108	1190	-82	-7.4%
Loudspeaker	1013	1026	-13	-1.3%
Total DiW, Win, Misc	29269	28625	644	2.2%
Trim	3128	3254	-126	-4.0%
Front Door Seal	128	57	71	55.5%
Total Trimmed Door	32525	31936	589	1.8%

8.3.1 Updating Inertia Properties

After taking the door apart to as small parts as possible without damaging the parts too much, every article was weighed. The results, seen in table 8.1, shows some serious mismatches. The door in white model weighs 150 g or 0.8% less than the physical door. This is not that serious but difficult to correct. It is preferred not to change the density of steel. However, this mismatch was solved when the model was put in an optimization loop, varying the shell element thicknesses with mass included in the β -method. Good results were achieved. More serious mismatch was that the window was 381 g or 11.7% too light. This will have major impact on prediction

8.3. Updating the Door Model

performance of the model. As it turned out, the mismatch was due to the specification of glass density and could easily be corrected. Another major mismatch was the rear view mirror model mass which was 221 g or 13.7% too light. At first this was solved by smearing non-structural mass over the shell elements but as will be explained later an alternative updating had to be used. All other mismatches was solved either with non-structural mass or by decreasing material density. The latter was done for the trim since the model was extensively simplified and the density of the FE model not as well understood as for steel.

8.3.2 Door in White

The door in white model is in general composed of a number of sheets of steel fastened with spotwelds. From the start the correlation was quite good but could probably be made better. It is important that the door in white configuration correlates very well since all other configurations will inherit the correlation mismatch.

The model parameters or techniques that were considered during the updating was the following:

- Shell element thicknesses
- Young's modulus
- Poisson's ratio
- Antiflutter
- Hemflange adhesive
- Spotwelds

Consideration of these will be addressed below then the model is updated using optimization.

Shell Element Thicknesses

In the door in white configuration the panel thicknesses are important parameters to investigate. The thicknesses of the panels affects the stiffness of the structure and can alter resonance frequencies as well as mode shapes. Additionally, it also affects the mass of the structure.

When modeling the panels a uniform nominal thickness is applied to each article through an entry on the `PSHELL` card. This nominal thickness

8. Model Updating

is set to the specifications given to the supplier of sheet metal. When the sheets are stamped into door panels the stamping process alters the thickness distribution and one ends up with a model that has the wrong shell element thicknesses.

To investigate the effects of the stamping process simulations were performed and the results for the major panels are shown in figure 8.2 to 8.6. The details of these simulations are left out from this report. What can be said is that the same simulations are used when developing and manufacturing stamping tools.

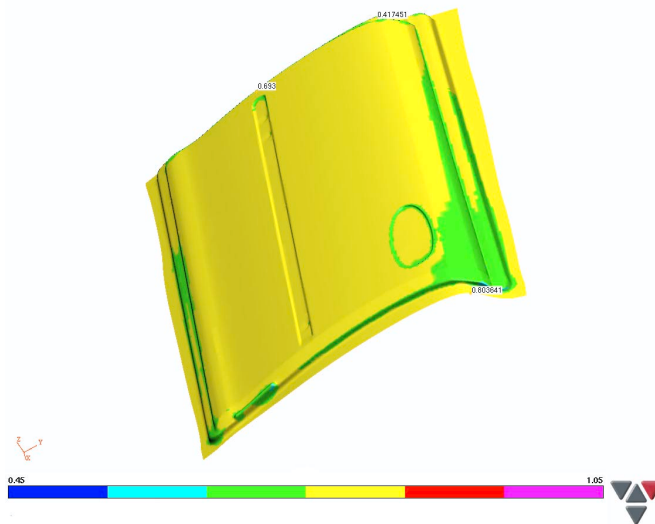


Figure 8.2 *Outer panel thickness distribution after stamping.*

The simulations show that the effects of the stamping process varies in magnitude depending on the shape of the panels, as can be expected. The worst case is with the front end of the inner panel where as much as a 15 % thickness loss exists locally.

To implement the thickness investigation in the modeling of the door the simulated thickness distributions were applied to the models of the corresponding panels through sectioning of the panels according to the color scheme depicted in the figures. This would give an approximation of the distribution. Of course this is a time and effort consuming job and the result will never reach the simulated distributions.

The correlation results after an eigenmodes simulation can be seen in

8.3. Updating the Door Model

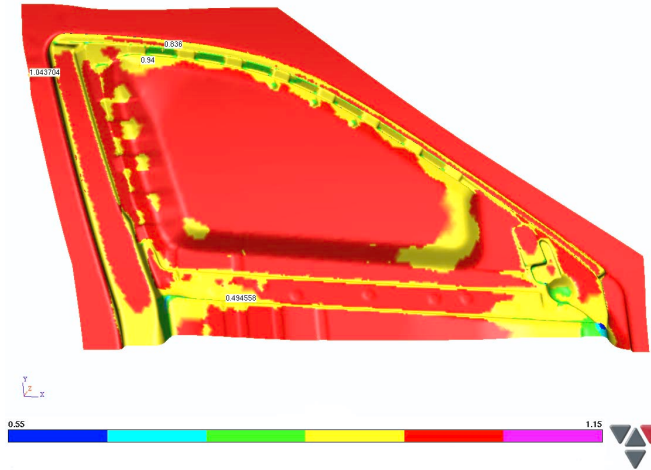


Figure 8.3 Door arch thickness distribution after stamping.

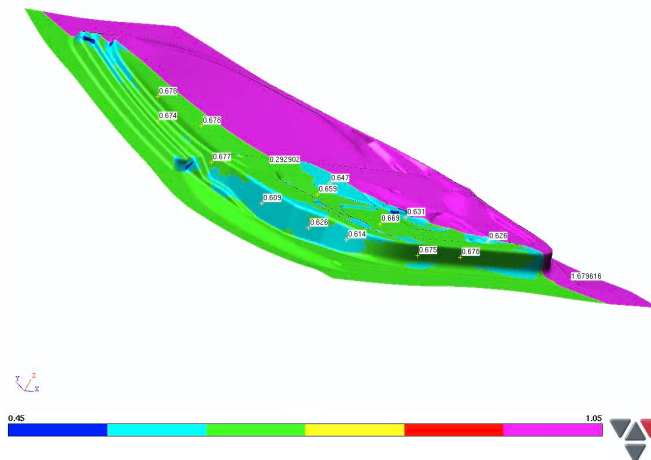


Figure 8.4 Rear of inner panel thickness distribution after stamping.

8. Model Updating

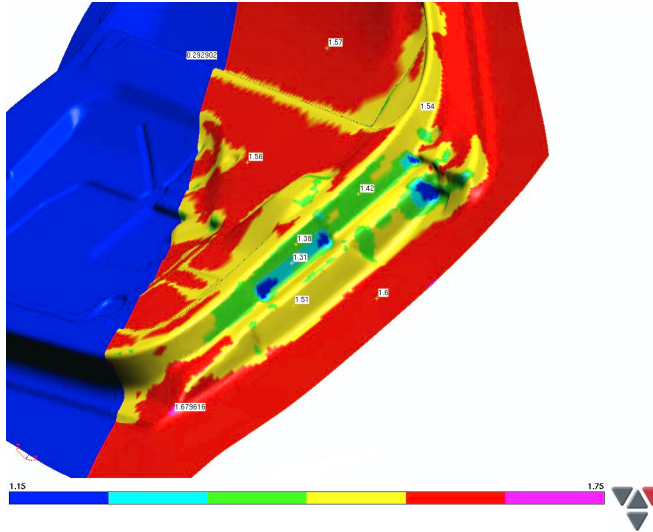


Figure 8.5 Front of inner panel thickness distribution after stamping.

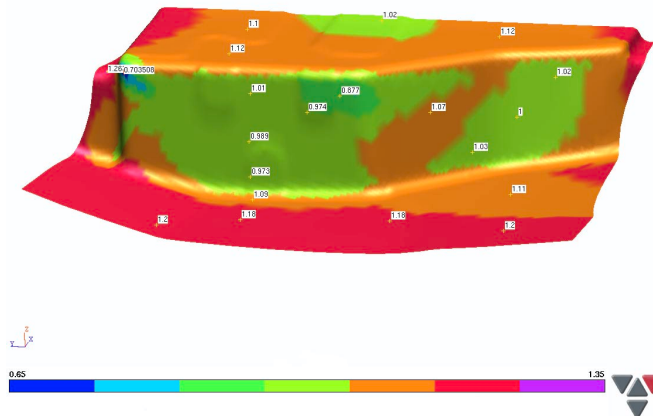


Figure 8.6 Lock reinforcement thickness distribution after stamping.

8.3. Updating the Door Model

figure 8.7. It shows somewhat better mode shape correlation for lower frequencies but the modification destroys the correlation above 85 Hz. Also the resonance frequency mismatch increases. This is all due to a minor change of panel thickness.

This approach to deal with panel thicknesses does not seem to be good but the results show the impact of variations of shell element thickness on correlation, especially for higher frequencies. The panel thicknesses will therefore be considered when the door in white model is put through the optimization procedure.

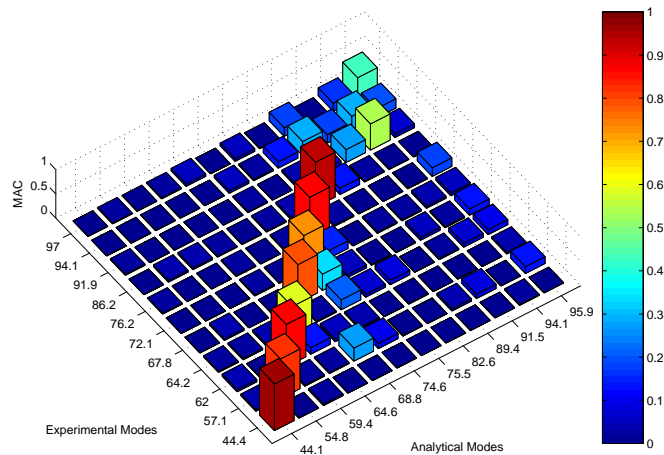


Figure 8.7 *MAC matrix for door in white with modified panel thickness sectioned according to stamping data.*

Young's Modulus and Poisson's Ratio

Young's modulus and Poisson's ratio are natural parameters to consider. These will in general not affect the mode shapes but have great impact on resonance frequencies. Since the door in white consists mostly of sheets of steel, these parameter must be varied with care. Data on these parameters for steel has been extensively researched and should be correct, although some statistical deviation still exists. Only Young's modulus for the major panels are entered in the optimization procedure.

Antiflutter and Hemflange Adhesives

When it comes to Young's modulus and Poisson's ratio for materials as the antiflutter or hemflange adhesives the question is another. These are rubber like materials and the isotropic linear material model does not hold. These materials generally have non-linear stress-strain relationship as well as some velocity or frequency dependance. Further on, the adhesives are pre-stressed when the door is assembled and when the rubbers goes through the paint shop they are exposed to temperature differences. The uncertainty on what material properties to assign these elements is great.

The hemflange adhesive is applied to the rear edge of the door, between the outer waist reinforcement and the outer panel. These are all quite stiff parts of the structure. Even in the rear of the door the panels are spotwelded. The effects of varying the material parameters for the hemflange adhesive is expected to be limited. They are still entered in the optimization procedure.

The antiflutter is a another matter. Its purpose is mainly to keep the distance between the outer panel and the side impact rail and the outer waist reinforcement. The outer panel is a very weak part of the structure which can be seen in the first eigenmode at approximately 44 Hz. The coupling of this weak panel to much stiffer parts can be expected to have greater impact on correlation.

In the original model the antiflutter was modeled as a soft linear isotropic material with a Poisson's ratio close to the one of steel. Investigations of the material properties has been done in cooperation with the material supplier and another approach exists. When working in the time domain it is possible to use hyper-elastic materials and such a model definition was available. The new definition could easily be approximated with a linear model and the results show a somewhat higher Young's modulus and a Poisson's ratio close to 0.5. Rubber materials in general ought to have Poisson's ratios close to 0.5 which indicates incompressible materials.

When implemented in the eigenmodes analysis the new material definition destroys correlation as a whole. The hyper-elastic material probably works fine when working in the time domain. Then, effects as pre-stresses can be taken into account.

When running the model in the optimization procedure the results indicates a Poisson's ratio close to zero. This means a completely compressible material much like chewing gum. A Poisson's ratio of zero decouples the stress-strain relationship to a uniaxial one. Therefore the approach of exchanging the antiflutter models (same as spotwelds) to linear springs. Different spring stiffnesses were tried on an ad hoc basis in eigenmodes simulations so that the experimental and analytical mode shapes could be paired. The

8.3. Updating the Door Model

results are a remarkable improvement as will be shown later. Thereafter, the parameters could be entered into the optimization procedure. The result of which is shown below.

Spotwelds

As mentioned earlier, the spotwelds are modeled as mesh independent solids and assigned material properties of steel, a reasonable assumption. However, studies performed at Saab Automobile indicate that the welds should be much stiffer. Therefore, also the spotweld Young's modulus was entered in the optimization procedure.

Another problem with spotwelds are that the placement is highly dependent on what is possible to achieve in the production facilities. To be sure that the placements on the physical door was in order with the specifications entered into the model a visual inspection was performed. This inspection showed no mismatches and the spotweld positions could be kept as they were.

Optimization

The door in white model was updated with the β -method optimization routine described above. The parameters used in the optimization and the results can be seen in table 8.2. The β -method was applied to the mass and the MAC values but the resonance frequencies were left out. The frequencies correlated well and to get the optimization routine to optimize the MAC values, the frequencies had to be left out.

The initial value of the springs, representing the antifleutter, was chosen on an ad hoc basis after some trial and error with eigenmodes simulations. This initial value was slightly increased. Almost all Young's modulus entered in the optimization was increased. The results show that the hemflange adhesive can be somewhat stiffer and that the spotwelds must be stiffer but not as much as previous studies show. When it comes to the shell element thicknesses the only affected article is the front end of the inner panel, where thickness is decreased.

Correlation After Model Updating

Model updating through optimization leads to better mode shape correlation as can be seen in figure 8.8, especially for modes at higher frequencies. There is still some frequency mismatch and the worst case is between 65 and 75 Hz. A MAC matrix with diagonal values over 0.8 must be considered good correlation.

Table 8.2 Optimization results for door in white configuration.

	K-tr (N/m)		K-rot (N/rad)			
Article	Init	Rslt	Init	Rslt		
Antiflutter	4000	4300	4000	4300		
	E (MPa)		ν		t (mm)	
Article	Init	Rslt	Init	Rslt	Init	Rslt
Door Arch	200000	207000			1.00	1.00
Hemflange	2500	2700	0.30	0.29		
Inner Panel, Fr	200000	207000			1.60	1.52
Inner Panel, Rr	200000	206000			0.70	0.70
Lock Reinf.	200000	207000			1.20	1.20
Outer Panel	200000	200000			0.80	0.80
Spotwelds	206000	220000				
Waist Reinf. In	200000	210000			2.00	2.00
Waist Reinf. Out	200000	200000			0.80	0.80

The frequency response correlation is also improved, see figure 8.9 and 8.11. In the modal frequency response analysis the measured modal damping was implemented in the model. The sum-blocks plot shows a perfect correlation of the first mode and the modes between 70 and 80 Hz are better separated.

The frequency response correlation for the modified model are worse than the original model for frequencies above 80 Hz. The updated model shows less damping at these frequencies. This is due to that the material model of the antiflutter was assigned a material specific damping in the original model. Then the damping assumption of this model is somewhat distorted and the model is over-damped.

The *FRAC* values also show an increase in correlation.

8.3. Updating the Door Model

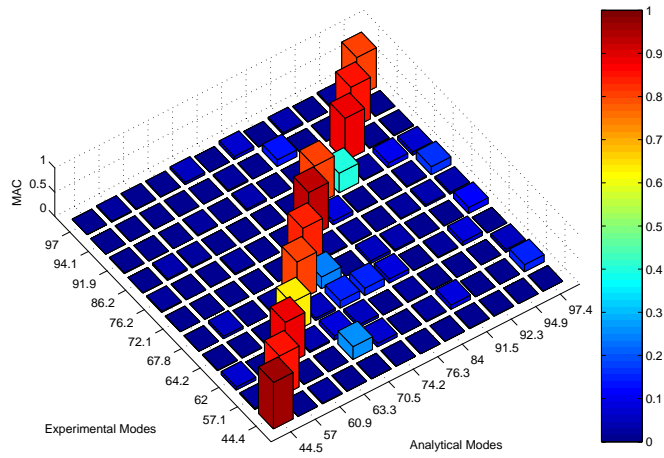


Figure 8.8 *MAC matrix for door in white configuration after updating model parameters.*

8. Model Updating

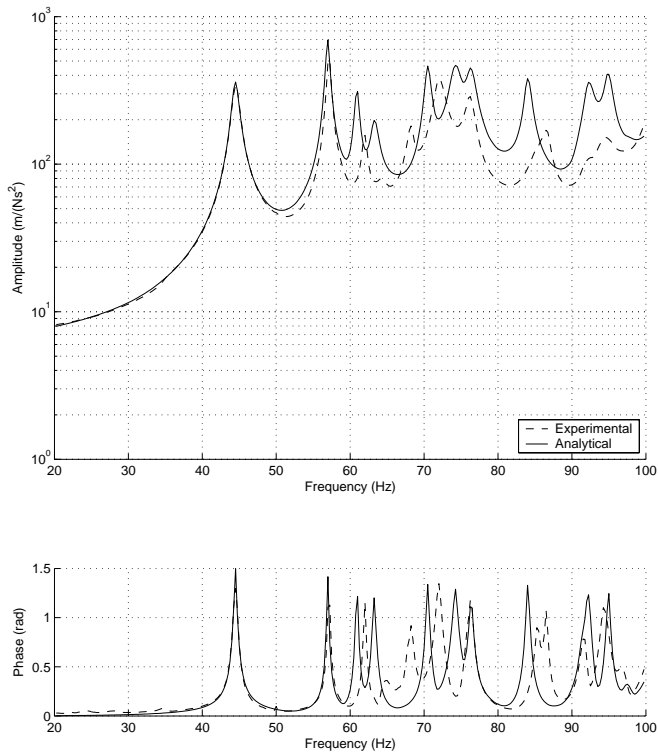


Figure 8.9 *Sum-blocks for door in white configuration after updating model parameters.*

8.3. Updating the Door Model

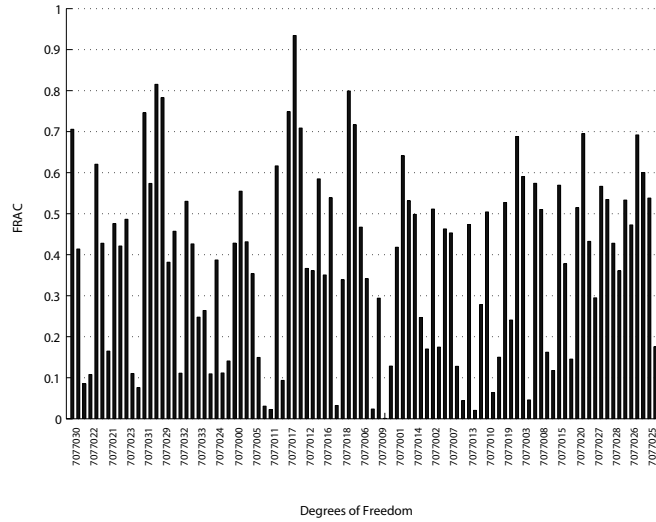


Figure 8.10 *FRAC for door in white configuration, excitation on arch in xy-plane, after updating model parameters.*

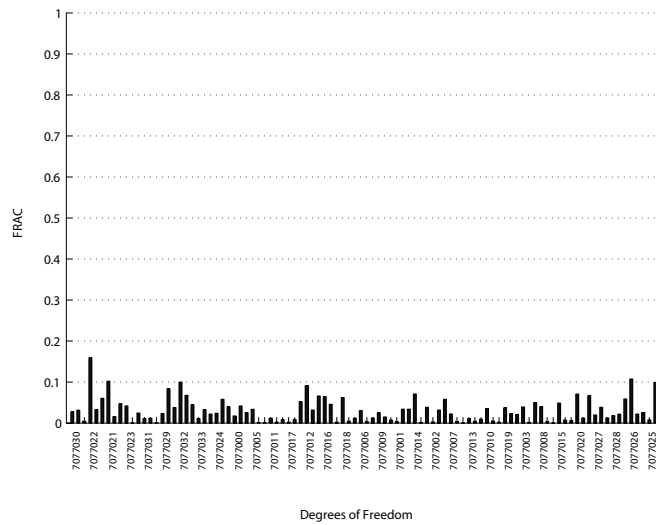


Figure 8.11 *FRAC for door in white configuration, excitation on outer panel in y-direction, after updating model parameters.*

8.3.3 Door in White, Window

In this configuration the window, window seals, guide rails and electrical motor are added to the door in white. As was stated in section 7.2.2 the correlation of the original model was poor.

After updating the inertia properties and implementing the updated parameters from the previous configuration the mode shape correlation is improved, see figure 8.12.

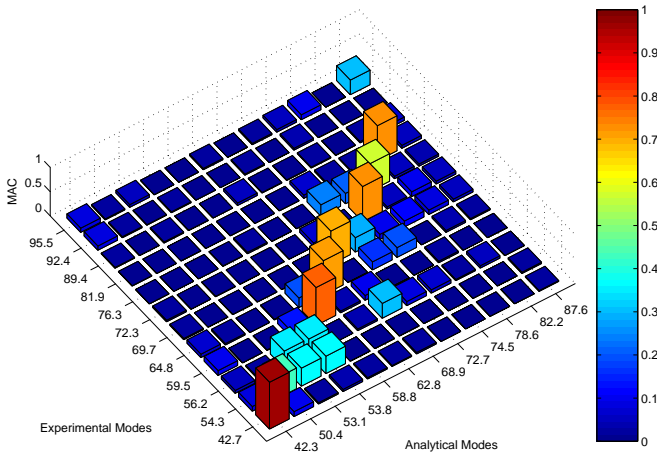


Figure 8.12 *MAC matrix for door in white, window configuration with updated parameters on previous configuration and updated bracket thickness.*

The analytical mode at 69.2 Hz can be considered a pure motor twisting mode much like the one at 59.5 Hz in the experimental set, see figure E.5, i.e. the analytical mode is off by 9.7 Hz or 14.0%. A measurement of the thickness of the actual bracket where the motor and gear is mounted gives the reason. The bracket is assigned a thickness of 1.5 mm in the model but the measurement reads 1.2 mm. When this change is made the correlation of that mode is improved drastically.

Friction Assumptions

The gap in the *MAC* matrix after the first mode is related to the window seal spring stiffness. A visualization of the experimental and analytical mode shapes indicates that the springs must be stiffer in the plane of the window. This can be achieved by increasing the spring stiffness in those directions.

8.3. Updating the Door Model

All springs are only assigned stiffness in the direction of the spring, due to the fact that certain spring properties that can only be assigned in the direction of the spring is used when working in the time domain. This means that the springs are either perpendicular to the plane of the window or in the plane. This is a sound assumption looking at the geometry of the window seals. However, effects of friction between the window and seals are not taken into account.

Modeling friction accurate in modal analysis is impossible but correlation may improve by assigning some stiffness to act as friction. This is already done in the original model, for instance, in the contacts between the window and the clips that connects the window to the guide rails.

By assigning stiffness in the plane of the window for those springs that are perpendicular to this plane, the effects of friction between the window and seals are simulated. The magnitude of the stiffness was set to one third of the corresponding stiffness in direction of the window plane normal. This change improves the correlation of the second and third mode drastically.

Spring Stiffness Assumptions

The spring stiffnesses assigned in the original model was based on non-linear static simulations performed on the different seal components. The results of the simulations was summarized in force-displacement relationships. These could then be entered into the models when, again, working in the time domain. But when performing eigenmodes- or modal frequency response simulations these non-linear relationships cannot be implemented. It should be mentioned that when performing door slam simulations the displacements that the seals are subjected to are far greater than in vibration simulations.

The stiffness assigned to each spring used in the vibration model was taken as the difference in force over the difference in displacement on a 4 mm interval around the initial position. To assume a maximum displacement of 2 mm in vibration analysis can be questioned and therefore all spring stiffnesses was entered into the optimization routine.

Optimization

To be able to perform the optimization all the modes included must be paired. This was not possible considering the correlation at this point. Above 70 Hz it was difficult pairing modes and the modal density seemed too high. A thorough study of what could cause the problems using visualization showed that the waist seals were too weak. Only by increasing the stiffness of these 50 times the original it was possible to pair the modes. This increase seem

questionable but was needed. The value was determined using trial and error eigenmodes simulations.

With paired modes the spring stiffnesses was updated using optimization. The initial values and the optimization results are seen in table 8.3.

Table 8.3 Optimization results for door in white, window.

Article	K_1 (N/mm)		K_2, K_3 (N/mm)		Change
	Init	Rslt	Init	Rslt	
Rear Seal (X)	1.588	1.710			8%
Rear Seal (Y), In	0.230	0.148		0.044	-36%
Rear Seal (Y), Out	183.800	143.000		42.900	-22%
Front Seal (X)	1.588	1.050			-34%
Front Seal (Y), In	0.230	0.185		0.056	-20%
Front Seal (Y), Out	183.800	365.000		109.5	99%
Top Seal (Y)	12.120	17.200		5.160	42%
Top Seal (Z)	121.300	319.000			163%
Waist Seal, Inner	0.304	65.800		19.74	21545%
Waist Seal, Outer	0.147	2.730		0.819	1757%

Although the waist seals stiffness was increased considerably before the optimization the results show additional increase. One remarkable observation is that the major increase is in the inner waist seal stiffness. This was the upside of the door when the measurements were performed and the load on the seal should be very low, hence should have low spring stiffness.

Correlation After Model Updating

After the model updating of the door in white, window configuration remarkable improvements in mode shape correlation can be observed, see figure 8.13. This justifies the somewhat questionable assumptions made. Now the model shows good correlation up to 70 Hz and better mode shape correlation overall.

A comparison of resonance frequencies shows improved correlation. The worst case is between 60 to 80 Hz, where the frequencies are off about 2 Hz or 2.8%.

The frequency response correlation is also improved. The sum-blocks plot, see figure 8.14, shows good frequency response correlation as a whole, although still amplitude mismatch at higher frequencies and the resonance frequency mismatch more accentuated. The *FRAC* values for the excitation in the *xy*-plane are in general improved but still indicates poor correlation, see figure 8.15.

8.3. Updating the Door Model

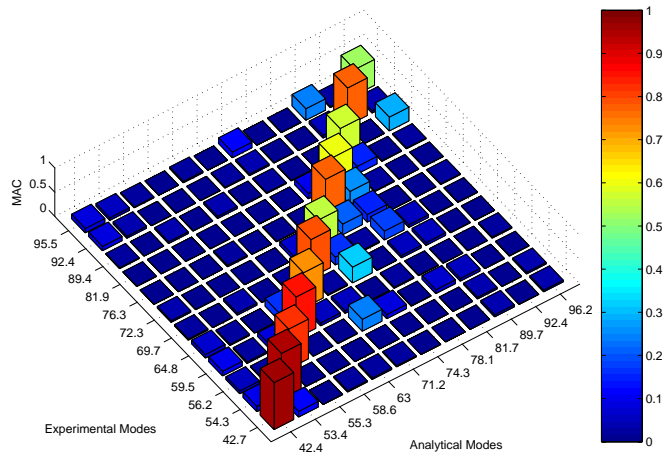


Figure 8.13 *MAC matrix for door in white, window configuration after updated model parameters.*

8. Model Updating

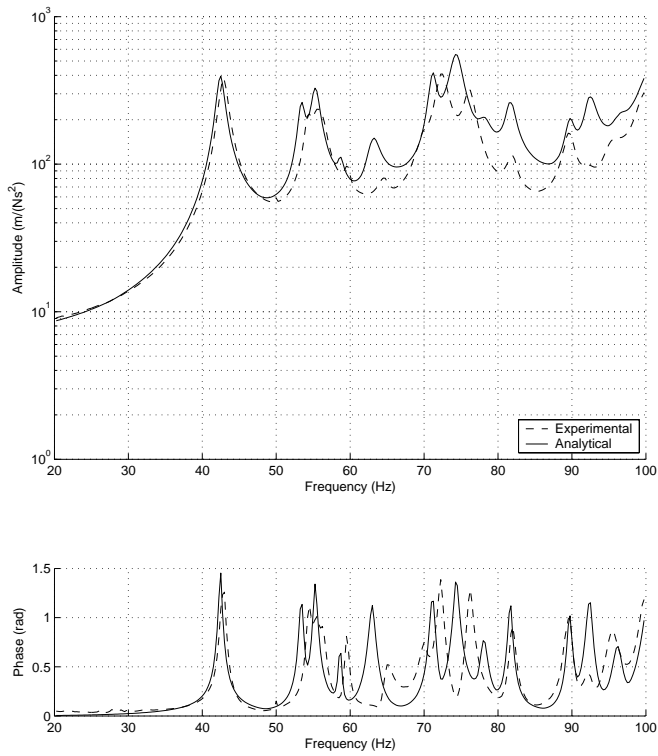


Figure 8.14 Sum-blocks for door in white, window configuration after updating model parameters.

8.3. Updating the Door Model

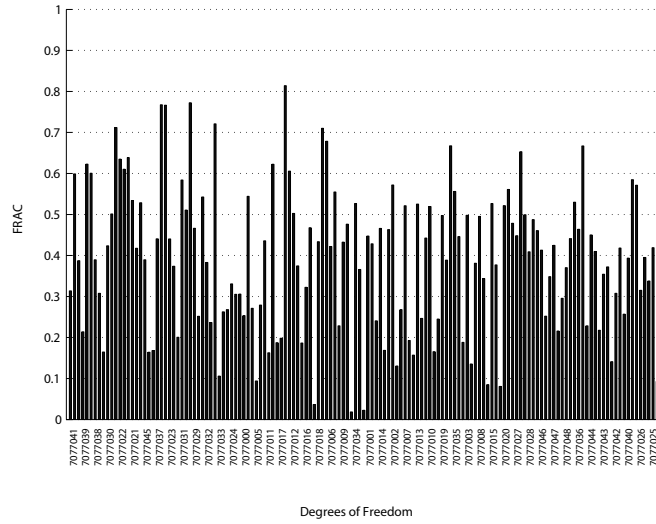


Figure 8.15 *FRAC for door in white, window configuration, excitation on arch in xy -plane, after updating model parameters.*

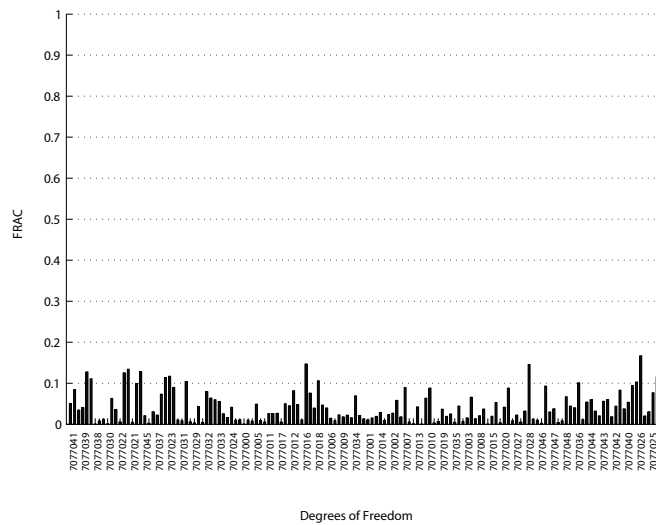


Figure 8.16 *FRAC for door in white, window configuration, excitation on outer panel in y -direction, after updating model parameters.*

8.3.4 Door in White, Window, Misc

In this configuration the door handle, lock mechanism, loudspeaker and rear view mirror are added to the structure. These are all parts carrying mass but will not add any significant structural stiffness. Therefore it is expected that the correlation after adding the parts will resemble that for the previous configuration. This is not the case. An eigenmodes simulation with the updated parameters from previous door configurations shows very poor correlation of mode shapes, see figure 8.17.

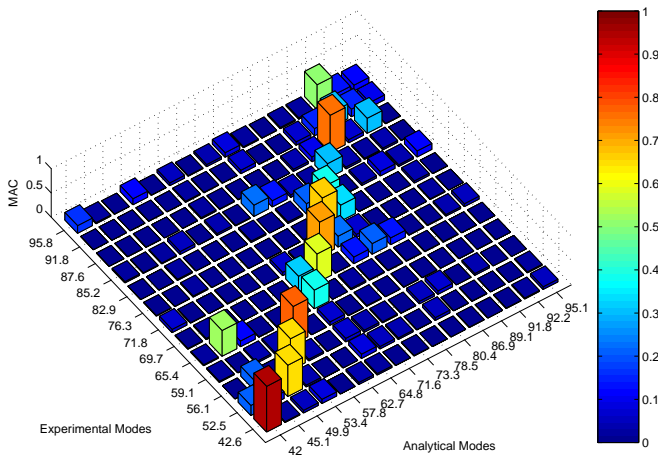


Figure 8.17 *MAC matrix for door in white, window, misc configuration after updating model parameters in previous configurations.*

Looking at the parts added it is difficult to relate the correlation mismatch to any model parameters. Above 60 Hz the mode shapes shows local motion. To be able to relate the correlation mismatch of local motions a much denser grid of response locations must be used. To be sure to capture all relevant motion special care must be taken with the now added parts. This is of course a too time consuming job and often not possible due to the geometry and assembly of the structure.

One obvious mismatch can be identified. The experimental mode at 65.4 Hz can be identified as a rear view mirror twisting mode. This mode corresponds to the second analytical mode which shows that the rear view mirror mode is off by 20.3 Hz or 31.0%. A further investigation of the rear view mirror is needed.

No other correlation mismatch could be related to the newly added parts.

8.3. Updating the Door Model

The Rear View Mirror

The rear view mirror mainly consists of a inner structure of aluminium mounted on an aluminum foot and a case in plastic. Mounted on the inner structure is also electronics and motors for adjusting and heating the mirror and the mirror glass itself.

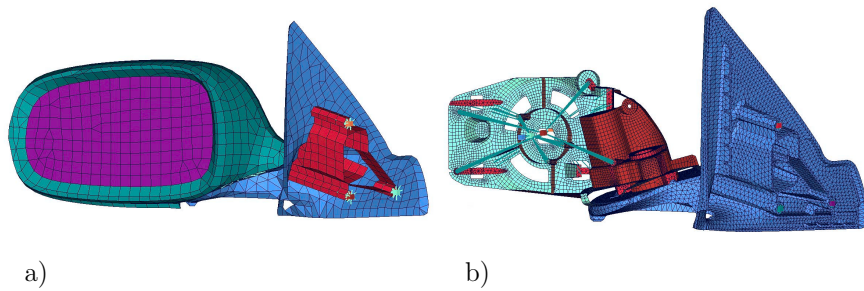


Figure 8.18 Rear view mirror models. a) Original model.
b) Detailed model.

In the original model, see figure 8.18a, shell elements are used to model the foot (with interior), the casing and the mirror. Mass and stiffness was assigned to these shells to compensate for stiffness and mass of the inner structure. This model looks as if it is quite detailed given the number of elements used. At first an approach to achieve better correlation through updating the Young's modulus, Poisson's ratio, density and shell element thickness was tried without success. Updating through optimization did not produce any good results due to that the model parameters had too little impact on correlation as a whole. Luckily, another model, supplied by the manufacturer, could be used, see figure 8.18b. This model was much more detailed and could not be used in vehicle system models or even in door slam models because of the number of elements in the model. The model is simply too detailed when considering the computational power available. However, for this project the model was applicable.

The new model is build up mainly by solid elements and focuses the interior structure. The casing and mirror is modeled with point inertia. This new model was then used in simulations and the results are shown below.

Correlation after Model Updating

After model updating of the door in white window, misc configuration the mode shape correlation is not satisfactory, see figure 8.19. Only the first four

8. Model Updating

modes correlate well and the modal density in the simulation below 100 Hz is too high. The maximum resonance frequency difference for these modes is some 2.5 Hz.

The rear view mirror mode can now be found on the diagonal in the MAC matrix, which means the new rear view mirror model correlates better although the MAC value is still too low and the resonance frequency is off by 3.3 Hz or 5.0%.

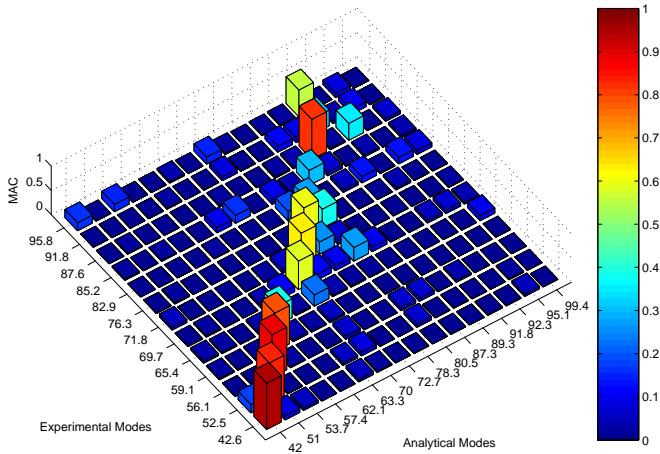


Figure 8.19 MAC matrix for door in white, window, misc configuration after updating model parameters.

After updating model parameters the frequency response correlation is improved for low frequencies. The frequency mismatch is obvious in the sum-blocks plot, see figure 8.20. The $FRAC$ values for excitation in xy -plane shows a general improvement but still indicates poor frequency response correlation, see figure 8.21.

8.3. Updating the Door Model

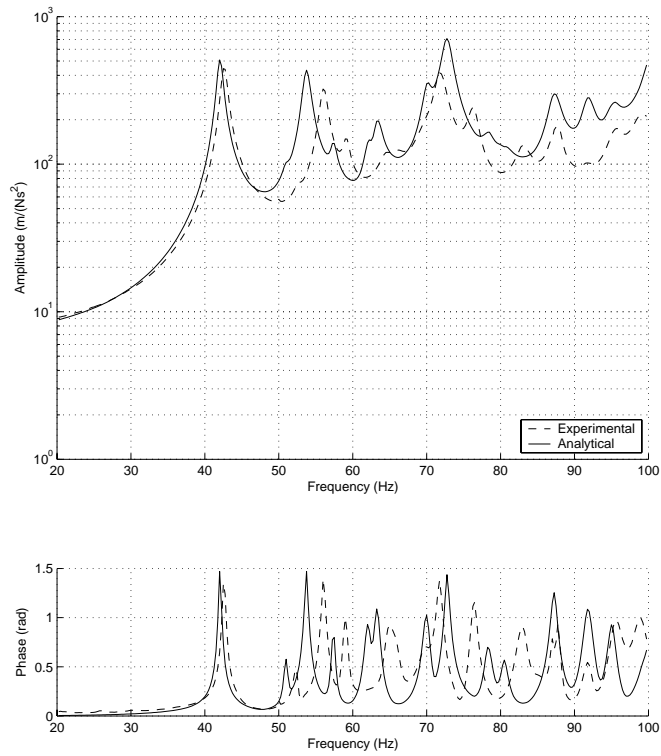


Figure 8.20 Sum-blocks plot for door in white, window, misc configuration after updating model parameters.

8. Model Updating

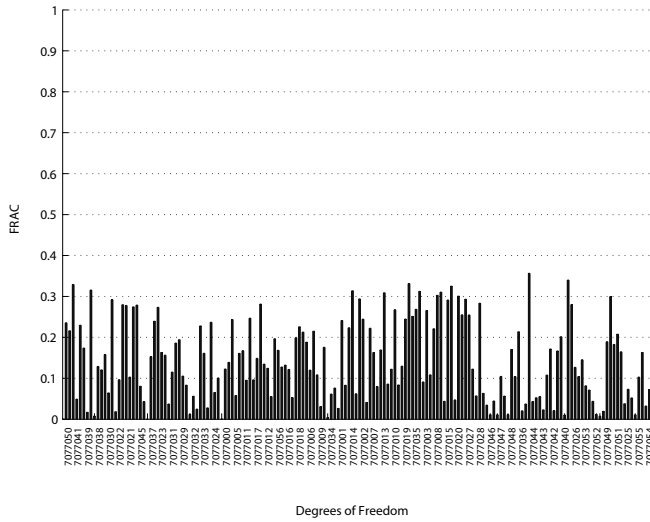


Figure 8.21 *FRAC for door in white window, misc configuration after updating model parameters. Excitation on arch inxy-plane.*

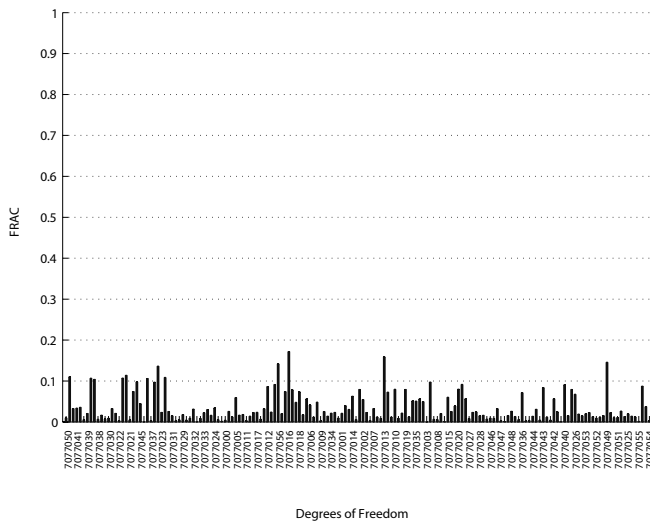


Figure 8.22 *FRAC for door in white, window, misc configuration after updating model parameters. Excitation on outer panel in y-direction.*

8.3. Updating the Door Model

8.3.5 Trimmed Door

The original model in the trimmed door configuration did not correlate at all. An eigenmodes simulation with model parameters updated in previous configurations does not show much improvement, see figure 8.23.

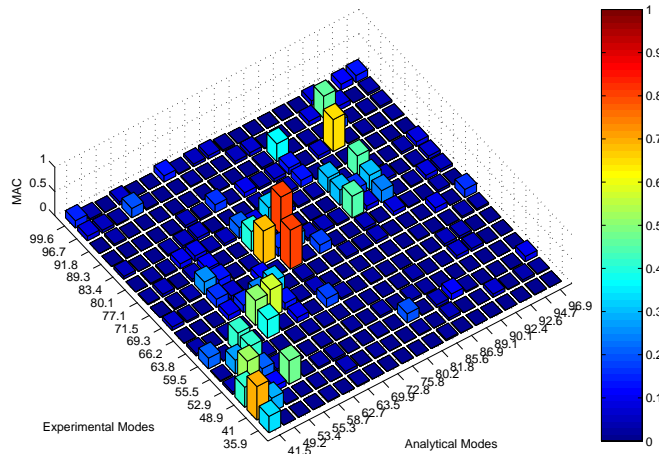


Figure 8.23 *MAC matrix for trimmed door configuration after updating model parameters in previous configurations.*

This door configuration differs drastically from the previous in terms of response locations used. When the door trim is attached the structure behind becomes inaccessible. Therefore it is more difficult to distinguish between mode shapes. Over 60 Hz the mode shapes all show local motion. When parts of the structure is inaccessible these local motions cannot be analyzed. This also lead to difficulties already at the pre-test stage. Still, the global behavior was expected to be captured.

The added components in this configuration are the trim itself and the attachment clips. Also, the trim is fixed with a friction contact to the inner panel at the waist, which is simulated with spring elements.

The trim itself is simply modeled as a uniform shell. This is an extensive simplification of the actual article. The actual geometry and material composition is much more complex.

Looking at the *MAC* matrix in figure 8.23 it is not possible to pair the experimental and analytical modes so the use of optimization is excluded at this stage.

Trial and error eigenmodes simulations with the variation of the few model

8. Model Updating

parameters available were performed to get an idea of how the parameters affect correlation. This did not shed any light on the problem at hand.

Starting from the correlation with parameters updated in previous configurations it was not possible to achieve a better correlation.

It should also be mentioned that the first experimental mode at 35.9 Hz displayed an unexpected window lateral bending motion. This opens the question if the measurements are really reliable for this configuration. The same window motion should also be captured in the door in white, window configuration.

The frequency response correlation for the trimmed door configuration is shown in figures 8.24 to 8.26. Despite the poor mode shape correlation and neglecting the first experimental mode the analytical sum-blocks shows remarkable resemblance with the experimental.

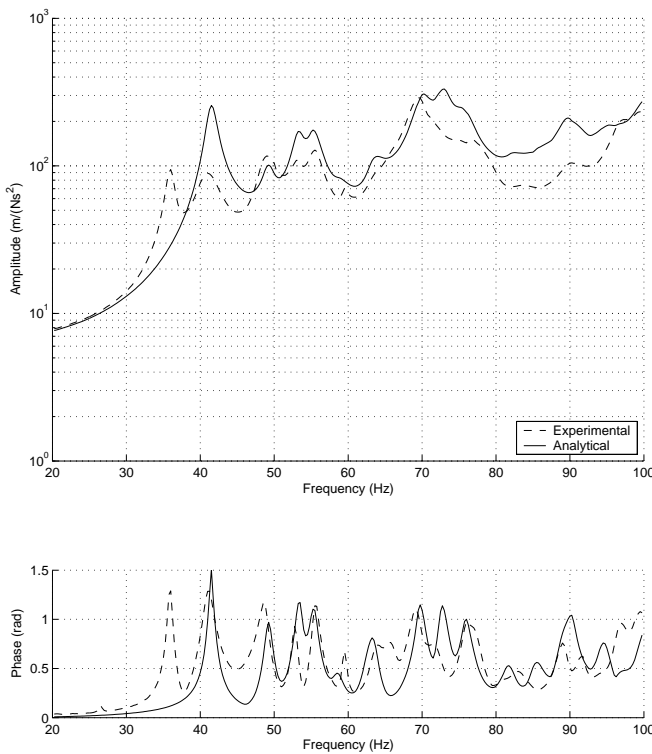


Figure 8.24 Sum-blocks for trimmed door configuration after updating model parameters in previous configurations.

8.3. Updating the Door Model

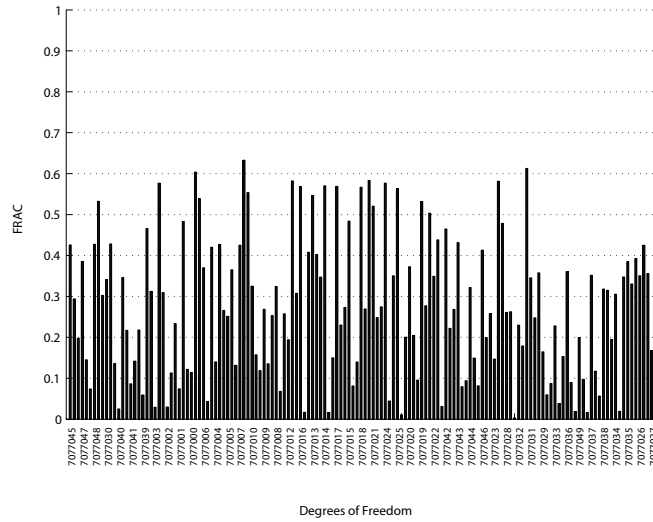


Figure 8.25 *FRAC for trimmed door configuration after updating model parameters in previous configurations. Excitation on arch in xy -plane.*

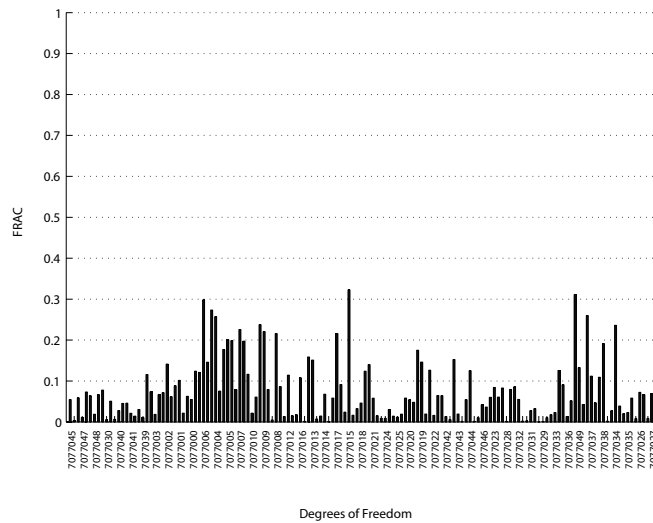


Figure 8.26 *FRAC for trimmed door configuration after updating model parameters in previous configurations. Excitation on outer panel in y -direction.*

Chapter 9

Conclusions

The conclusions, presented in this chapter, are divided in two parts. First, the modeling of the door structure is addressed, second, comments on the methodology used is presented.

9.1 The Modeling of Doors

First of all, achieving reasonable deterministic correlation for complex structures as vehicle closures is difficult. The simulation models represents an ideal, discretized world but when it comes to measurements, variability is present. The correlation work depends very much on the quality of the measurements performed. At higher frequencies, with increased modal density and modes displaying local motions the experimental modal analysis becomes unreliable. Also, the simulation models of today are still extensively simplified, especially when used under steady-state conditions where most non-linear effects cannot be addressed.

To summarize the results of this project, the door in white configuration correlates well, although the implementation of the measured modal damping in the frequency response analysis may have to be revised. This frequency response correlation mismatch is then inherited throughout the project. Also, the door in white, window configuration displays fair correlation for the frequency band under study, after the assumptions of friction. An important issue in these configurations are how to relate the optimization results to specifications known before building the models.

The correlations of the next two configurations are poor. This indicates that addition of quite simple components can alter the structural dynamic response considerably. The mass loading of the components added in the door in white, window, misc configuration shows that there is an evident trade-off

9. Conclusions

between accuracy and computational effort. Neglecting the odd occurrence of the window lateral bending mode in the final configuration, the plastic trim on the inside of the door alters the dynamic response drastically, although the frequency response plots show remarkable resemblance.

As mentioned above, all non-linearities cannot be implemented under steady-state conditions. When modeling rubber materials as the antiflutter, hemflange adhesive and window seals modal analysis is weak. By simplifying the models with linear springs it is possible to achieve good correlation for a narrow frequency band. The problem is what stiffness properties to assign the springs.

Material data exists on these material but are non-linear. Also, uncertainties in the application of these materials on the actual door as pre-stresses or contact issues are present. Therefore, it is not necessary to build too complex models of these components. A good thing would be to develop a strategy to relate the simplified model properties to the material or component data at hand. One conclusion in this project is that it is not sufficient to assume previously measured static stiffness properties.

The difficulties in modeling seals is widely recognized and is an important issue in the noise and vibration simulations that makes up the background to this project. The results of the model updating of the door in white, window configuration indicates that it is necessary to take into account the friction forces. One way has been presented here but much can still be done.

The seals act as weak connectors between much stiffer parts that are allowed a certain freedom of motion. Under these circumstances the contact between seal and structural elements becomes vital and must be addressed in the modeling of seals. In this project linear springs was used and the problem of how to relate properties to existing data is evident. The method used initially in the work, based on static force-displacement simulations of the seals, is not sufficient but may be a good starting point.

The friction constant assumed in this project can be questioned but it gives the general idea of how to manage the problems.

An important issue in this project has been the investigation of how well the nominal shell element thickness represents the actual thickness distribution of the panels. The attempt to take this distribution into account was not successful but shows that the shell element thickness play an important role. A small alteration can improve or worsen the correlation drastically, especially at higher frequencies.

9.2 Model Updating Methodology

The methodology used in this project follow an intuitive pattern both when it comes to the analyzes performed and the resources used. But as the process is implemented here it has a major drawback. After updating a model the structural dynamic response changes extensively. This means that if a pre-test analysis for the next configuration was performed on a now outdated model the test set-up will not be the best one possible. Therefore, it would be better if the analysis and measurement reconciliation goes through every step depicted in figure 2.2, including the model updating before the eigenmodes simulation and pre-test for the next configuration are performed.

It should also be mentioned that if the model updating process does not reach sufficient results for a certain configuration, the analysis and measurement reconciliation may be started over for this particular configuration.

Another conclusion concerning the methodology is that, although the use of optimization routines are effective, these should be used with care. If the procedure is set up correct it will surely give the correct results. The problem is that a structures complete dynamic response cannot be rolled down into a single scalar. As mentioned earlier there exists a number of different formulations and only one was addressed in the report of this project.

Also, the optimization procedure will only give a local minimum point. Nothing can be said about the global minimum. It is the engineer that have to decide if the optimization output is reasonable.

Chapter 10

Future Work

The work performed in this project should be thought of as only one part of the process depicted in figure 1.1. There is still a number of unsolved issues.

First, since the correlation of the last two configuration was not satisfactory, these may have to be addressed again on component level. The plastic trim model on the inside of the door needs to be modeled much more detailed. Suggestions of how this can be addressed have been encountered during the work on this project, but not for a front door.

One way of handling the trade-off between accuracy and effort for these parts is to optimize a simple model to fit the response of a more detailed on component level. Another main issue that needs further investigation is the dynamic stiffness of rubber material and how this can be approximated in linear analysis within a given frequency band. It should be noted here that it is possible to implement frequency dependent springs in frequency response analysis in MSC.Nastran.

The implementation of panel thickness distribution in the simulation models can also be addressed further. Since the simulation results of the stamping process exists they can be implemented in MSC.Nastran models by assigning shell element thicknesses for every grid point. This may be something that can be implemented in the general development process of new automotive vehicles. However, first the impact of the thickness distribution must be established.

Last, considering the product-to-product and test-to-test variability it is necessary to develop statistical methods in the analysis and measurement reconciliation.

Appendix A

Normal Modes Analysis in MSC.Nastran

Normal Modes Analysis is performed in MSC.Nastran with the executive control command SOL 103. The following entries are the most important ones used when performing modal analysis on the door. In order of appearance:

METHOD	Selects the real eigenvalue extraction method. Calls the EIGRL entry.
SET	Defines a set of element or grid point numbers to be plotted, called by the DISPLACEMENT statement.
DISPLACEMENT	Requests the form and type of displacement vector output, in this case a sorted punch file (*.pch). REAL requests rectangular format of complex output.
PARAM,GRDPNT,0	Causes the grid point weight generator to be executed, which computes the center of gravity and mass inertia properties.
EIGRL	Defines data needed to perform real eigenvalue analysis with the Lanczos method.

A. Normal Modes Analysis in MSC.Nastran

A.1 MSC.Nastran SOL 103 Input File

```
$----- FILE MANAGEMENT SECTION -----
$----- EXECUTIVE CONTROL SECTION -----

SOL 103
TIME 10000
DIAG 8
CEND

$----- CASE CONTROL SECTION -----

METHOD=1
INCLUDE 'response_grids.set'      $--- (SET 1 GRID,GRID,GRID,...)
DISPLACEMENT(SORT2,PUNCH,REAL)=1

ECHO=NONE

PARAM,GRDPNT,0                    $--- GRID POINT WEIGHT GENERATOR REFERENCE
PARAM,AUTOSPC,YES                 $--- AUTOMATIC CONSTRAIN OF SINGULARITIES
PARAM,POST,-1                     $--- 0=>.xdb, -1=>.op2(PATRAN), -2=>.op2(IDEAS)
$                                  -4=>.op2(LMS)
PARAM,SNORM,20.0                  $--- SHELL NORMAL PARAMETER
PARAM,DBALL,SCRATCH               $--- REDUCE DISK SPACE USAGE => slower restart
PARAM,PRGPST,NO                   $--- SINGULARITY PRINTOUT
PARAM,NEWSEQ,-1                   $--- NO RESEQUENCING

$----- BULK DATA SECTION -----

BEGIN BULK

EIGRL          1      10.0  200.0

INCLUDE 'model.bdf'

ENDDATA
```

Appendix B

Modal Frequency Response Analysis in MSC.Nastran

Modal frequency response analysis is performed in MSC.Nastran with the executive control statement SOL 111. The most important control statements in order of appearance are the following:

PARAM, RESVEC, YES	Selects the use of residual vectors to represent excluded modes.
METHOD	Selects the real eigenvalue extraction method, calls the EIGRL statement.
FREQUENCY	Selects the set of forcing frequencies to be solved, calls the FREQi statement.
SDAMPING	Requests modal damping as a function of natural frequency, calls the TABDMPi statement.
SET	Defines a set of element or grid point numbers to be plotted, called by the DISPLACEMENT statement.
SUBCASE	Delimits and identifies a subcase. The following case control statements are included in this subcase only.

B. Modal Frequency Response Analysis in MSC.Nastran

DISPLACEMENT	Requests the form and type of displacement vector output, in this case a sorted punch file (*.pch). PHASE requests polar format.
DLOAD	The case control statement selects a dynamic load to be applied, calls the bulk data section statement DLOAD. In turn this defines a dynamic loading condition as a linear combination of load sets defined via RLOAD1.
RLOAD1	Defines a frequency dependent dynamic load, calls the DAREA and TABLED1 statement.
DAREA	Defines scale, direction and load grid of dynamic loads.
TABLED1	Defines a tabular function for use in generating frequency dependent loads.
TABDMP1	Defines modal damping as a tabular function of natural frequency.
EIGRL	Defines data needed to perform real eigenvalue analysis with the Lanczos method.
FREQ1	Defines a set of frequencies to be used in the solution.
SUPPORT	Defines determinate reaction degrees of freedom for a free-free body.

B.1. MSC.Nastran SOL 111 Input File

B.1 MSC.Nastran SOL 111 Input File

```
$----- FILE MANAGMENT SECTION -----
$----- EXECUTIVE CONTROL SECTION -----

SOL 111
TIME 10000
DIAG 8
CEND

$----- CASE CONTROL SECTION -----

PARAM,GRDPNT,0          $--- GRID POINT WEIGHT GENERATOR REFERENCE
PARAM,AUTOSPC,YES      $--- AUTOMATIC CONSTRAIN OF SINGULARITIES
PARAM,SNORM,20.0      $--- SHELL NORMAL PARAMETER
PARAM,DBALL,SCRATCH    $--- REDUCE DISK SPACE USAGE => slower restart
PARAM,PRGPST,NO        $--- SINGULARITY PRINTOUT
PARAM,NEWSEQ,-1        $--- NO RESEQUENCING

PARAM,RESVEC,YES

METHOD=1
FREQUENCY=1
SDAMPING=1

INCLUDE'response_grids.set'  $--- (SET 1 GRID,GRID,GRID,...)

SUBCASE=101
DLOAD=101
DISPLACEMENT(SORT2,PUNCH,PHASE)=1
ECHO=NONE

SUBCASE=102
DLOAD=102
DISPLACEMENT(SORT2,PUNCH,PHASE)=1
ECHO=NONE

$----- BULK DATA SECTION -----

BEGIN BULK

DLOAD      101      1.0      1.0      1001
RLOAD1     1001     1001
DAREA      1001 7077004      2      1.0

DLOAD      102      1.0 -0.8290      1002 -0.5592      1003
RLOAD1     1002     1002
RLOAD1     1003     1003
DAREA      1002 7077034      1      1.0
DAREA      1003 7077034      2      1.0

TABLED1    1
           0.0      1.0      400.0      1.0      ENDT

TABDMP1    1      CRIT
           44.9467  0.0104 56.5331  0.0046 60.3155  0.0051 65.4632  0.0075
           70.4235  0.0060 75.7648  0.0103 76.4273  0.0076 85.1659  0.0058
           93.0562  0.0075 94.9449  0.0056 97.8545  0.0095      ENDT

EIGRL      1      0.0      400.0
```

B. Modal Frequency Response Analysis in MSC.Nastran

```
FREQ1      1  10.0  0.25  760
SUPPORT  7013513  123 7053520  12 7013511  1
INCLUDE 'model.bdf'
ENDDATA
```

Appendix C

Pre-Test Results

C.1 Excitation Point Selection

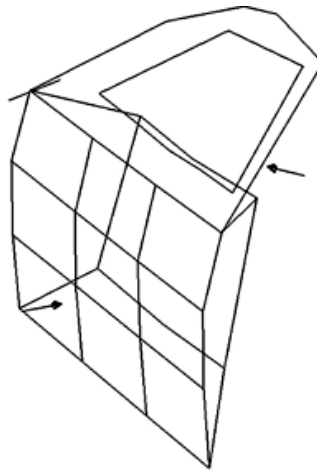


Figure C.1 *Excitation locations and directions used to excite the door in the test shown as arrows on the wire frame.*

C.2 Response Point Selection

C.2.1 Door in White

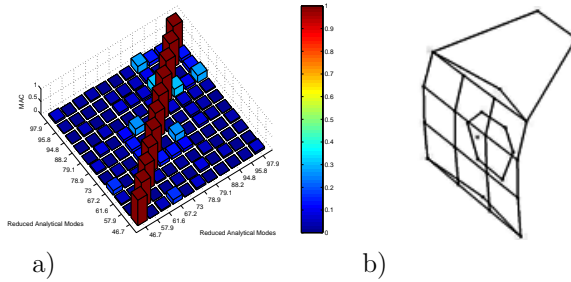


Figure C.2 Initial set of 27 response nodes for door in white, chosen to visualize the door structure and to make sure to capture the first global modes. a) MAC matrix. b) The initial set of response nodes shown as dots on the wire frame.

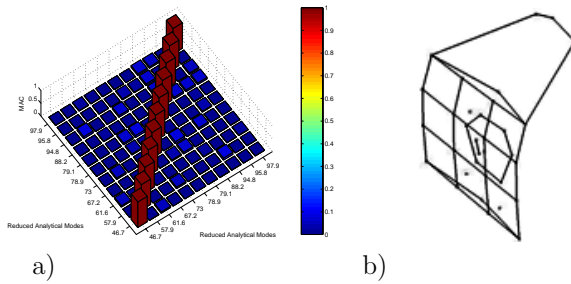


Figure C.3 Final set of 33 response nodes for door in white after the point that was chosen as excitation locations was omitted. a) MAC matrix b) The final set of response nodes shown as dots on the wire frame.

C.2. Response Point Selection

C.2.2 Door in White, Guide Rails

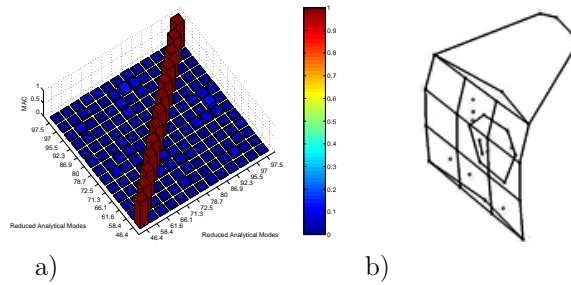


Figure C.4 Initial set of 37 response nodes for door in white, guide rails. a) MAC matrix. b) The initial set of response nodes shown as dots on the wire frame.

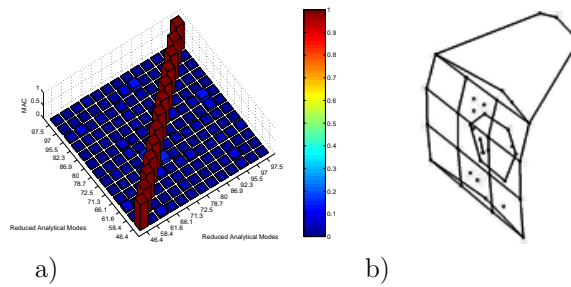


Figure C.5 Final set of 39 response nodes for door in white, guide rails after the point that was chosen as excitation location was omitted. a) MAC matrix b) The final set of response nodes shown as dots on the wire frame.

C.2.3 Door in White, Window

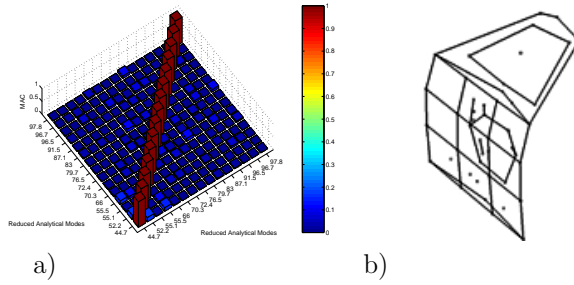


Figure C.6 Initial set of 46 response nodes for door in white, window. a) MAC matrix. b) The initial set of response nodes shown as dots on the wire frame.

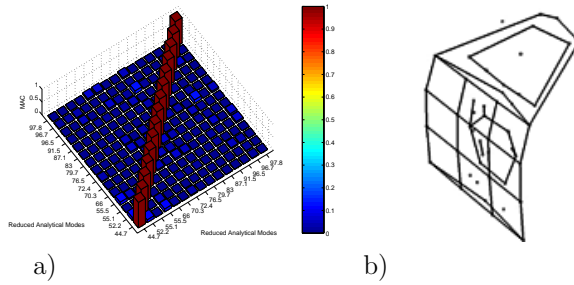


Figure C.7 Final set of 48 response nodes for door in white, window after the point that was chosen as excitation location was omitted. a) MAC matrix b) The final set of response nodes shown as dots on the wire frame.

C.2. Response Point Selection

C.2.4 Door in White, Window, Misc

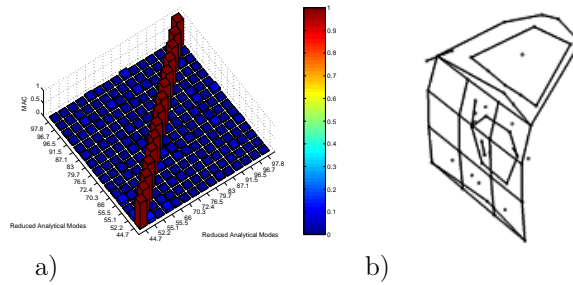


Figure C.8 Initial set of 54 response nodes for door in white, window, misc. a) MAC matrix. b) The initial set of response nodes shown as dots on the wire frame.

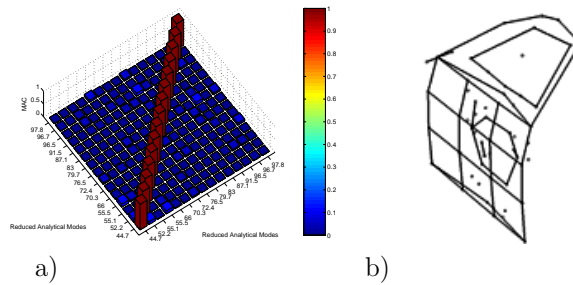


Figure C.9 Final set of 56 response nodes for door in white, window, misc after the point that was chosen as excitation location was omitted in addition with two other points that were omitted before performing the test, due to the impossibility to place accelerometers on those locations. a) MAC matrix b) The final set of response nodes shown as dots on the wire frame.

C.2.5 Trimmed Door

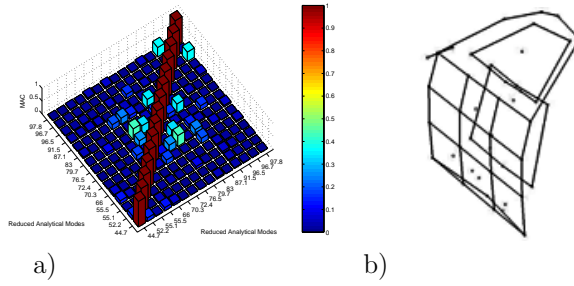


Figure C.10 Initial set of 46 response nodes for trimmed door. a) MAC matrix. b) The initial set of response nodes shown as dots on the wire frame.

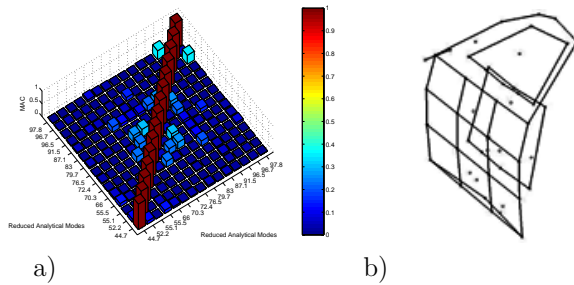


Figure C.11 Final set of 49 response nodes for trimmed door, after the point that was chosen as excitation location was omitted. a) MAC matrix b) The final set of response nodes shown as dots on the wire frame.

Appendix D

Measurement Results

D.1 Mode Maps

Table D.1 *Mode map and estimated modal damping for door in white configuration.*

Mode	Freq (Hz)	Damping (%)	Description
1	44.4	1.04	Outer panel lateral bending
2	57.1	0.46	Global torsion
3	62.0	0.51	Global lateral bending
4	64.2	0.75	
5	67.8	0.60	
6	72.1	1.03	
7	76.2	0.76	
8	86.2	0.58	
9	91.9	0.75	
10	94.1	0.75	
11	97.0	0.95	
Mean value for modal damping: 0.73%			

D. Measurement Results

Table D.2 Mode map and estimated modal damping for door in white, window configuration.

Mode	Freq (Hz)	Damping (%)	Description
1	42.7	1.24	Outer panel lateral bending
2	54.3	0.91	Global lateral bending
3	56.2	1.08	Global torsion
4	59.5	0.54	Motor twisting
5	64.8	1.29	
6	69.7	0.84	
7	72.3	1.14	
8	76.3	1.02	
9	81.9	0.72	
10	89.4	0.62	
11	92.4	0.85	
12	95.5	1.09	
Mean value for modal damping: 0.95%			

Table D.3 Mode map and estimated modal damping for door in white, window, misc configuration.

Mode	Freq (Hz)	Damping (%)	Description
1	42.7	1.00	Outer panel lateral bending
2	52.5	0.82	Global torsion
3	56.1	1.04	Global lateral bending
4	59.1	0.66	Motor twisting
5	65.4	1.40	Rear view mirror twisting
6	69.1	1.27	
7	71.8	1.17	
8	76.3	0.91	
9	82.9	1.23	
10	85.2	1.34	
11	87.6	0.51	
12	91.8	0.88	
13	95.6	1.03	
Mean value for modal damping: 1.02%			

D.1. Mode Maps

Table D.4 Mode map and estimated modal damping for trimmed door configuration.

Mode	Freq (Hz)	Damping (%)	Description
1	36.0	1.75	Window lateral bending
2	41.0	3.65	Outer panel lateral bending
3	48.9	2.34	Global torsion
4	52.9	1.42	Global lateral bending
5	55.5	1.64	
6	59.5	0.69	
7	63.8	2.04	Rear view mirror twisting
8	69.3	1.59	
9	71.5	2.09	
10	77.1	2.05	
11	80.1	2.19	
12	83.4	1.96	
13	91.8	1.15	
14	96.7	1.38	
15	99.6	1.22	
Mean value for modal damping:			1.81%

D.2 Model Validation

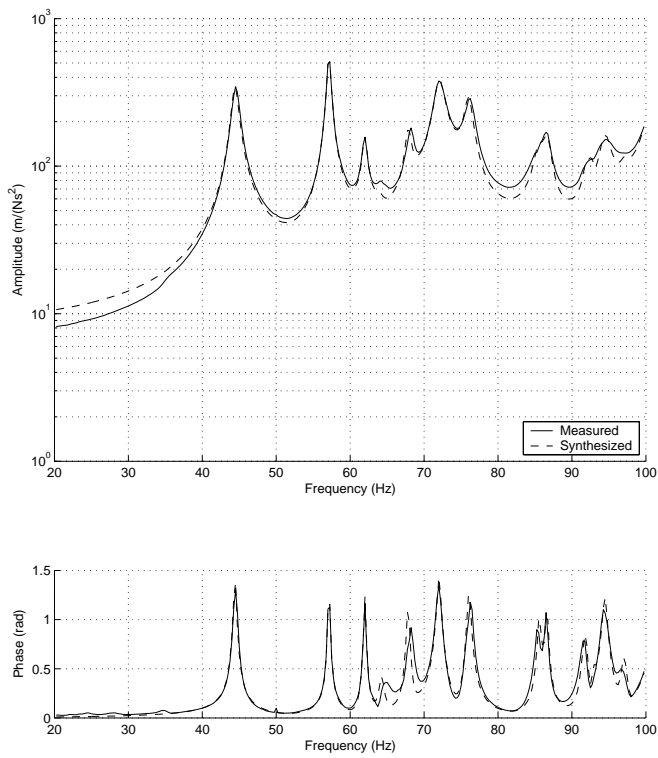


Figure D.1 *Synthesized frequency response for door in white configuration.*

D.2. Model Validation

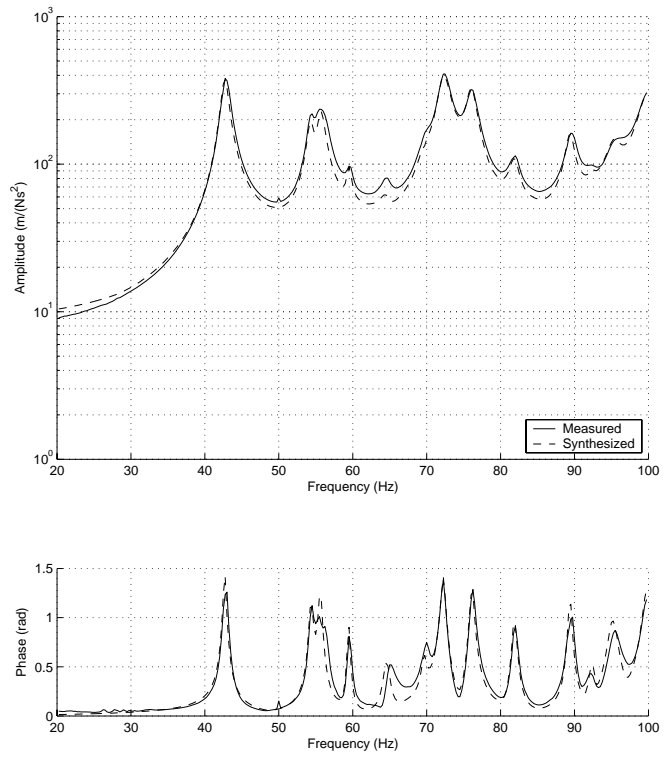


Figure D.2 Synthesized frequency response for door in white, window configuration.

D. Measurement Results

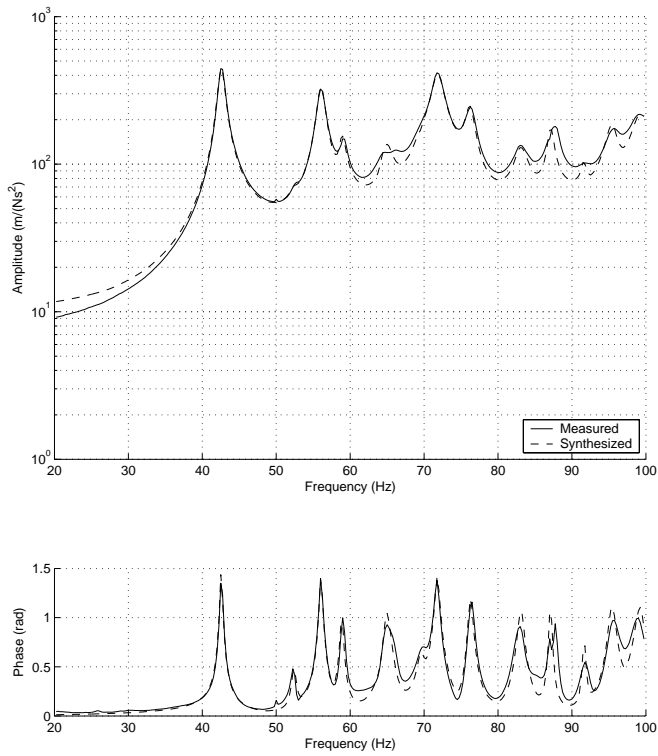


Figure D.3 Synthesized frequency response for door in white, window, misc configuration.

D.2. Model Validation

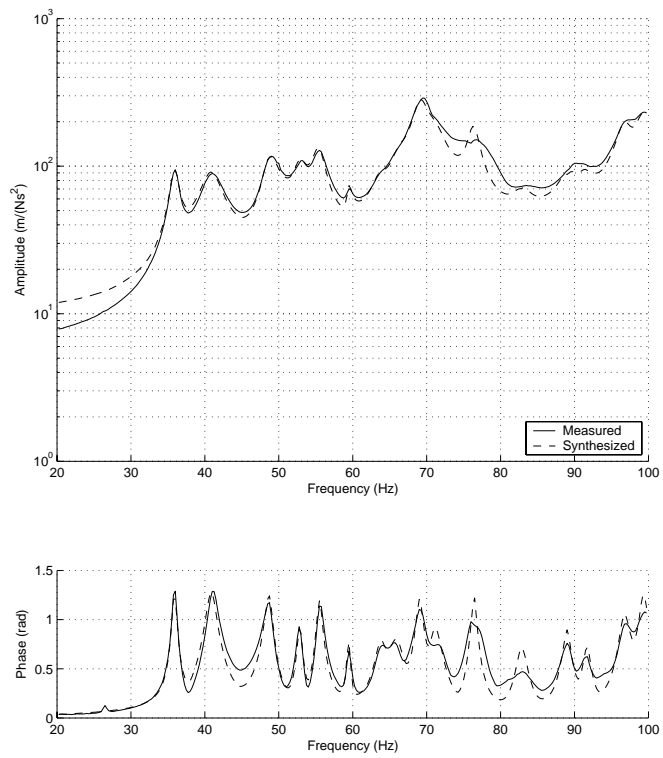


Figure D.4 *Synthesized frequency response for trimmed door configuration.*

D. Measurement Results

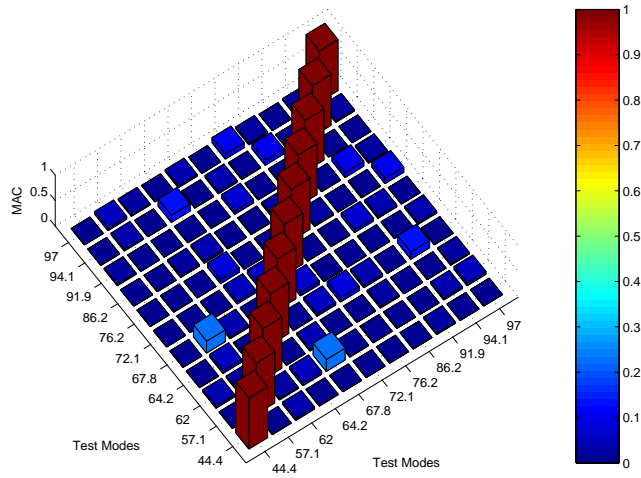


Figure D.5 *MAC matrix for test modes for door in white configuration.*

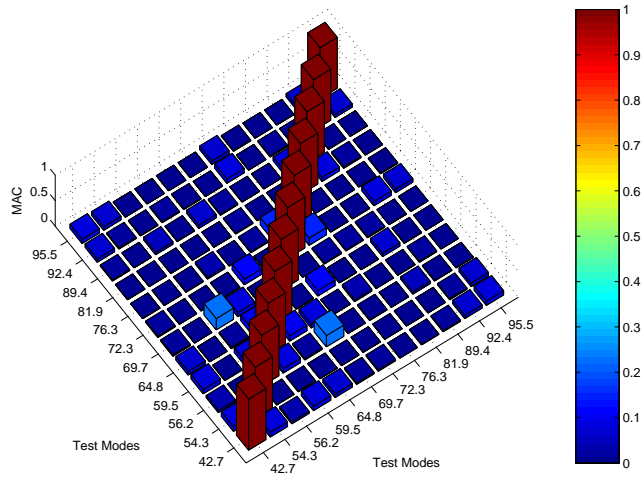


Figure D.6 *MAC matrix for test modes for door in white, window configuration.*

D.2. Model Validation

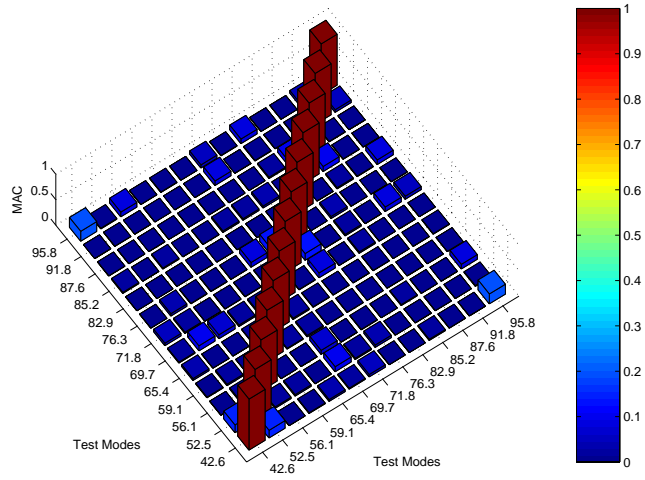


Figure D.7 *MAC matrix for test modes for door in white, window, misc configuration.*

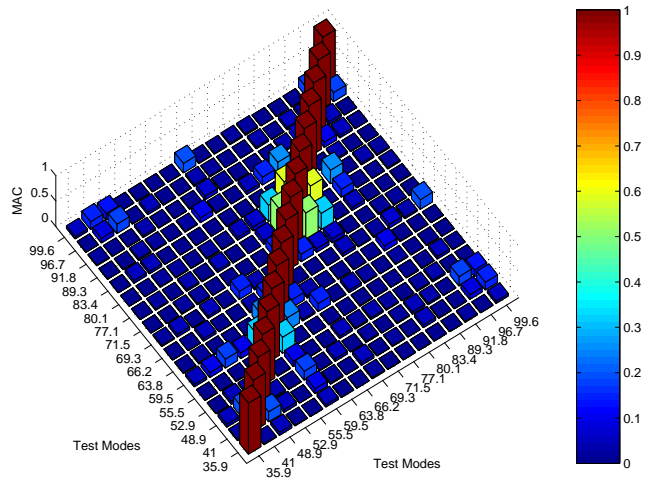


Figure D.8 *MAC matrix for test modes for trimmed door configuration.*

D.3 Sum-Blocks with Separated Excitations

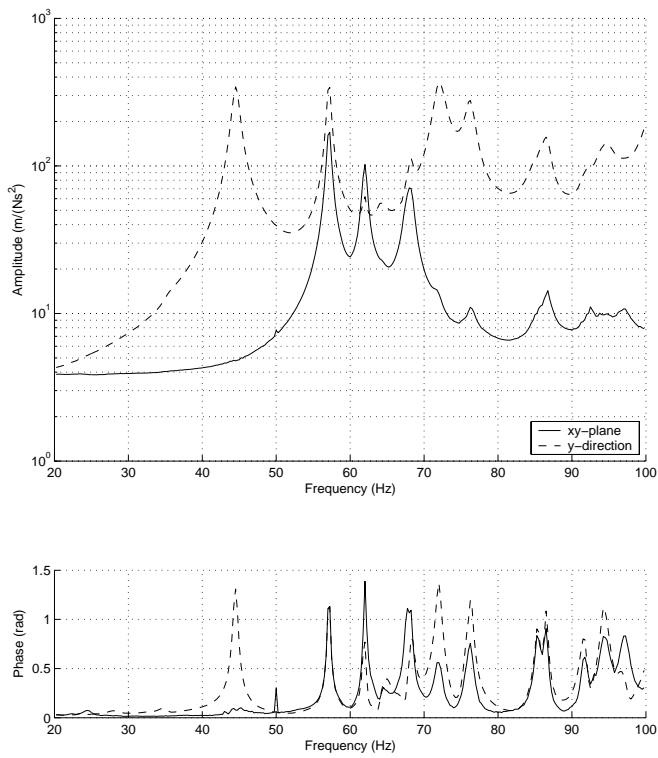


Figure D.9 Sum-blocks for door in white configuration with separated excitations.

D.3. Sum-Blocks with Separated Excitations

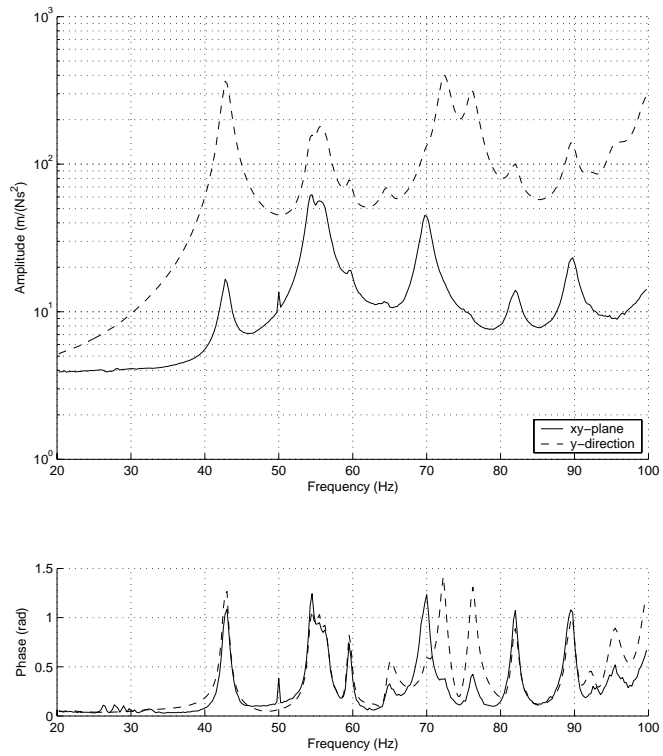


Figure D.10 Sum-blocks for door in white, window configuration with separated excitations.

D. Measurement Results

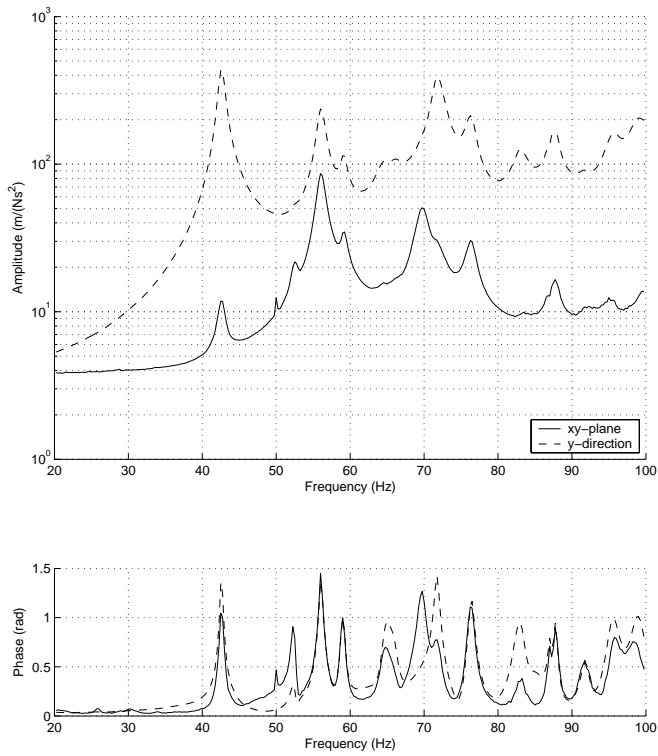


Figure D.11 Sum-blocks for door in white, window, misc configuration with separated excitations.

D.3. Sum-Blocks with Separated Excitations

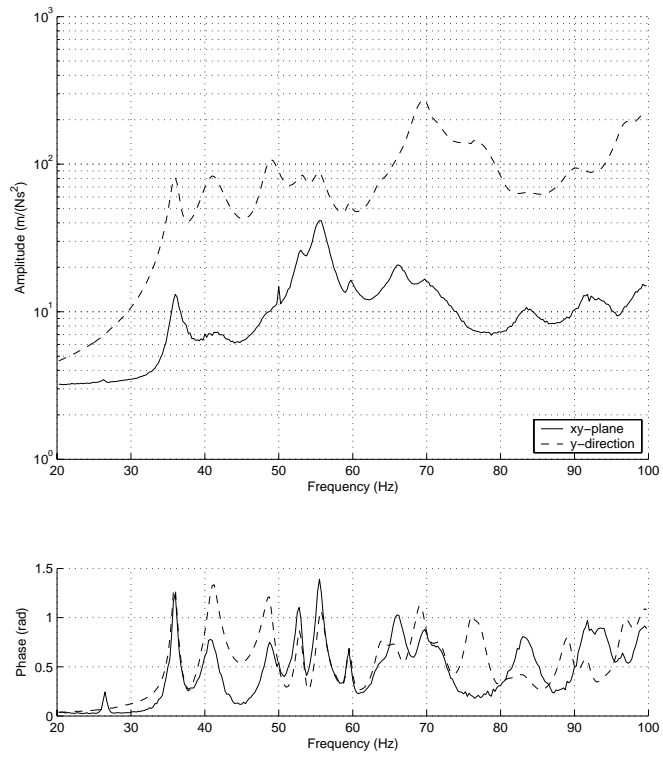


Figure D.12 Sum-blocks for trimmed door configuration with separated excitations.

Appendix E

Correlation Results

E.1 Door in White

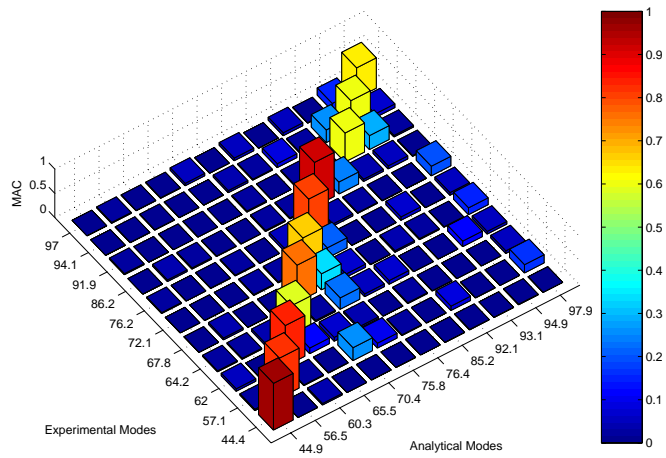


Figure E.1 MAC matrix for door in white configuration.

E. Correlation Results

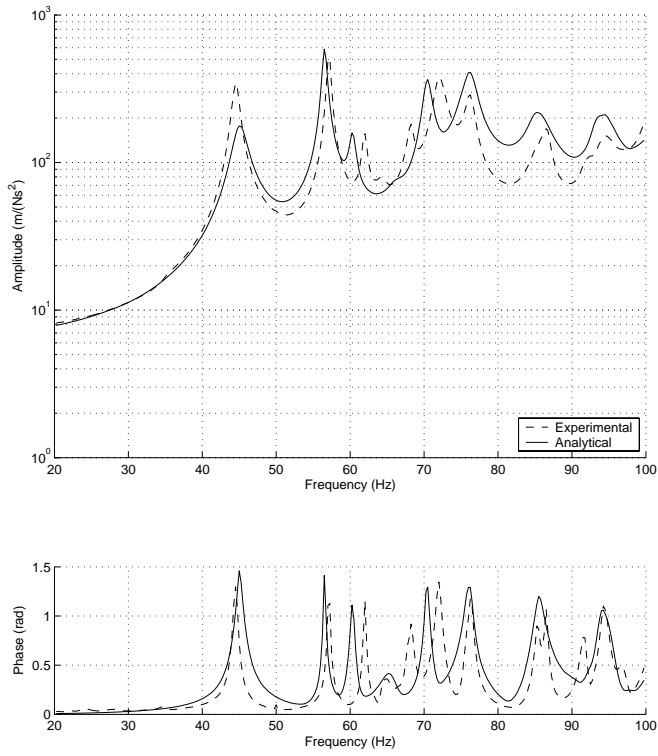


Figure E.2 *Sum-blocks for door in white configuration.*

E.1. Door in White

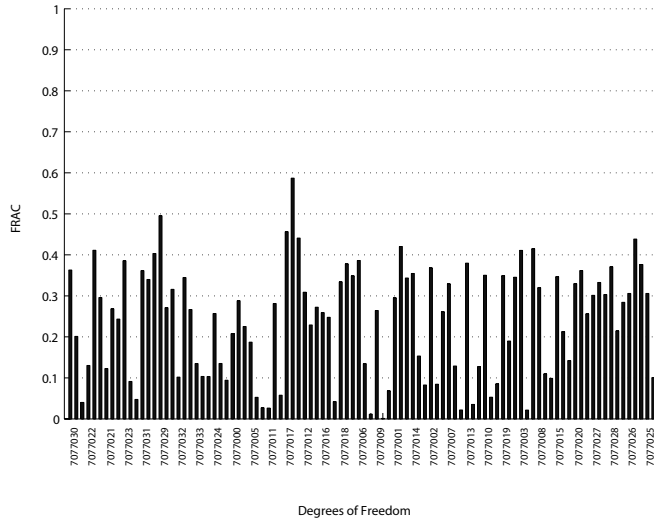


Figure E.3 *FRAC for door in white configuration. Excitation on arch in xy-plane.*

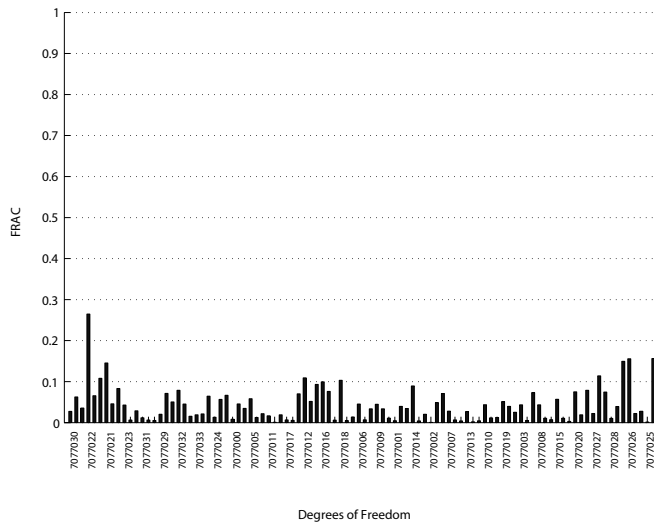


Figure E.4 *FRAC for door in white configuration. Excitation on outer panel in y-direction.*

E.2 Door in White, Window

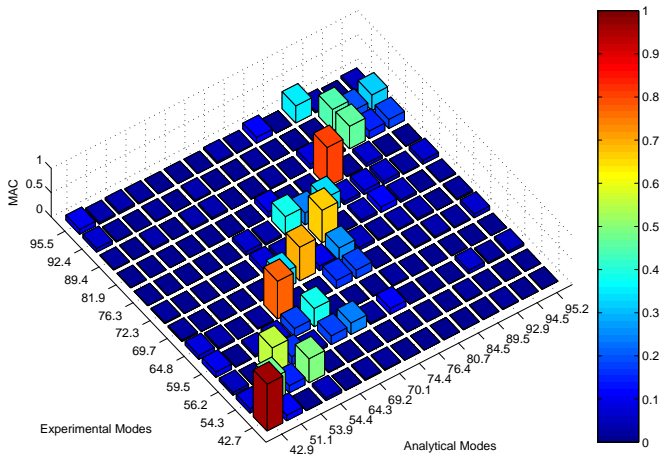


Figure E.5 MAC matrix for door in white, window configuration.

E.2. Door in White, Window

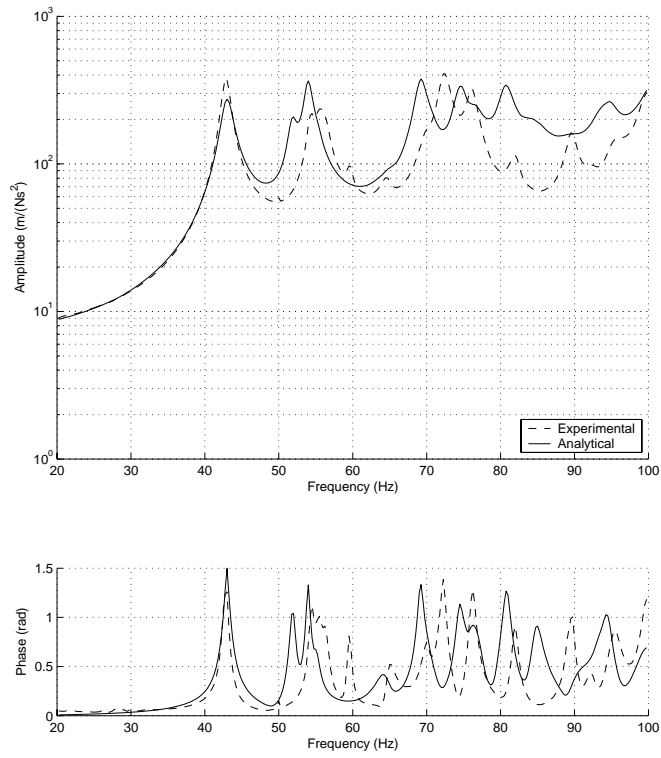


Figure E.6 Sum-blocks for door in white, window configuration.

E. Correlation Results

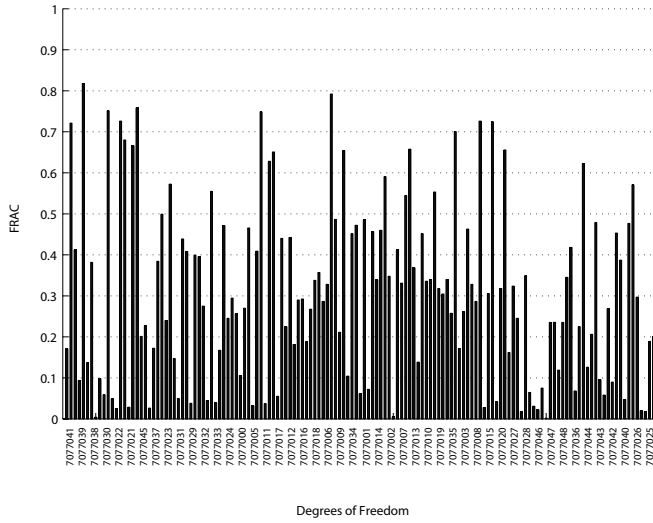


Figure E.7 *FRAC for door in white, window configuration. Excitation on arch in xy -plane.*

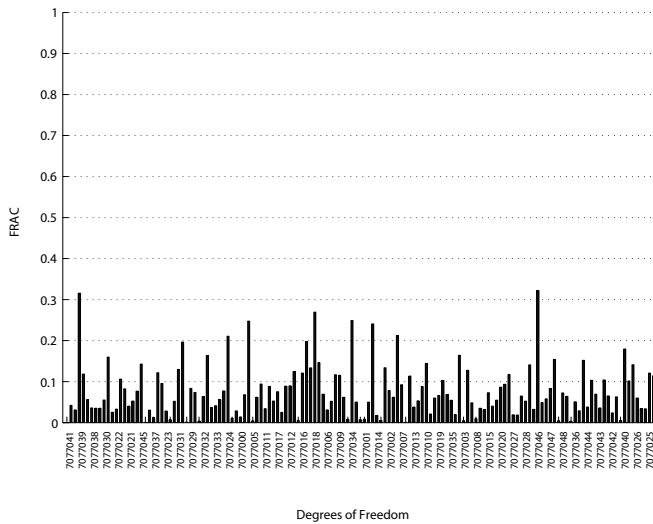


Figure E.8 *FRAC for door in white, window configuration. Excitation on outer panel in y -direction.*

E.3 Door in White, Window, Misc

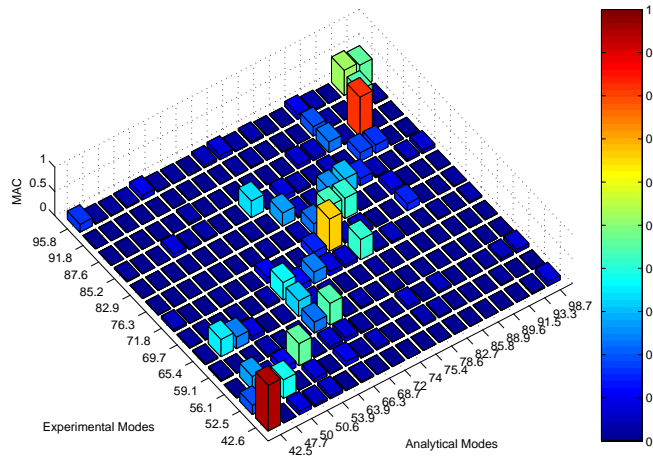


Figure E.9 MAC matrix for door in white, window, misc configuration.

E. Correlation Results

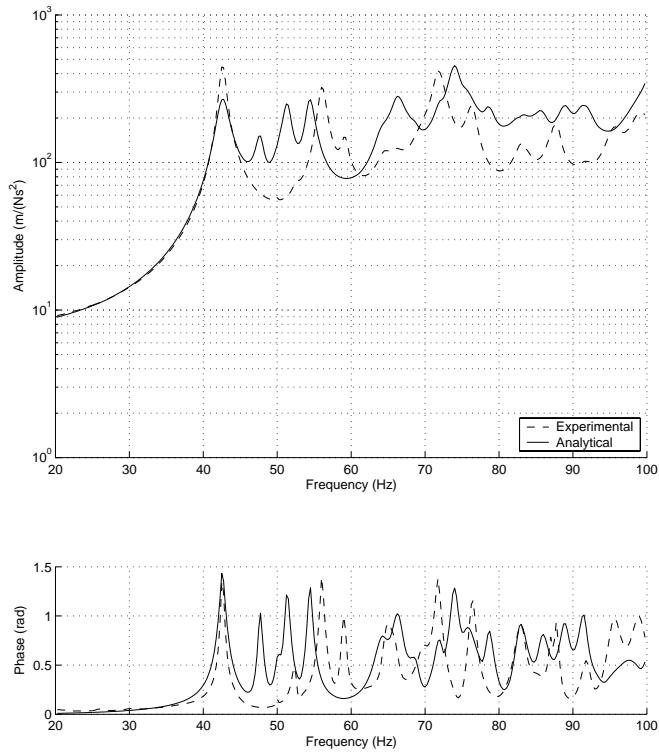


Figure E.10 Sum-blocks for door in white, window, misc configuration.

E.3. Door in White, Window, Misc

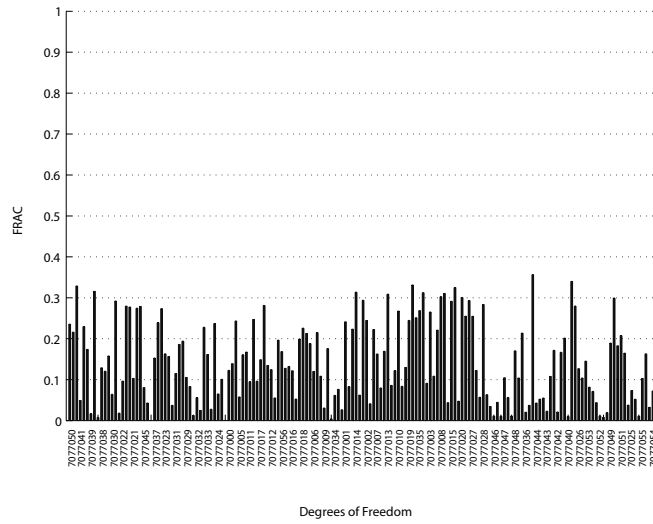


Figure E.11 *FRAC* for door in white, window, misc configuration. Excitation on arch in *xy*-plane.

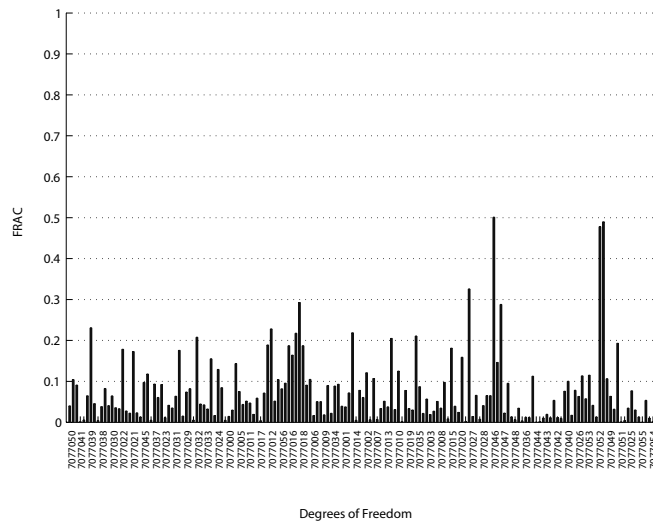


Figure E.12 *FRAC* for door in white, window, misc configuration. Excitation on outer panel in *y*-direction.

E.4 Trimmed Door

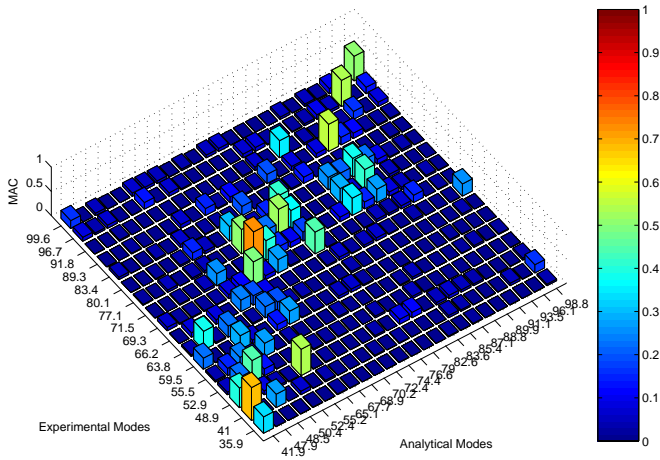


Figure E.13 *MAC matrix for trimmed door configuration.*

E.4. Trimmed Door

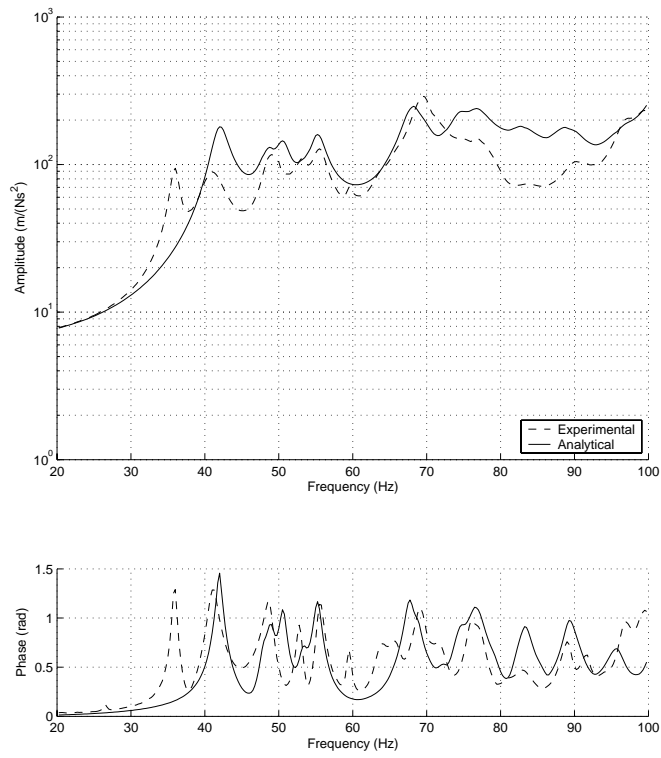


Figure E.14 Sum-blocks for trimmed door configuration.

E. Correlation Results

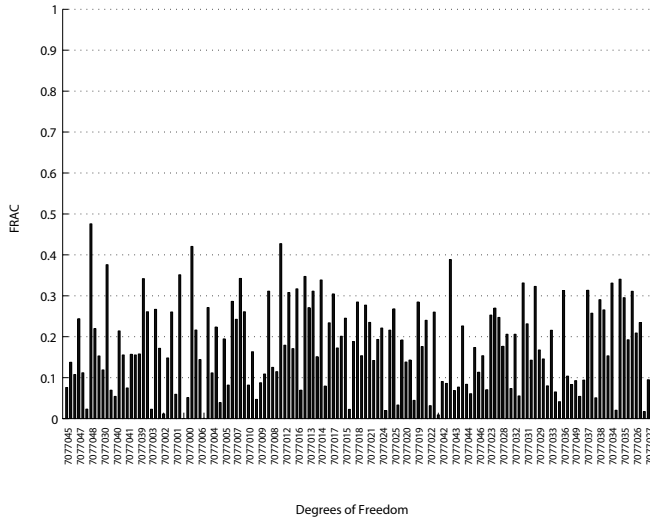


Figure E.15 *FRAC for trimmed door configuration. Excitation on arch in xy -plane.*

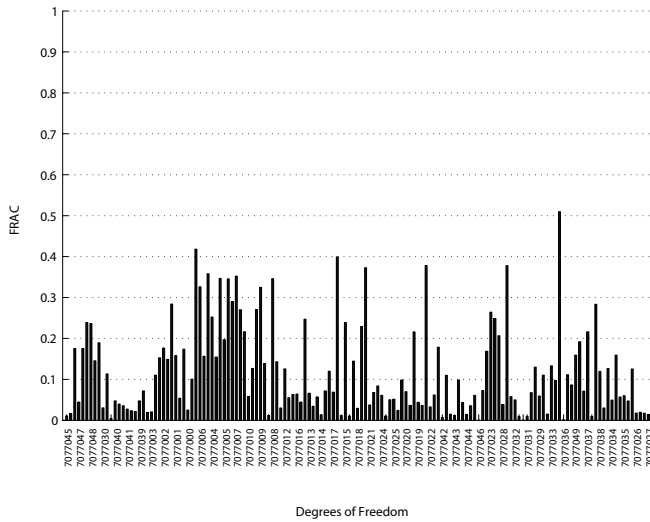


Figure E.16 *FRAC for trimmed door configuration. Excitation on outer panel in y -direction.*

Appendix F

Optimization in MSC.Nastran

Optimization is performed in MSC.Nastran using the executive control statement SOL 200. The most important control statements in order of appearance are the following:

ANALYSIS	specifies the type of analysis being performed for the current subcase. MODES requests normal modes analysis.
DESOBJ	Selects the DRESP<i>i</i> entry to be used as objective function.
DESSUB	Selects the optimization constraints to be used, calls DCONSTR entries.
DOPTPRM	Overrides default values of parameters used in optimization.
DESVAR	Defines design variables used in optimization.
DVMREL1	Defines the relation between a material property and design variable previously defined in DESVAR .
DVPREL1	Defines the relation between element property and design variable previously defined in DESVAR .

F. Optimization in MSC.Nastran

DRESP2	Defines equation responses that are used in the optimization, either as constraints or as an objective function.
DEQATN	Defines equations for use in optimization.
DRESP1	Defines a set of structural responses that is used in the optimization, either as constraints or as an objective. For instance global mass, modal displacements or eigenfrequencies.
DCONSTR	Defines optimization constraints.
DTABLE	Defines a table of real constants that are used in equation entries DEQTN

F.1. MSC.Nastran SOL 200 Input File

F.1 MSC.Nastran SOL 200 Input File

```
$----- FILE MANAGMENT SECTION -----
$----- EXECUTIVE CONTROL SECTION -----

SOL 200
TIME 100000
DIAG 8
CEND

$----- CASE CONTROL SECTION -----

ANALYSIS=MODES
METHOD=1
DESOBJ(MIN)=900000
DESSUB=900001

DISPLACEMENT(SORT2,PUNCH,REAL)=ALL
ECHO=NONE

PARAM,GRDPNT,0           $--- GRID POINT WEIGHT GENERATOR REFERENCE
PARAM,AUTOSPC,YES       $--- AUTOMATIC CONSTRAIN OF SINGULARITIES
PARAM,SNORM,20.0        $--- SHELL NORMAL PARAMETER
PARAM,DBALL,SCRATCH     $--- REDUCE DISK SPACE USAGE => slower restart
PARAM,PRGPST,NO        $--- SINGULARITY PRINTOUT
PARAM,NEWSEQ,-1        $--- NO RESEQUENCING

$----- BULK DATA SECTION -----

BEGIN BULK

EIGRL          1    10.0  200.0                                MAX

$DOPTPRM PARAM1,  VALU1, PARAM2,  VALU2,    ...,

DOPTPRM  CONV1  1.0E-6  DELB  1.0E-05  DESMAX  200  DXMIN  1.0E-05
          P1      1  CONVDV  1.0E-06  CONVPR  1.0E-06  DELX   0.01
          METHOD  1  APRCOD   1         CT   -3.0E-4  CTMIN  5.0E-05

$DESVAR,  ID, LABEL,  XINIT,  XLB,  XUB,  DELXV,

DESVAR    101  E_00    2.00    2.0    2.1
.
.
.

DESVAR    211  NU_26   3.0
.
.
.

DESVAR    401  T_25    0.8     0.7    0.8
.
.
.

DESVAR    501  K_47_T   4.0     0.1
DESVAR    502  K_47_R   4.0     0.1
.
.
```

F. Optimization in MSC.Nastran

```

.
$DVMREL1, ID, TYPE, MID, MPNAME, MPMIN, MPMAX, CO, , +
$+ DVID1, C1, DVID2, C2, ...,

DVMREL1 101 MAT1 7000000 E
        101 1.0E5
.
.
.
DVMREL1 211 MAT1 7000026 NU
        211 1.0E-1
.
.
.
$DVPREL1, ID, TYPE, PID, FID, PMIN, PMAX, CO, , +
$+ DVID1, C1, DVID2, C2, ...,

DVPREL1 401 PSHELL 7000025 4
        401 1.0
.
.
.
DVPREL1 501 PBUSH 7000047 K1
        501 1.0
DVPREL1 502 PBUSH 7000047 K2
        501 1.0
DVPREL1 503 PBUSH 7000047 K3
        501 1.0
DVPREL1 504 PBUSH 7000047 K4
        502 1.0E3
DVPREL1 505 PBUSH 7000047 K5
        502 1.0E3
DVPREL1 506 PBUSH 7000047 K6
        502 1.0E3
.
.
.
$ --- OBJECTIVE FUNCTION

DESVAR 90001 BETA 1.0 1.0E-06
DRESP2 900000 BETA 900000
        DESVAR 90001
DEQATN 900000 OBJ(BETA) = 1.0 * BETA

$ --- CONSTRAINTS

DRESP1 100 MASS WEIGHT
DRESP2 200 BETAM 200
        DESVAR 90001
        DTABLE MASS
        DRESP1 100
DEQATN 200 F(BETA,TM,AM) =
        0.0100 * BETA - ABS((TM-AM)/TM) + 100.0
DCONSTR 900001 200 100.0

DRESP1 1 F01 FREQ 1
DRESP2 201 BETAF01 201

```

F.1. MSC.Nastran SOL 200 Input File

```

      DESVAR      90001
      DTABLE      TF01
      DRESP1      1
DEQATN      201      F(BETA,TF01,AF01) =
              0.0500 * BETA - ABS((TF01-AF01)/TF01) + 100.0
DCONSTR      900001      201      100.0

      DRESP1      2      F02      FREQ      2
      DRESP2      202      BETA F02      202

      DESVAR      90001
      DTABLE      TF02
      DRESP1      2
DEQATN      202      F(BETA,TF02,AF02) =
              0.0500 * BETA - ABS((TF02-AF02)/TF02) + 100.0
DCONSTR      900001      202      100.0

      .
      .
      .

      DRESP2      101      BETA01      101
      DESVAR      90001
      DRESP2      100001
DEQATN      101      F(BETA,MAC) =
              1.0000 * BETA - (1.0-MAC) + 100.0
DCONSTR      900001      101      100.0

      DRESP2      102      BETA02      102
      DESVAR      90001
      DRESP2      100002
DEQATN      102      F(BETA,MAC) =
              1.0000 * BETA - (1.0-MAC) + 100.0
DCONSTR      900001      102      100.0

      .
      .
      .

$ --- TEST DATA

      DTABLE      MASS      0.019      TF01 44.4220      TF02 57.1340      ...      ...
      .
      .
      .
      TD01001      0.0022      TD01002 -0.0240      TD01003 -0.0036      TD01004      0.0205
      TD01005      0.0078      TD01006 -0.0111      ...      ...      ...      ...
      .
      .
      .

$ --- MAC 1, 1

      DRESP1      1001      AD01001      DISP      1      1 7077000
      DRESP1      1002      AD01002      DISP      2      1 7077000
      DRESP1      1003      AD01003      DISP      3      1 7077000
      DRESP1      1004      AD01004      DISP      1      1 7077001
      DRESP1      1005      AD01005      DISP      2      1 7077001
      DRESP1      1006      AD01006      DISP      3      1 7077001
      .
      .
      .

```

F. Optimization in MSC.Nastran

```
DRESP2  10001  MAC0101  10001
DTABLE  TD01001 TD01002 TD01003 TD01004 TD01005 TD01006 ...
.
.
.
DRESP1  1001  1002  1003  1004  1005  1006  ...
.
.
.
```

```
DEQATN  100001  MAC(TD01001,TD01002,TD01003,TD01004,TD01005,
TD01006, ..., ..., ..., ..., ...,
.
.
.
AD01001,AD01002,AD01003,AD01004,AD01005,
AD01006, ..., ..., ..., ..., ...,
.
.
.
..., ..., ..., ..., ...,) =
(TD01001*AD01001+TD01002*AD01002+
TD01003*AD01003+TD01004*AD01004+
TD01005*AD01005+TD01006*AD01006+
...* ...+ ...* ...+
.
.
.
...* ...+ ...* ...)**2 /
((TD01001**2+TD01002**2+TD01003**2+TD01004**2+
TD01005**2+TD01006**2+ ...**2+ ...**2+
.
.
.
...**2+ ...**2+ ...**2+ ...**2) *
(AD01001**2+AD01002**2+AD01003**2+AD01004**2+
AD01005**2+AD01006**2+ ...**2+ ...**2+
...**2+ ...**2+ ...**2+ ...**2))
```

\$ --- MAC 2, 2

```
DRESP1  2001  AD02001  DISP  1  2  7077000
DRESP1  2002  AD02002  DISP  2  2  7077000
DRESP1  2003  AD02003  DISP  3  2  7077000
DRESP1  2004  AD02004  DISP  1  2  7077001
DRESP1  2005  AD02005  DISP  2  2  7077001
DRESP1  2006  AD02006  DISP  3  2  7077001
```

```
DRESP2  100002  MAC0202  100002
DTABLE  TD02001 TD02002 TD02003 TD02004 TD02005 TD02006 ...
.
.
.
DRESP1  2001  2002  2003  2004  2005  2006  ...
.
.
.
```

```
DEQATN  100002  MAC(TD02001,TD02002,TD02003,TD02004,TD02005,
TD02006, ..., ..., ..., ..., ...,
.
.
.
```


F.1. MSC.Nastran SOL 200 Input File

```

      .
      AD02001,AD02002,AD02003,AD02004,AD02005,
      AD02006,   ... ,   ... ,   ... ,   ... ,
      .
      .
      .
      ... ,   ... ,   ... ,   ... ,   ... ,) =
      (TD02001*AD02001+TD02002*AD02002+
      TD02003*AD02003+TD02004*AD02004+
      TD02005*AD02005+TD02006*AD02006+
      ...*   ...+   ...*   ...+
      .
      .
      .
      ...*   ...+   ...*   ...+)**2 /
      ((TD02001**2+TD02002**2+TD02003**2+TD02004**2+
      TD02005**2+TD02006**2+   ...**2+   ...**2+
      .
      .
      .
      ...**2+   ...**2+   ...**2+   ...**2) *
      (AD02001**2+AD02002**2+AD02003**2+AD02004**2+
      AD02005**2+AD02006**2+   ...**2+   ...**2+
      ...**2+   ...**2+   ...**2+   ...**2))

INCLUDE 'model.bdf'

ENDDATA

```


Bibliography

- H. Bedrossian, M. L. Tinker, and H. Hidalgo. Ground vibration test planning and pre-test analysis for the X-33 vehicle. *American Institute of Aeronautics and Astronautics*, (2000-1586), 2000.
- L. C. Böiers. *Lectures on Optimization*. Mathematics Department, Lund Institute of Technology, Lund, Sweden, 2001.
- J. A. Cafeo. Mac and cross-orthogonality variability of vehicle modal vectors. 1st GM CAE Conference, June 1998.
- J. A. Cafeo, R. V. Lust, and U. M. Meireis. Uncertainty in mode shape data and its influence on the comparison of test and analysis models. *Simulation*, 75(5):264–275, 2000.
- A. K. Chopra. *Dynamics of Structures, Theory and Applications to Earthquake Engineering*. Prentice Hall Inc., Upper Saddle River, NJ, USA, 2nd edition, 2001.
- P. Davidsson. *Structure-Acoustic Analysis; Finite Element Modeling and Reduction Methods*. Ph.D. dissertation, Division of Structural Mechanics, Lund Institute of Technology, Lund University, Lund, Sweden, 2004.
- G. H. Golub and C. F. Van Loan. *Matrix Computations*. Johns Hopkins University Press, Baltimore, MD, USA, 1983.
- W. Heylen, S. Lammes, and P. Sas. *Modal Analysis Theory and Testing*. Katholieke University, Leuven, Belgium, 1997.
- L. Komzsik. *MSC.NASTRAN 2001 Numerical User's Guide*. The MacNeal-Schwendler Corporation, Los Angeles, CA, USA, 2001.
- LMS International. *LMS PolyMAX - A Revolution in Modal Parameter Estimation*. LMS International, Leuven, Belgium, 2003.

Bibliography

- G. J. Moore. *MSC/NASTRAN Design Sensitivity and Optimization; Version 68*. The MacNeal-Schwendler Corporation, Los Angeles, CA, USA, 1994.
- MSC.Software Corporation. *MSC.Nastran 2004 - Release Guide*. MSC.Software Corporation, Santa Ana, CA, USA, 2003a.
- MSC.Software Corporation. *MSC.Nastran Quick Reference Guide - Volume 2*. MSC.Software Corporation, Santa Ana, CA, USA, 2003b.
- N. S. Ottosen and H. Pettersson. *Introduction to the Finite Element Method*. Prentice Hall Europe, 1992.
- B. J. Schwarz and M. H. Richardson. *Experimental Modal Analysis*. Vibrant Technology Inc., CA, USA, 1999.
- S. Spanne. *Föreläsningar i Matristeori*. Mathematics Department, Lund Institute of Technology, Lund, Sweden, 1994.
- The MacNeal-Schwendler Corporation. *MSC/NASTRAN V68 Basic Dynamic Analysis User's Guide*. The MacNeal-Schwendler Corporation, Los Angeles, CA, USA, 1996.
- G. N. Vanderplaats. *Numerical Optimization Techniques for Engineering Design*. McGraw-Hill, New York, NY, USA, 1984.
- Vanderplaats Research & Development Inc. *DOT User's Manual; Version 4.20*. Vanderplaats Research & Development Inc., Colorado Springs, CO, USA, 1995.
- T. von Langenhove and M. Brughmans. Using MSC/NASTRAN and LMS/Pretest to find optimal sensor placement for modal identification and correlation of aerospace structures. *LMS International*, 1999. Leuven, Belgium.